

GHENT UNIVERSITY

FACULTY OF VETERINARY MEDICINE

Academic year 2013 - 2014

**THE SATIN SYNDROME IN GUINEA PIGS**

Nephropathy, hyperparathyroidism  
and bone disease of satin cavies

by

Eva Stoffels-Adamowicz

Promoter: Prof. Dr. Katleen Hermans

Research project as part of the  
Master's Dissertation

*Universiteit Gent, its employees and/or students, give no warranty that the information provided in this thesis is accurate or exhaustive, nor that the content of this thesis will not constitute or result in any infringement of third-party rights.*

*Universiteit Gent, its employees and/or students do not accept any liability or responsibility for any use which may be made of the content or information given in the thesis, nor for any reliance which may be placed on any advice or information provided in this thesis.*

## TABLE OF CONTENTS

SUMMARY .....	1
SAMENVATTING .....	2
1. INTRODUCTION .....	4
1.1. THE SATIN FACTOR IN GUINEA PIGS: ORIGIN AND CONSEQUENCES .....	4
1.2. THE SATIN SYNDROME.....	6
1.3. THE SCOPE OF THIS WORK.....	6
2. REVIEW OF PAST RESEARCH.....	8
2.1. STUDIES OF SATIN DISEASE .....	8
2.1.1. First clinical examinations, medical imaging and blood tests .....	8
2.1.2. Fibrous osteodystrophy .....	10
2.2. DIFFERENTIAL DIAGNOSES .....	11
2.2.1. Vitamin C deficiency (scurvy) .....	11
2.2.2. Osteomalacia (vitamin D deficiency) .....	12
2.2.3. Metastatic calcification.....	13
2.2.4. Primary (idiopathic) osteoarthritis .....	13
2.2.5. Osteoporosis.....	13
2.2.6. Neoplasia .....	14
2.2.7. Paget disease of bone .....	15
2.2.8. Other conditions.....	15
3. THE SATIN SYNDROME: CLINICAL PRESENTATION AND EPIDEMIOLOGY .....	17
3.1. INTRODUCTION.....	17
3.2. MATERIALS AND METHODS .....	17
3.2.1. Husbandry and diet.....	17
3.2.2. Weight, lifespan and lameness scores .....	18
3.2.3. Acquired dental disease .....	18
3.2.4. Statistical analyses .....	19
3.3. RESULTS.....	19
3.3.1. Vitality of satin guinea pigs .....	19
3.3.2. Lameness prevalence and scores .....	19
3.3.3. Acquired dental disease .....	21
3.3.3.1. Clinical manifestation .....	21
3.3.3.2. ADD in satin guinea pigs .....	21
3.4. DISCUSSION .....	22
3.4.1. Acquired dental disease .....	22
3.4.2. General discussion and concluding remarks.....	23
4. CALCIUM HOMEOSTASIS.....	25
4.1. INORGANIC IONS IN THE ORGANISM .....	25
4.2. REGULATION OF CALCIUM AND PHOSPHATE LEVELS.....	26
4.2.1. Solubility in physiological fluids.....	26
4.2.2. Intermezzo: tissue calcification inhibitors .....	28
4.3. THE RENAL-BONE AXIS .....	29

4.3.1. The parathyroid gland and hormone.....	30
4.3.2. Calcitonin .....	32
4.3.3. The biochemistry of vitamin D .....	32
4.3.4. The intestine .....	34
4.3.5. The bone.....	35
4.4. THE KIDNEY.....	36
4.4.1. Anatomy.....	36
4.4.2. Glomerular filtration .....	36
4.4.3 Proximal tubule .....	38
4.4.4. Loop of Henle.....	39
4.4.5. Distal tubule .....	40
4.4.6. Renin-angiotensin-aldosterone system .....	40
4.4.7. Acid-base regulation .....	41
4.5 CALCIUM, SODIUM AND PROTEIN INTERACTIONS.....	42
4.5.1 Modeling tubular ion flows .....	42
4.5.2. Calcium-sodium interaction .....	45
4.5.3. Calcium-protein interaction .....	47
4.5.4. Conclusion .....	49
5. RENAL OSTEODYSTROPHY.....	50
5.1. CKD IN ANIMAL MODELS .....	50
5.2. BONE REMODELING .....	52
5.2.1. Bone matrix and cells .....	52
5.2.2. Bone remodeling.....	54
5.2.3. Bone morphology.....	55
5.3. BONE IN SECONDARY RENAL HYPERPARATHYROIDISM .....	57
5.3.1. Fibrous osteodystrophy .....	57
5.3.2. Osteomalacia.....	58
5.3.3. Adynamic bone disease.....	58
6. COMPUTED TOMOGRAPHY AND BONE DENSITY MEASUREMENTS.....	60
6.1. INTRODUCTION.....	60
6.2. MATERIALS AND METHODS .....	60
6.3. RESULTS.....	63
6.3.1. General bone morphology .....	63
6.3.2. Dental disease .....	63
6.3.3. Bone density measurements .....	65
6.4. DISCUSSION .....	67
6.5. CONCLUSION .....	70
7. CLINICAL DIAGNOSTICS AND HISTOPATHOLOGY .....	71
7.1. INTRODUCTION.....	71
7.2. MATERIALS AND METHODS .....	71
7.3. RESULTS.....	72
7.3.1. Anamneses and necropsy findings.....	72

7.3.2. Blood and urine parameters .....	74
7.3.3. Histopathology .....	76
7.3.3.1. Integument.....	76
7.3.3.2. Parathyroid .....	76
7.3.3.3. Bone .....	77
7.3.3.4. Kidneys.....	79
7.4. DISCUSSION .....	83
7.4.1. Blood and urine parameters .....	83
7.4.2. Parathyroid glands.....	84
7.4.3. Bones .....	86
7.4.4. Kidneys .....	88
7.5. CONCLUSION .....	91
8. GENERAL REMARKS AND CONCLUSION .....	92
8.1. WHAT HAVE WE LEARNED FROM GUINEA PIGS?.....	92
8.1.1. Lesions in satins and satin carriers.....	92
8.1.2. Is the satin syndrome an “exotic” disorder?.....	92
8.2. WHAT CAN WE LEARN FROM GUINEA PIGS? .....	93
9. REFERENCES .....	95

## **SUMMARY**

The satin guinea pig breed gained popularity due to its attractive lustrous coat. However, inexplicable disease symptoms such as lameness, dental malocclusion and failure to thrive are associated with this breed. In this work a multi-disciplinary study involving experimental and modeling efforts was undertaken to characterize the satin syndrome and its underlying pathophysiological processes. The compromised vitality of the satin breed, reflected by a shorter lifespan and a lower weight of animals as compared with their non-satin peers, was statistically proven in observational studies. Computed tomography and bone densitometry revealed advanced bone lesions with loss of bone mass in satin guinea pigs, and provided insights in dental pathology. In clinical studies, blood serum characteristics of satins were suggestive of homeostatic imbalances in calcium metabolism, while urine tests revealed proteinuria. At necropsy, gross kidney lesions were found. Histopathologically, hyperplasia of the parathyroid gland, fibrous osteodystrophy and glomerulopathy reminiscent of human diabetic kidney disease were observed. Pronounced changes were present in homozygotic and heterozygotic satin guinea pigs. These findings were attributed to secondary renal hyperparathyroidism and metabolic bone disease. An extensive literature study was carried out to support this diagnosis. To explain the relationship between glomerulopathy and renal calcium losses, numerical modeling of renal mineral handling was performed. Codependencies of urinary calcium, sodium and protein excretion were demonstrated. It was shown that proteinuria attendant to glomerulopathy can account for the observed hyperparathyroidism and bone disease. Finally, the potential of a satin guinea pig as a model in human kidney research was evaluated.

## SAMENVATTING

Satijncavia's werden veel gefokt vanwege hun opvallend glanzende vacht. Er circuleren echter veel anekdotische verhalen over onverklaarbare ziekteverschijnselen bij dit ras, zoals mankheid, tandproblemen en algemene zwakte. De symptomen zijn veelal aspecifiek. Dit werk beschrijft een multi-disciplinaire studie naar verschillende aspecten van het satijnsyndroom, en heeft als doel te komen tot verklaring van de onderliggende pathofysiologische verschijnselen.

Ten eerste werd er in een vergelijkende studie uitgevoerd tussen satijn- en niet-satijncavia's. Er werd aangetoond dat satijncavia's een kortere levensverwachting en een lager lichaamsgewicht hebben. Opmerkelijk is echter dat er in deze studie geen statistisch significant verschil werd gevonden in het voorkomen van mankheid en tandproblemen tussen satijncavia's en de controle dieren. Enkele cavia's werden onderzocht met behulp van computertomografie. Beeldvorming visualiseerde vergaande botletsels, zoals botcysten en veranderde trabeculaire patronen bij satijncavia's. Bovendien verschaftte het inzichten in de tandproblemen bij satijn- en niet-satijncavia's. Botdichtheidsmetingen toonden lagere botmassa's bij satijncavia's in vergelijking met niet-satijncavia's.

Vervolgens werden klinische studies en lijkschouwingen uitgevoerd om abnormaliteiten bij satijncavia's te beschrijven. Bloedtesten toonden verlaagde calcium- en verhoogde alkalische fosfataseconcentraties in het serum. Deze afwijkende waarden wijzen op een homeostatische imbalans van het calcium metabolisme. Daarnaast bleek uit urinetesten dat er sprake is van ernstige proteïnurie. Bij lijkschouwing werden er macroscopische nierletsels vastgesteld. Histologie toonde hyperplasie van de bijschildklier en botaantasting aan. De normale lamellaire structuur van corticaal bot werd vervangen door een netwerk van trabeculae die hoofdzakelijk uit geweven bot bestonden. Er was toename van cellulariteit en bindweefsel in de peritrabeculaire ruimte, en onderdrukking van beenmerg. Deze pathologie kon geïdentificeerd worden als fibreuze osteodystrofie. In de nier werd een aantasting van de glomeruli vastgesteld: toename van mesangiale cellulariteit, focale glomerulaire sclerose en verdikking van basale membranen van Bowman capsules. De waargenomen glomerulopathie heeft morfologische kenmerken die overeenkomen met humane diabetische nierinsufficiëntie. Tevens is gebleken dat ook de dragers van het satijngen, die anderszins fenotypisch niet te onderscheiden zijn van niet-satijncavia's, ook dergelijke letsels kunnen ontwikkelen.

Op basis van deze observaties werd de diagnose van secundaire renale hyperparathyreoidie en daaruitvoortvloeiende metabole botziekte gesteld. Een uitgebreide literatuurstudie ondersteunt deze diagnose. Vergelijkbare presentaties van botziekten zijn namelijk ook terug te vinden in de humane pathologie. Om kwantitatief aan te tonen dat er een significant calciumverlies kan optreden bij glomerulopathie werd er een numeriek niermodel ontwikkeld. Hierbij werden de transportvergelijkingen van de filtraatflux door renale tubuli afgeleid en in een numeriek model verwerkt. De verbanden tussen calcium-, natrium- en eiwitexcretie werden berekend. De resultaten laten zien dat proteïnurie ten gevolge van glomerulopathie tot substantiële calciumverliezen kan leiden, welke de waargenomen hyperparathyreoidie en botaantasting kunnen verklaren.

De resultaten suggereren dat het satijnsyndroom bestaand uit renale hyperparathyreoidie en osteodystrofie niet specifiek is voor satijncavia's. Het kan bij verschillende diersoorten en bij de mens

voorkomen. Dit maakt de satijncavia een potentiëel model voor overeenkomstige humane nier- en botaandoeningen.

# 1. INTRODUCTION

## 1.1. THE SATIN FACTOR IN GUINEA PIGS: ORIGIN AND CONSEQUENCES

The guinea pig or cavy (*Cavia porcellus*) is a large herbivorous rodent indigenous to South America. Guinea pigs were domesticated around 2000 BC and became an important part of the cultural heritage of Native South Americans (Morales, 1995). The guinea pig was taxonomically classified by Linnaeus in 1758. Elementary biological facts on this species are summarized in Table 1.1.

	Values	Remarks
Adult body weight (BW)	700-1200 g	up to 2100 g*
Surface area	$10.1 \times (\text{BW in g})^{2/3} \text{ cm}^2$	
Life span	4-6 years	up to 10 years*
Body temperature	37-39.8 °C	
Respiratory rate	42-104/min	
Heart rate	280-380/min	
Blood pressure	80-94/55-58 mmHg	
Puberty	♂ 3-4 months, ♀ 2-3 months	♂ 400-500 g, ♀ 300-400 g*
Gestation	68.8 days	68-72 days*
Litter size	2-5	1-7*
Weaning	21 days	21-28 days*

Table 1.1: Normative values for guinea pigs, after Hrapkiewicz and Medina; 2007 Suckow et al., 2012. \* author's observations.

Guinea pigs have a docile character and modest requirements; they adapt easily to captivity, are inexpensive in maintenance and breed readily. These features have made guinea pigs popular both as laboratory and as companion animals. Their use in biomedical research was extensive throughout the 20th century: the term *guinea pig* is still a synonym of *test animal* in the English language. Guinea pigs bear many resemblances to humans, particularly with regard to nutrition (dietary vitamin C requirements), reproduction and susceptibility to intoxication and infection (Clarke et al., 1980; Barth, 2004; Hrapkiewicz and Medina, 2007; Carter, 2007). Although the number of new scientific records on guinea pigs tends to decline due to the introduction of more efficient rat and mouse models, guinea pig models are still used in research on human immune-mediated and endocrine disorders (Canning and Chou, 2008; Kumar et al., 2012).



Fig. 1.1: A short-haired gold agouti guinea pig.

Breeding pet cavy has become increasingly popular in the past decades. Many new breeds and varieties have been developed. Along with the short-haired agouti (Fig. 1.1), derived from the wild ancestor of the domestic guinea pig (Rowlands and Weir, 1974), numerous rough-coated and long-haired breeds with diverse coat colors and patterns are available (Fig. 1.2). The satin guinea pig breed emerged in 1977 in the United States as a spontaneous mutation in local short-haired lines. Soon it



Fig. 1.2: Guinea pig breeds: top – short-haired self-white (type Dunkin-Hartley), middle – rough-haired (Abyssinian), bottom – peruvian.

gained popularity among breeders because of its esthetically attractive lustrous coat (Robinson and Seaborne, 1988).

Robinson and Seaborne (1988) described the satin factor as a monogenic recessive autosomal mutation (*sa*) that affects the hair structure. The satin factor can be also present in other animal species, such as mice and hamsters. Macroscopically, the hairs of homozygotic animals (*sasa*) display a typical shine due to light reflection and refraction; the hairs are markedly thinner than in other guinea pig breeds. Microscopically, the hair medulla is reduced (Robinson and Seaborne, 1988). These phenotypic features are however not always evident. Firstly, lustrous coats can appear in animals with a totally different genetic background, see e.g. Fig. 1.1. Secondly, there is much variation between individuals that carry the double *sa* gene. The satin shine is more pronounced in light-coated animals and particularly in the US-Teddy breed. According to specialized breeders, also the US-Teddy heterozygotes (*Sasa*) can be distinguished from non-satin



Fig. 1.3: Examples of satin cavies, clockwise from top left: peruvian, short-haired (solid silver agouti variety), US-teddy, short haired (tortoiseshell variety). Note the large diversity within the breed.

animals by the sheen of their coats. Conversely, the satin phenotype is not apparent in dark-coated animals and agoutis (Fig. 1.3). Therefore one may hypothesize that the inheritance patterns are more complex than indicated by Robinson and Seaborne (1988), and that the phenotype is not only determined by the major gene (*sa*), but also by not yet identified minor genes, gene interaction

(epistasis) and environmental factors. In hobby breeding, animals are often arbitrarily assigned to “satin” or “satin-carrier” groups based on visual evaluation and genealogy. Reliable tests based on genotyping are unfortunately not available to date.

The satin cavy was imported to Europe in 1986. Although there were no previous indications of any health problems, neither in American nor in other satin guinea pig lines, the European pet owners noticed some peculiarities. The satin cavies appeared to perform poorer than their non-satin peers: their growth was often retarded and their adult weight was low. The life expectancy of satins was also said to be shorter. Interestingly, motoric and dental problems typical for advanced age or malnutrition (Ding et al., 2006; Hawkins and Bishop, 2012) were observed frequently in relatively young and well-fed satins. Isolated cases were subjected to veterinary examination. Skeletal abnormalities, bone loss,

pathological fractures and dental disease were diagnosed by radiography (Chapter 2). Simultaneously, the satin breeders fiercely denied the existence of any genetic disorders in their lines. This discussion was situated outside the scientific community. The information originated mainly from private individuals and no systematic statistic studies were performed to verify their observations. Nevertheless, a reluctant attitude towards satin guinea pigs and their breeders, or the “satin fear”, arose and peaked in 2000s. The satin issue was even addressed by Dutch political parties devoted to animal welfare (see <https://zoek.officielebekendmakingen.nl/kst-31389-125.odt>). Presently, the satin guinea pig has become rather scarce. It is unclear whether this is due to propaganda campaigns or due to time-varying trends in guinea pig breeding.

## 1.2. THE SATIN SYNDROME

The *satin syndrome* - the entire complex of disorders related to the satin factor – is difficult to describe in quantitative terms. It has diverse manifestations, ranging from subtle effects like retarded growth and failure to thrive, through mild motoric dysfunction, to severe debilitation, anorexia and death. One cannot predict the age onset nor the penetrance of the disease. A fraction of satin cavies does not develop any visible symptoms throughout their lifetime (5-6 years), while other animals succumb before 1 year of age. After the onset of symptoms, the typical time scale of disease progression is several months up to 2 years (see also Chapter 3). There are virtually no pathognomonic signs of the satin disease, because similar problems are also encountered in non-satin breeds. Moreover, as indicated in the previous section, the observations of health problems in satin cavies originate largely from pet owners; the reliability of such observations can be often questioned. The scientific literature data is rather scarce (see Chapter 2) and the pathophysiology and epidemiology of the satin syndrome have not yet been thoroughly investigated.

In the light of the above, it is a scientific challenge to provide an unbiased, systematic description of the satin syndrome and to unravel the underlying pathophysiological mechanisms. At the first instance, new therapeutic methods may be developed, and the breeding schemes may be adapted so as to control the disease. On a longer term, understanding the satin syndrome may have implications that reach far beyond hobby breeding and routine veterinary practice. The satin guinea pig may become a model for human disease when sufficient parallels in the pathogenesis and clinical manifestations are identified. This possibility will be discussed in the current manuscript.

## 1.3. THE SCOPE OF THIS WORK

The present work attempts a systematic description of the satin syndrome and is the outcome of a multi-diagnostic study conducted by the author in the years 2008-2013. This research comprised daily observations of satin guinea pigs, recording their health status and vital parameters, results of blood and urine tests, and necropsy findings followed by medical imaging (computed tomography) and histopathological studies. When feasible, statistical analyses of the experimental data were performed. Simultaneously, theoretical models were developed to explain the experimental findings.

In Chapter 2 a review of the hitherto published scientific findings on satin guinea pigs is presented. A scrupulous analysis of previously described symptoms and lesions in satins, combined with the author’s observations of guinea pig herds, leads to the work hypothesis on the renal origin of

the satin syndrome. This hypothesis is further elaborated and supported by experimental data in the course of this research. Chapter 3 contains a detailed description of clinical manifestations of the satin syndrome, a new lesion scoring system and the results of epidemiological studies. Chapter 4 deals with fundamental physiological mechanisms of maintaining mineral homeostasis, with special attention given to kidney function: renal filtration and reabsorption, renal handling of calcium, phosphate and other minerals. Humoral control and the influences of acid-base regulation and renine-angiotensin-aldosterone systems are discussed in detail. A model is developed for the evaluation of calcium excretion in normal versus compromised kidney function. The interactions of calcium with other urinary components such as sodium and protein are described quantitatively. In Chapter 5 current research topics in the area of kidney and bone pathophysiology are reviewed. State of the art animal models for kidney and bone disease are discussed, and their advantages and drawbacks are indicated. Normal versus pathological bone remodeling processes and the most common presentations of renal bone disease are described. Chapter 6 contains computed tomography and bone density measurement data for satin guinea pigs, non-satin guinea pigs with normal renal function and non-satin guinea pigs with previously diagnosed chronic kidney disease. Chapter 7 presents the outcome of clinical case studies performed in the framework of this research. The results of diagnostic laboratory tests (blood, urine) and macroscopic and histopathological findings in bones and soft tissues are discussed. Finally, general remarks, conclusions and recommendations are given in Chapter 8.

## 2. REVIEW OF PAST RESEARCH

### 2.1. STUDIES OF SATIN DISEASE

#### 2.1.1. First clinical examinations, medical imaging and blood tests

The relatively high prevalence of health problems among satin guinea pigs attracted attention from veterinary practitioners. However, diagnosis could not be readily established because of vagueness and diversity of the clinical picture. The only remarkable symptoms were: anorexia, weight loss and lameness (see also Chapter 3). Based on these observations, it was tentatively concluded that satin guinea pigs were affected by primary skeletal (bone) pathology.

Radiographic studies followed clinical examinations. Unfortunately, the major part of medical imaging data was collected by private veterinary practitioners; these data were not made available to the scientific community. Few reports of clinical case studies were published (Schwartz et al., 2001; Rapsch-Dahinden et al., 2009). Schwartz et al. (2001) described two satin guinea pig patients that displayed lethargy and reluctance to move; in addition, dental disease was diagnosed in one of the animals. Upon radiographic examination, bone deformities and alterations of the trabecular bone pattern, polyarticular osteoarthritis, pathological fractures and osteopenia were found. The disorder was tentatively described as fibrous osteodystrophy (*osteodystrophia fibrosa*). Links to nutritional imbalances such as calcium deficiency or a low calcium-to-phosphorus ratio in feed, were considered. However, no conclusions were drawn at that stage.

An extensive study was conducted in 1997-2002 by Jordan and coworkers (Jordan, 2008; Jordan et al., 2009) at the Small Animal Clinic, Freie Universität Berlin (Germany). A total number of 52 satin animals, 7 satin carriers and 25 non-satin controls were subjected to clinical evaluation and radiographic examination. In this particular study (snapshot data), the penetrance of the disease symptoms in satins was found to be 38%. Twenty satin cavies showed at least one of the following clinical symptoms: weight loss, inappetence, salivation, dental abnormalities and motoric dysfunction. Necropsy was performed on 11 animals. X-ray imaging revealed osteopenic lesions in the hip joint, tibia and femur, as well as in the mandibula, zygomatic arch and other skull bones. A lesion scoring system was developed, based on the radiographic appearance of the bones. Scores of 1, 2 or 3 points were assigned to bone lesions based on their severity, and a total score per animal was calculated. Significantly higher lesion scores were found in satin cavies that displayed clinical symptoms, as compared with clinically normal satins, satin carriers and controls. Furthermore, blood serum biochemistry and haematology tests were performed. The satin guinea pigs with symptoms of disease had significantly lower serum calcium than the satin animals without symptoms and the control groups. There was no significant elevation of serum phosphate in clinically affected animals. The alkaline phosphatase activity was higher ( $p < 0.05$ ) in satins than in satin carrier and control groups. Fibrous osteodystrophy was diagnosed at necropsy. The authors investigated possible causes, including nutritional or renal secondary hyperparathyroidism, vitamin C deficiency and vitamin D deficiency (osteomalacia). Interestingly, out of 11 necropsied satin guinea pigs, 8 showed macroscopic (interstitial nephritis, pyelonephritis) and microscopic (renal calcinosis) kidney lesions. Nevertheless, the authors considered the observed kidney damage not to be sufficiently pronounced. Besides, no

abnormalities were found in serum renal parameters (urea, creatinine) and in haematological characteristics (no evidence of anemia). Based on these arguments the authors excluded the possibility of renal origin of the satin osteodystrophy. The study remained inconclusive with regard to the pathophysiology of the disease.

In 2008-2009 another study was conducted by Massop (Massop 2009) at the Faculty of Veterinary Medicine, Ghent University (Belgium), with the participation of the author at the Department of Biomedical Engineering, Eindhoven University of Technology (The Netherlands). A limited number

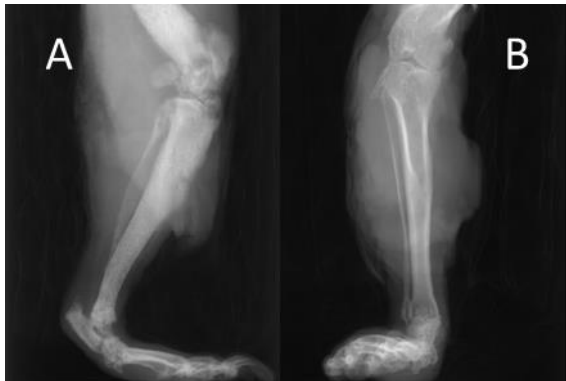


Fig. 2.1: Typical radiographic images of a hind leg of a satin (A) and a non-satin (B) guinea pig. Note the radiopacity of the medulla of the satin tibia and femur.

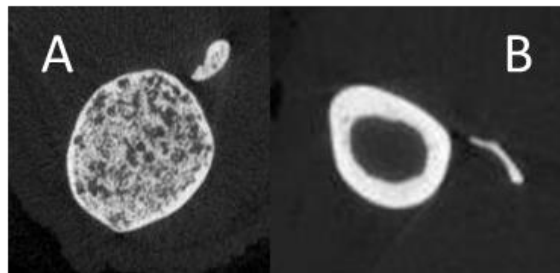


Fig. 2.2: CT imaging: mid-diaphyseal cross sections of a satin (A) and a non-satin (B) tibia.

of clinically affected satin guinea pigs was examined post-mortem by conventional X-ray radiography and by high-resolution X-ray computed tomography (CT). Two animals were necropsied and subjected to pathohistological examination. Routine blood tests to determine serum biochemistry parameters were performed in another group of guinea pigs, consisting of both clinically healthy and diseased satin individuals. Although the limited scale of this project did not allow statistical data analyses, the global outcome was similar to this of Jordan and coworkers (Jordan, 2008; Jordan et al., 2009). Similar radiographic features were observed and the activity of alkaline phosphatase was found to be elevated in satin cavies, in accordance with the previous findings. However, several minor discrepancies were present. Unlike in the study of Jordan, the satin guinea pigs displayed mild hypocalcaemia regardless of the presence of clinical symptoms. Furthermore, phosphate retention was found in all satin animals. Typical radiograms are presented in Fig. 2.1. CT imaging provided the most important new insight. The long bones of satin guinea pigs showed dramatic periosteal bone resorption and osteolytic lesions. The cortex was expanded and the medullary cavity was constricted (Fig. 2.2). The most pronounced lesions were found in hind extremities (femur, tibia, stifle joint and foot), the jaws (ramus mandibulae), and the skull (frontal and parietal bones, and bulla tympanica). Preliminary histopathology results indicated irregular trabecular patterns. The cortex was markedly thickened and contained large amounts of vascularized fibrous tissue. Bone marrow was largely replaced by fibrous tissue, as depicted in Fig. 2.3. One of the two necropsied animals had bilaterally cysteous kidneys. Massop rejected metabolic bone disease as the potential pathophysiology of the satin syndrome. Instead, several other hypotheses were posed (see Section 2.2) but not verified due to lack of experimental evidence.

### 2.1.2. Fibrous osteodystrophy

The majority of scientific records describe the satin syndrome in terms of fibrous osteodystrophy (*osteodystrophia fibrosa*). Fibrous osteodystrophy is a collective term that refers to bone abnormalities caused by hyperparathyroidism. This condition was produced experimentally in guinea pigs (Bodansky et al., 1930). In human medicine one distinguishes between primary (neoplastic), secondary

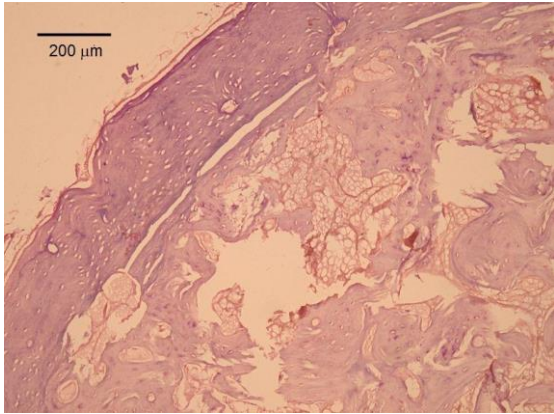


Fig. 2.3: A mid-diaphyseal cross section of a satin guinea pig tibia. H&E stain.

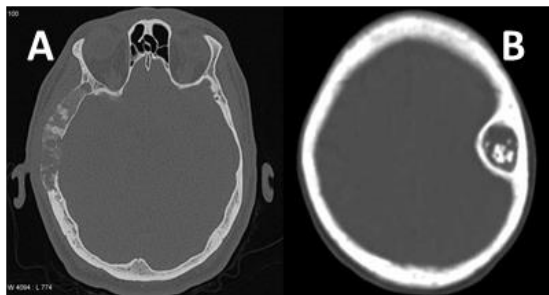


Fig. 2.4: CT imaging: transverse scans of a human skull affected by renal osteodystrophy. A – fibrous dysplasia, B – a brown tumor of the calvarium. Contributed by Dr. M.T. Niknejad to radiopaedia.org. Reproduced by courtesy of Dr. F. Gaillard, Editor, <http://radiopaedia.org>.

(nutritional or renal) and tertiary (sequel to secondary) hyperparathyroidism. In veterinary sciences this strict classification is much less frequently applied. The pathogenesis of various types of parathyroidism with the attendant bone diseases, including the molecular markers and signaling systems, is reviewed in Chapter 5. Shortly, fibrous osteodystrophy is one of three possible manifestations of hyperparathyroidism, the two others being osteomalacia and adynamic bone disease. Fibrous osteodystrophy is characterized by a drastic increase in bone turnover. Histopathological changes are: replacement of lamellar bone by woven bone, increase of unmineralized osteoid (Christiansen, 2001; Parfitt, 2003), and periosteal bone resorption (Triantafillidou et al., 2006). The condition progresses from *osteitis dissecans*, or the early stage characterized solely by microscopic changes, through *osteitis fibrosa* (also called fibrous dysplasia) with a marked increase of fibrous tissue, cortex thickening and medullary constriction, towards the end stage termed *osteitis cystica fibrosa* (Schiller and Teitelbaum, 1999). Dependent on the stage of the disease, radiographic findings are: osteopenia,

mineralization defects, cortex thickening and cystic lesions (Tigges et al., 1995). Typically, the skull and the jaws are affected (Lautenbach et al., 1968; Cooper, 1989). In *osteitis fibrosa*, computed tomography reveals a spongy network of poorly mineralized trabeculae, often referred to as “ground glass” (Chang et al., 2007). The skull displays a typical “salt and pepper” pattern of mixed osteolytic and osteosclerotic zones (Jevtic, 2003). In the most advanced form, *osteitis cystica fibrosa*, large osteolytic lesions termed *brown tumors* may be present. Brown tumors often mimic neoplasia (Chew and Huang-Hellinger, 1993). The characteristic jaw hypertrophy is termed *leontiasis ossea* (Lee et al., 1996). The latter features: brown tumors and *leontiasis ossea* are specific for advanced renal osteodystrophy.

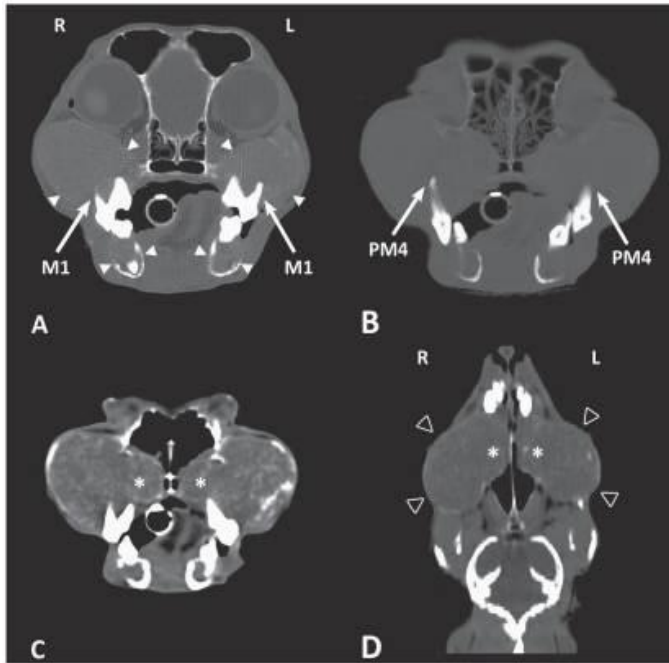


Fig. 2.5: CT images of a canine skull affected by renal osteodystrophy. A – transverse image at the level of maxillary M1, demonstrating demineralization of the calvaria. White arrowheads: enlarged maxillae, mandibulae and the zygomatic arches. B – transverse image at the level of P4, showing loss of alveolar bone and “floating teeth” (white arrows). C (transverse) and D (frontal) images showing 2 fibrous maxillary masses (open white arrowheads).

Reproduced from Vanbrugge et al., (2011) by courtesy of Dr. L. Blond, Département de Sciences Cliniques, Centre Hospitalier Universitaire Vétérinaire (CHUV), Faculté de Médecine Vétérinaire de l'Université de Montréal (Canada).

Fibrous osteodystrophy is known to affect companion animals: dogs (Hogg, 1947), and to a lesser extent cats (Lucke, 1968). In dogs, bone deformities similar to those in humans and guinea pigs are observed (Vanbrugge et al., 2011). Jaws are the predilection site in dogs; canine osteodystrophy (renal or nutritional) is often termed “rubber jaws” (Hogg, 1947). Jaw hypertrophy in dogs with secondary renal hyperparathyroidism bears much resemblance to *leontiasis ossea* in humans. Typical CT images of human and canine kidney patient’s skulls are shown in Figures 2.4 and 2.5; images of a satin guinea pig’s skull are given for comparison in Fig. 2.6.

There is striking morphological similarity between bone lesions of human or canine chronic kidney disease and the findings in satin guinea pigs. The typical salt and pepper appearance and the cystic lesions reminiscent of brown tumors are observed in guinea pigs with end stage satin syndrome. Kidney disease in satins

was excluded in previous studies (Jordan, 2008; Massop, 2009). However, renal insufficiency has many manifestations, and one cannot reject on the basis of a mere absence of uraemia or gross kidney lesions (Meyer and Hostetter, 2007). In fact, the early necropsy data (Massop, 2009) provided strong indications for the underlying renal pathology. This issue will be further elaborated in Chapters 5-8.

## 2.2. DIFFERENTIAL DIAGNOSES

It is important to note that the clinical symptoms found in satin patients are neither pathognomonic for fibrous osteodystrophy nor for any other skeletal disorder. Several authors considered different causes of the observed abnormalities (Jordan, 2008; Massop, 2009). Differential diagnoses for lameness, anorexia and dental problems are discussed below.

### 2.2.1. Vitamin C deficiency (scurvy)

Most species are capable of biosynthesis of vitamin C (L-ascorbic acid) from glucose. However, guinea pigs and primates lack L-gulonolactone oxidase, a liver enzyme that converts L-gulonolactone into L-ascorbic acid (Burns, 1957). These species are thus dependent on dietary L-ascorbic acid

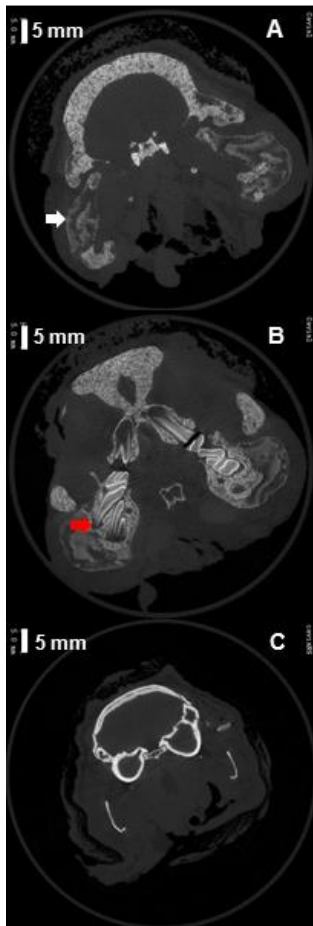


Fig. 2.6: Transverse CT images of guinea pig skulls. A – satin, rostral to bulla tympanica, B – same satin, at the level of M1/M2, C – control, at the level of bulla tympanica. White arrow: thickening and osteolytic lesions in mandibulae, red arrow: resorption of alveolar bone and “floating teeth”.

supply. The daily requirement for a guinea pig is 10 mg/kg, increasing to 30 mg/kg in gestation (Quesenberry et al., 2012). Deficiency leads to a potentially lethal metabolic disorder, known as scurvy. Guinea pig is an important model for human scurvy (Kipp et al., 1996).

Vitamin C is involved in many important metabolic processes. Besides being an intracellular antioxidant, L-ascorbic acid is necessary for collagen synthesis and functioning of innate immune system (Chojkier et al., 1989; Meister, 1994; Preedy et al., 2010). Furthermore, vitamin C is required for the synthesis of osteocalcin and other osteoblast-related proteins (Franceschi et al., 1994). Since vitamin C plays a role in collagen synthesis, its deficiency causes defective formation of extracellular matrix. This in turn can lead to vascular wall fragility (haemorrhages), cartilage degeneration (Bonucci, 1970; Bonucci 1978), decreased bone density and periodontal disease (Kipp et al., 1996; Fain, 2005). Bone, joint and dental pathology in vitamin C-deficient guinea pigs has been confirmed in many studies (Clarke et al., 1980; Richardson 2000; Suckow et al., 2012). Nowadays it is widely recognized that vitamin C is of vital importance to guinea pigs, and adequate supplementation schemes are applied (Suckow et al., 2012). As a result, clinical scurvy has become extremely rare. Scurvy as the sole cause of the satin syndrome is unlikely, because the satin cavies involved in the current and past studies (Massop, 2009) were fed a vitamin-rich diet (see also Chapter 3). Moreover, no typical signs of scurvy such as subcutaneous ecchymoses or calcification of epiphyseal cartilage (Bonucci, 1970) were found upon necropsy. However, since vitamin C deficiency is known to affect bones and joint cartilage, it may in certain cases exacerbate the symptoms of the satin syndrome.

### 2.2.2. Osteomalacia (vitamin D deficiency)

Osteomalacia (in juveniles: rickets) is a disorder characterized by inadequate mineralization of newly deposited bone matrix, caused by disturbances in vitamin D metabolism. This condition affects human as well as animals (Schiller and Teitelbaum, 1999; McGavin and Zachary, 2007). Clinically it presents as bone and muscle weakness, bone deformities and pathological fractures, including greenstick fractures (Schiller and Teitelbaum, 1999; Leon et al., 2008). The principal parameter in osteomalacia is the level of circulating calcitriol (1,25-dihydroxycholecalciferol). Calcitriol acts in concert with the parathyroid hormone (PTH) and sustains the serum calcium balance by stimulating intestinal calcium absorption and bone resorption, and reducing renal calcium excretion (Guyton and Hall, 2000). Low levels of calcitriol are associated with osteomalacia. The underlying causes are diverse: too low dietary intake of vitamin D2 and D3 (ergocalciferol, cholecalciferol), failure of synthesis of cholecalciferol in the skin, and inadequate transformation to 25-OH and 1,25-OH active derivatives in liver and kidney, respectively. In fact,

osteomalacia is one of the possible manifestations of renal bone disease (Berry et al., 2002; De Schutter, 2012). The pathways of vitamin D biosynthesis and actions in a healthy organism and in renal disease will be discussed in detail in Chapter 4. Vitamin D and its metabolism may be altered in the satin syndrome; however, this issue remains hitherto unresolved.

### **2.2.3. Metastatic calcification**

Metastatic calcification, or soft tissue mineralization, is a relatively common disorder in guinea pigs. Clinical signs include stiffness and impaired gait followed by anorexia, lethargy and death (Richardson, 2000). Soft tissue calcification in guinea pigs in response to dietary imbalances was studied by many authors. Microscopically, calcium deposits in various tissues (skeletal and cardiac muscle, liver and kidney) were found (Maynard et al., 1958). In early studies, magnesium deficiency was suggested as the main etiological factor (O'Dell et al., 1957; Walter and Baldwin, 1963). Other factors included vitamin D intoxication and inadequate dietary calcium to phosphate ratios (Richardson, 2000). Preliminary histopathological and radiographic findings in satins did not indicate extensive soft tissue calcification, but this issue requires further exploration in the future. Soft tissue calcification in renal failure, also called *the calcification paradox*, is an important topic in contemporary kidney research (De Schutter, 2012). The underlying mechanisms will be reviewed in Chapter 4.

### **2.2.4. Primary (idiopathic) osteoarthritis**

Osteoarthritis or degenerative joint disease was found to occur spontaneously in Dunkin-Hartley guinea pig lines (Jimenez et al., 1997; Ding et al., 2006). Clinical symptoms included reluctance to move, joint stiffness and swelling. Radiographically, subchondral bone sclerosis of proximal tibia, cystic lesions in femur condyles, calcification of collateral bands and the presence of osteophytes were observed. The cortex of long bones was not affected. The effect of animal age on the progression of lesions was studied (Ding et al., 2006). Alterations in epiphyseal bone microstructure were found: the trabeculae increased in thickness and the mineral to collagen ratio decreased. These features are to a certain extent compatible with radiographic findings in satin cavies (Massop, 2009), except that the satin syndrome involves the whole bone and not only the joint region.

Vitamin C is one of the mediators of joint disease, and it plays a delicate role in its pathogenesis (Fain, 2005). Because of its antioxidant properties, vitamin C may act as a chondroprotectant in inflammatory processes (McAlindon et al., 1996). On the other hand, excessive vitamin C supplementation can exacerbate osteoarthritis, as was demonstrated in a guinea pig model (Kraus et al., 2004).

Degenerative joint disease, be it alone or in combination with vitamin C deficiency, cannot account for the whole spectrum of symptoms and lesions in satins. However, regarding its high prevalence (Ding et al., 2006), it may be a contributing factor to the satin syndrome.

### **2.2.5. Osteoporosis**

Osteoporosis is a bone disorder characterized by a decrease of total mineralized bone mass to the stage at which the mechanical stability of the bone is compromised (Schiller and Teitelbaum, 1999). At the tissue level, bone resorption exceeds new bone matrix deposition. There is deterioration of bone microstructure. Unlike in hyperparathyroidism and osteomalacia, the ratio of mineralized bone

tissue to unmineralized matrix is not altered in osteoporosis (Seeman, 2001). Primary osteoporosis affects mainly post-menopausal women and elderly of both sexes. Its etiology has not been fully resolved. Associations with levels of sex hormones, genetic factors and nutritional patterns are investigated (Seeman, 2001; Prentice, 2004; Gennari et al., 2005). Secondary osteoporosis has been linked to neoplastic changes (multiple myeloma), gastrointestinal malabsorption and endocrine imbalances such as Cushing disease (Schiller and Teitelbaum, 1999). The disease has no spontaneous analogues in animal species; however, female ovariectomized rats display patterns of bone loss similar to those of osteoporotic women (Wronsky et al., 1989; Brouwers et al., 2008). Corticosteroid-induced osteoporosis has been described in dogs (De Bruin et al., 2009).

One record described osteoporosis in a guinea pig after administration of high doses of vitamin D (Richardson, 2000). Symptoms included hind leg paralysis. However, since no histopathological studies of soft tissue and bone microstructure were carried out, it is difficult to differentiate this condition from the more common metastatic calcification induced by vitamin D overdoses (see Section 2.2.3). The radiographic findings in satin cavies (Massop, 2009) were not compatible with osteoporosis. The histopathological results presented in this work (Chapter 7) allow exclusion of osteoporosis from the list of differential diagnoses of the satin syndrome.

#### **2.2.6. Neoplasia**

Bone neoplasia occurs frequently in humans (Schiller and Teitelbaum, 1999) and in companion animals. Primary and secondary bone tumors were described in dogs (Liu et al., 1977); osteosarcoma was found to be the most prevalent one, followed by chondrosarcoma and metastases of other tumors. In cats, secondary tumors were observed as sequelae to lung carcinomas (Rosol et al., 2003). Guinea pigs are generally not considered to be prone to neoplasia (Rogers and Blumenthal, 1960). There are relatively few reports on spontaneous tumors in guinea pigs, and no bone tumors were described in the past.

The previous diagnoses of bone disease in satin cavies were mainly based on radiography. Radiographic findings need a cautious interpretation with regard to tumor diagnosis. The osteolytic patterns found in neoplasia, referred to as “moth-eaten” (Myers et al., 1991) are not specific. Many other conditions can present similarly, including infarcts, abscesses, cysts, fibrous dysplasia and brown tumors of advanced renal osteodystrophy (Gould et al., 2007). Although cystic bone lesions found in satins may in certain cases resemble tumors, no reliable conclusions can be drawn from medical imaging data.

The main arguments against neoplasia are: the simultaneous involvement of many different bones in the same individual, the relatively slow progression of the disease, and the reported low susceptibility of guinea pigs to tumors. An aggressive tumor is unlikely in guinea pigs. Moreover, a tumor that affects virtually the whole skeleton would probably manifest itself systemically and lead to severely altered haematological profiles, general malaise and quick death. This is contradicted by clinical observations. Based on histopathological features (see Chapter 7) neoplasia can be ruled out.

### 2.2.7. Paget disease of bone

Paget disease, also termed *osteitis deformans*, is a chronic condition characterized by disordered bone remodeling. In its clinical presentation, Paget disease can mimic virtually any bone and joint disorder, including bacterial infections such as syphilis (as primarily suggested by Sir James Paget), tumors and gout (Paget, 1877; Schiller and Teitelbaum, 1999). The etiology is not fully resolved to date. Canine distemper virus (*Paramyxoviridae*) was suggested as a possible causative agent (Gordon et al., 1991); characteristic viral inclusion bodies were found in osteoclasts of nearly all patients. In Paget disease of bone, three phases can be distinguished: the osteoclastic resorptive phase where activated osteoclasts produce sharply defined lytic lesions in the cortex, the mixed osteoclastic-osteoblastic “compensatory” phase in which osteoblasts deposit large amounts of new bone in response to the osteoclastic activity, and the burn-out phase when the overall cellular activity declines. Macroscopically, the bones are markedly thickened and heavier. Signs of increased bone turnover are present; serum alkaline phosphatase is elevated. Microscopically, numerous osteoclasts and large activated osteoblasts, and trabeculae with a large surface to volume ratio are found. Lamellar bone is replaced by woven bone. At this stage the histopathological features resemble those of *osteitis fibrosa* (see Section 2.1.2). However, the osteoclasts in *osteitis fibrosa* have a normal appearance, while abnormal giant osteoclasts containing more than hundred nuclei are considered pathognomonic for Paget disease. In the burn-out phase, the architecture of the lamellar bone is altered (irregular or “mosaic-like”) with islands of bone formation separated by disordered cement lines (Schiller and Teitelbaum, 1999).

Paget disease of bone is unique to humans; however, there is anecdotal evidence of Paget-like bone deformities in reptiles. In a case study presented by Preziosi and coworkers (Preziosi et al., 2007), diagnosis in a Burmese python was established by comparing medical imaging and histopathology findings with the human data. Excessive new bone formation leading to osteopetrosis-like lesions was found upon radiography. Serum alkaline phosphatase of the patient was elevated. Histopathology revealed thickened trabeculae and unorganised mosaic-like bone reminiscent of the Paget disease. However, no specific signs such as abnormal osteoclasts with inclusion bodies were found.

Massop (Massop, 2009) tentatively ascribed the observed bone lesions in satin guinea pigs to a Paget-like deformity, referring to the case of a Burmese python. However, the only similarity between these cases was the elevated alkaline phosphatase, while the histopathological and radiographic features were essentially different (see Figs 2.2 and 2.3). No further research effort was undertaken to verify this diagnosis. In the light of the current knowledge, Paget disease of bone is extremely unlikely to be the underlying pathology of the satin syndrome.

### 2.2.8. Other conditions

Differential diagnoses for bone pathology have been reviewed in the previous sections. Naturally, there may be many extraskkeletal causes of lameness, dental problems and anorexia. Examples include muscular dystrophy due to vitamin E and selenium deficiency (The Merck Veterinary Manual, [http://www.merckmanuals.com/vet/exotic\\_and\\_laboratory\\_animals/rodents/guinea\\_pigs.html](http://www.merckmanuals.com/vet/exotic_and_laboratory_animals/rodents/guinea_pigs.html)), neurological problems of viral origin (Suckow et al., 2012), severe malnutrition and dental disease

caused by fiber-deficient diets (Richardson 2000). However, these causes were excluded based on anamnesis, evaluation of the general health condition, feed analysis, and absence of specific signs.

### 3. THE SATIN SYNDROME: CLINICAL PRESENTATION AND EPIDEMIOLOGY

#### 3.1. INTRODUCTION

The most often reported disease symptoms in satin guinea pigs are related to their skeletal disorder (Chapter 2). However, these signs may be intermittent and in some cases altogether not apparent. Moreover, many other, apparently unrelated symptoms may be present, such as digestive and dental problems, retarded growth, low body weight, unthriftiness and predisposition to infections. As stated in Chapter 2, none of the observed symptoms can be considered specific to satin guinea pigs. In order to be able to conclude on the severity and penetrance of the satin syndrome one has to conduct a comparative study by performing long-term observations of large numbers of satin and non-satin animals. In this chapter a retrospective cohort study, based on the facts collected by the author in her own guinea pig sheltering facility, is presented. Furthermore, pathogenesis and symptoms of acquired dental disease (ADD) are described, and the prevalence of dental problems in satin and non-satin cavies is discussed.



Fig. 3.1: A standard cage used in the current study.

#### 3.2. MATERIALS AND METHODS

##### 3.2.1. Husbandry and diet

In the period of observation (2008-2013), the rodent shelter run by the author housed 60 to 120 guinea pigs of different ages, genders and breeds. In total, 21 satin (N=21) and 54 non-satin (N=54) guinea pigs were taking part in this study. The gender distribution was: 5 males/16 females in the satin and 22 males/32 females in the non-satin group. These animals had spent the major part of their lifetime, and died in the shelter in the period 2008-2013. This assured the uniformity of living conditions: husbandry, feed and medical care, and allowed long periods of observation for every individual.

The animals were housed in open cages, as depicted in Fig. 3.1, with dimensions from 60x120 cm to 120x220 cm. The available surface per animal was at least 600 cm<sup>2</sup>. Satin and non-satin animals were housed together. The diet consisted of the commercial Supreme Petfoods guinea pig chow (crude protein 15%, crude fibre 10%, crude oils 3%, crude ash 5%, Ca 0.6%, P 0.5%, vitamin C

250 mg/kg, vitamin D 1500 IU/kg), about 40 g per animal per day. Additional vitamin C supplementation was realized as top dressing: about 2 g of L-ascorbic acid (Jiangsu Nutraceutical Ltd.) was dispensed per 20 animals per day. Other diet components were: fresh vegetables and grass, about 200 g per animal per day, hay and water (refreshed daily) *ad libitum*.

### 3.2.2. Weight, lifespan and lameness scores

The general condition of animals was assessed daily. The animals were weighed weekly and the average adult weights were determined. The following parameters were recorded: the condition score (body weight), the presence of motoric problems (lameness) and the lifespan. Lameness was defined as permanent or intermittent paresis or paraparesis, or a dysfunction of at least one extremity: a fore or a hindlimb. No differential diagnoses were attempted to distinguish between traumatic, neural or musculoskeletal origin of lameness.

A scoring system based on visual evaluation of the animal's gait was developed; a description of various phases is given in Table 3.1.

Phase	Score	Posture and gait	Other symptoms
0	0	Symmetric digitigrade diagonal gait. Equal support on all limbs.	None (healthy animal)
I	1	Plantigrade diagonal gait. Support on carpi/tarsi, toes elevated above the ground (often observed in aged non-satin cavies).	Weight loss.
II	2	Asymmetric gait with simultaneous movement of both hind limbs ("hare hop"). Elevation of one hind limb in recumbency.	Weight loss, joint swelling. Subtle radiographic signs of bone pathology in hind limbs.
III	3	Reduced support on hind limbs, reluctance to move. Elevation of both hind limbs in recumbency.	Severe weight loss, anorexia, dental disease, jaw swelling. Pronounced radiographic signs in the whole skeleton.
IV	4	No support on fore and hindlimbs. Sternal or lateral decubitus.	Cachexia, debilitation, secondary pathology (constipation/ileus or diarrhoea, metabolic acidosis).

Table 3.1: A scoring system based on evaluation of symptoms in satin guinea pigs.

### 3.2.3. Acquired dental disease

Dental problems were diagnosed symptomatically, by evaluation of the animal's ability to masticate hard feed such as hay and pellets. After detecting symptoms such as reduced feed intake, difficulty in chewing and weight loss, visual controls of incisors followed by inspections of the whole oral cavity were carried out. A Heine otoscope was used in unanaesthetized animals. In selected cases radiographic examination was performed.

### 3.2.4. Statistical analyses

To verify the significance of the differences in the measured variables, two-tailed Student t-tests

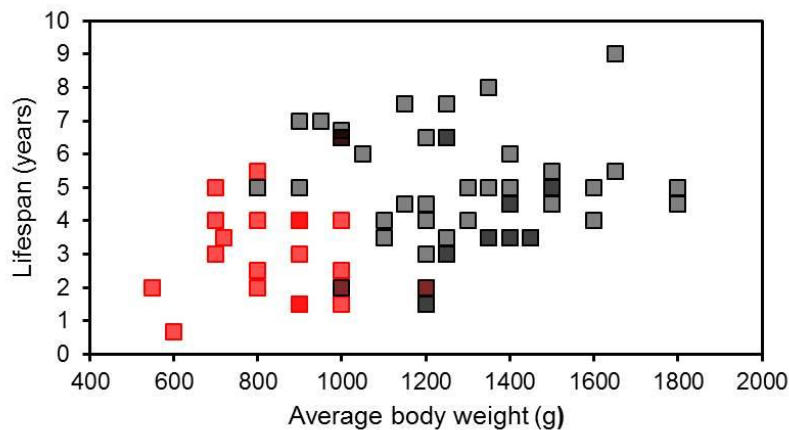


Fig. 3.2: The lifespan and the average adult body weight of satin (red squares) and non-satin (gray squares) guinea pigs.

were performed and confidence intervals were calculated using the Microsoft Excel software package.

### 3.3. RESULTS

#### 3.3.1. Vitality of satin guinea pigs

A scatter graph displaying the lifespan and the weight of animals in satin (N=21) and non-satin (N=54) groups is given in Fig. 3.2.

The averages and standard deviations are given in Table 3.2. There were no significant differences in weight and lifespan between male and female guinea pigs. The satin guinea pigs had a significantly shorter lifespan and a significantly lower body weight than the non-satin guinea pigs.

	Lifespan (years)	Body weight (g)
Satin	3.08 ± 1.49 ***	860 ± 157 ***
Non-satin	4.92 ± 1.69	1287 ± 229

Table 3.2: The lifespan and the adult average body weight of satin and non-satin guinea pigs: group averages and standard deviations.\*\*\* p < 0.001

#### 3.3.2. Lameness prevalence and scores

Lameness was frequently observed in both groups. The most common type of lameness was a dysfunction of one or both hind limbs. The total incidence during the 5 years of observation was 38% in satins (8 out of 21 animals), and 22% in non-satins (12 out of 54 animals). The odds ratio for satins was 2.15 (95% CI = 0.72 - 6.40). The satin guinea pigs had higher odds for motoric dysfunction; however, this result is not statistically significant. The incidence rate, defined as:

$$I = \frac{\#disease\ cases\ during\ observation}{\#observation\ years\ for\ all\ animals\ at\ risk}$$

was 0.16 for satin and 0.05 for non-satins, per year.

Despite the non-specificity of lameness as a symptom of the satin disease, some features were typical for satin guinea pigs. Lameness in non-satins was often intermittent; there was no typical age dependence. Severe lameness in the last weeks of the animal's life was observed in 9 non-satins. The onset was sudden and the average age at the onset was 5.5 years. In contrast, the motoric function in

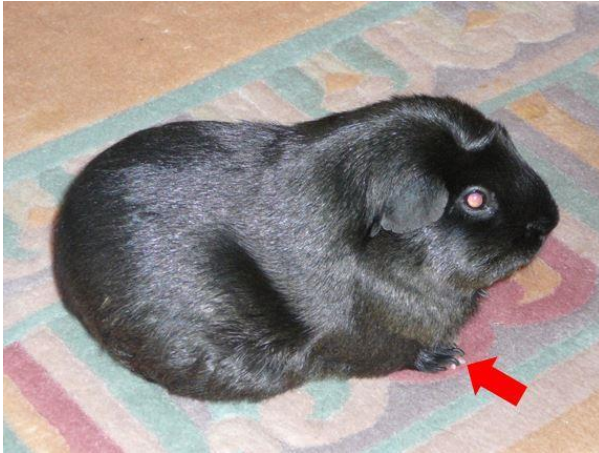


Fig. 3.3: Score 1. Arrow: elevated toes.



Fig. 3.4: Score 2. An elevated hind limb at rest.



Fig. 3.5: Score 3. Elevated hind limbs at rest.



Fig. 3.6: Score 4 - sternal decubitus.

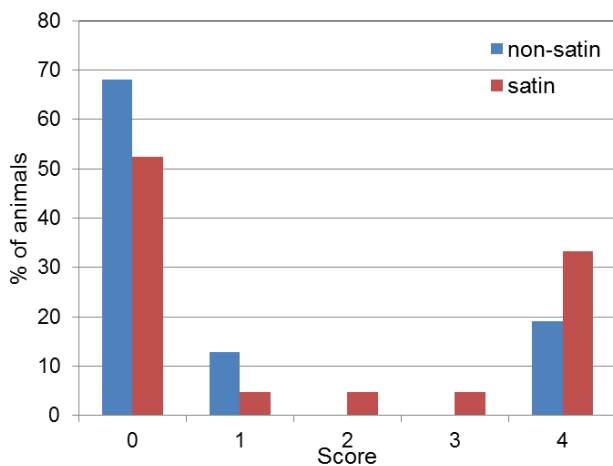


Fig. 3.7: The distribution of lameness scores in terminal non-satin (blue bars) and satin (red bars).

satin guinea pigs deteriorated progressively in the course of months/years. The average age at which the symptoms became apparent was 1.75 years.

As the disease progressed, one could distinguish between different phases, with symptoms ranging from altered gait to paralysis and debilitation (see lesion scores in Section 3.2.2). Typical images corresponding to phases I-IV (scores 1-4) are displayed in Figs 3.3-3.6.

The distribution of scores in the participating satin and non-satin guinea pigs is given in Fig. 3.7. These are snapshot scores, assigned to an animal in the terminal phase of its life. The whole spectrum of scores was observed in satins at the time of death, while non-satins displayed only the extreme values.

### 3.3.3. Acquired dental disease

#### 3.3.3.1. Clinical manifestation

The observable onset of the acquired dental disease (ADD) was often abrupt: the problems became evident within 1-2 weeks. The earliest signs were reduced appetite, weight loss and selective feeding. The animals avoided hard chow and hay while still attempting to gnaw at soft feed (vegetables). There were typical pain symptoms, such as hunched posture, tremors, slow mastication and finally loss of interest in feeding. Jaw closing appeared painful; the mouth remained open and the animals were unable to swallow. Thus, salivation and regurgitation were frequently observed. Atrophy of mastication muscles, especially the largest cheek muscle *m. masseter*, resulted in characteristic hollow cheeks, or a “hawk beak” appearance in affected animals (Fig. 3.8). In several cases, overgrown mandibular molar crowns with characteristic “spikes” pointing in the buccal direction were found (Fig. 3.9), but most of the affected animals had normal dentition upon visual inspection. Radiographic studies revealed the following deformities: elongation of molar reserve crowns in the

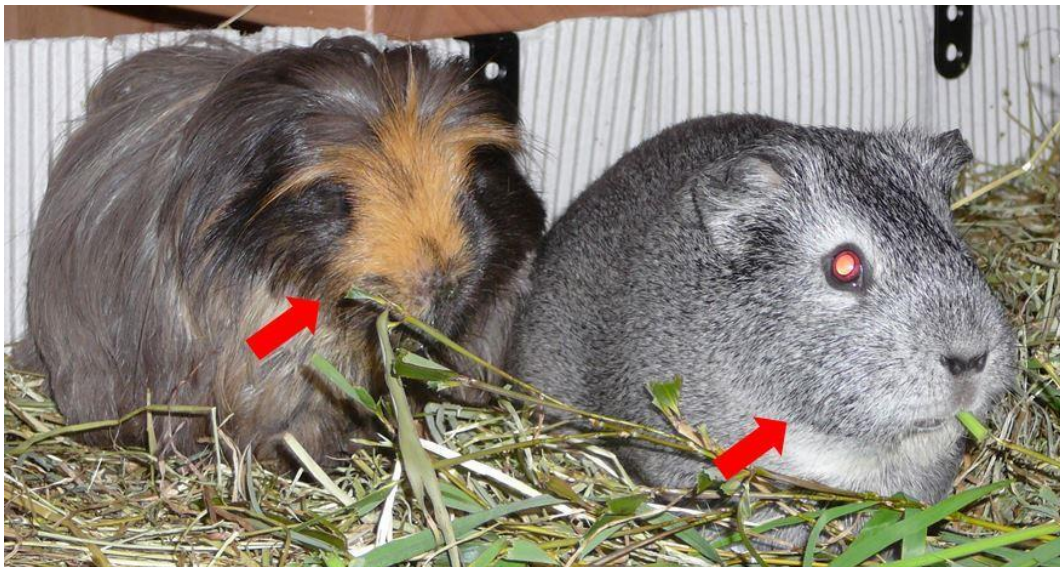


Fig. 3.8: A guinea pig suffering from ADD (left) next to a healthy animal (right). Note that the volume of the *m. masseter* (arrows) is markedly reduced in the affected animal.

upper and in the lower jaw, malocclusion of incisors and molars with clearly distorted occlusal planes (Fig. 3.10). The apices of the mandibular molars extended visibly beyond the mandibular margin. These deformities could be also palpated as firm and painful nodules in the ventral aspect of the mandibula (so-called “bulging”). Eventually, the animals had to be euthanized because of severe discomfort.

#### 3.3.3.2. ADD in satin guinea pigs

The incidence of ADD during the 5 years of observation was 29% (6 out of 21 animals) in the satin and 19% (10 out of 54 animals) in the non-satin group. The odds ratio for satins was 1.76 (95% CI = 0.55 – 5.67). The satin guinea pigs had higher odds for ADD, but the result was not statistically significant. The incidence rate was 0.10 in satins and 0.04 in non-satins, per year. After splitting both groups according to the animal’s gender, the odds ratio became 32 (95% CI = 2.3 – 448) for satin males with respect to satin females, and 8.57 (95% CI = 1.60 – 45.7) for non-satin males with respect

to non-satin females. Male guinea pigs had significantly higher odds for developing ADD than the female animals.

### 3.4. DISCUSSION

#### 3.4.1. Acquired dental disease

Dental problems are commonly encountered in rabbits, guinea pigs and chinchillas (Legendre, 2002; Harcourt-Brown, 2007; Capello and Cauduro, 2008; Capello and Lennox, 2008).

The teeth of guinea pigs are of the aradicular (open-rooted) hypsodont type (Reiter, 2008). Incisors as well as molars continue growing throughout the lifetime of the animal. Guinea pigs require



Fig. 3.9: Examination of the oral cavity reveals characteristic "spikes" formed by overgrown premolars. By courtesy of Dr. F. Verstappen, Veterinary Clinic Hoofdstraat, Driebergen, The Netherlands

abrasive feed components, such as vegetable fibers, to maintain healthy dentition (Suckow et al., 2012). Low fiber diets do not allow the teeth to wear off properly, and lead to overgrown crowns. Furthermore, many other factors influence tooth overgrowth in guinea pigs, such as infectious processes (abscesses), a low calcium to phosphate ratio in feed, vitamin C deficiency (Clarke et al., 1980) and prolonged anorexia secondary to other disorders (Richardson, 2000). The problems are readily diagnosed by visual inspection of the oral cavity. Inspection can be performed with an otoscope or another speculum, or with special mouth gags and buccal pad dilators (Legendre, 2002). Usually, premolars of the

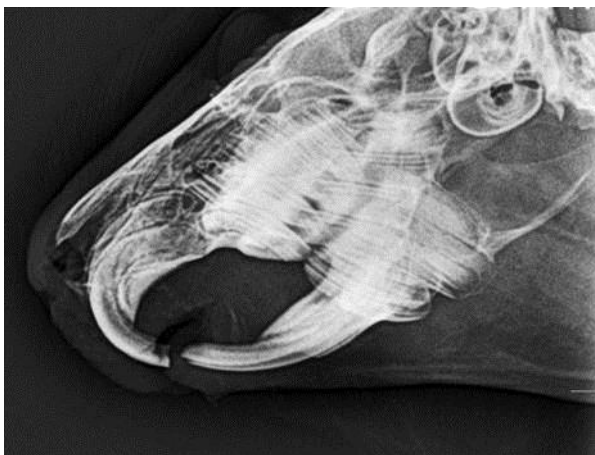


Fig. 3.10: A lateral oblique radiographic view of a skull of a guinea pig affected by ADD. By courtesy of Dr. P. Bastiaansen, Veterinary Clinic De Baronie, Prinsenbeek, The Netherlands.

mandibula are affected which manifests as typical "spikes" that often entrap the tongue (Fig. 3.9). Abnormal molars require filing so as to enable the animal to resume normal feeding. Inspection and trimming can be performed in conscious animals; however, this requires excellent skills and experience in handling guinea pigs. Therefore, most practitioners prefer to anaesthetize animals prior to examinations or interventions (Legendre, 2002; Boehmer and Crossley, 2009). The underlying causes of teeth abnormalities must always be identified and when possible, eliminated.

Acquired dental disease is a progressive jaw deformity secondary to the above-described teeth overgrowth. ADD has been described in rabbits, guinea pigs and chinchillas (Harcourt-Brown, 2007; Capello and Cauduro, 2008; Capello and Lennox, 2008). It affects animals of all ages, but the risk increases with advancing age. The mechanisms underlying ADD have not been fully resolved yet; however, instability of the alveolar bone secondary

to disturbances in calcium homeostasis (hyperparathyroidism) was proposed as a possible etiological factor in rabbits (Harcourt-Brown, 2007).

The symptoms are gradually reduced appetite and selective feeding. Affected animals tend to avoid abrasive feed (hay). This produces a vicious circle: the wear off of crowns is reduced due to a decreased intake of fiber-rich feed, and further overgrowth of apices exacerbates the existing lesions in the jaw bones.

Mere inspection of the oral cavity rarely reveals abnormalities, and is not reliable as a diagnostic method. Diagnosis is established by palpation and radiography. Currently, no treatment is available for advanced cases of ADD. Contrary to views circulating among certain veterinary practitioners (Boehmer and Crossley, 2009), restoring the normal occlusal plane by trimming the cheek teeth does not improve the animal's ability to masticate, neither does it reduce its discomfort. Palliative care with pain management is the only treatment option; however, to the author's knowledge, there exist no pain medication that can provide analgesia levels sufficient to improve the animal's quality of life. ADD is debilitating and eventually fatal.

Acquired dental disease has been observed both in satin and non-satin guinea pigs. The satin animals may seem to be predisposed, but statistical analyses do not support this observation. Interestingly, male guinea pigs are more frequently affected than the females. The latter association is statistically significant. The cause of this gender asymmetry is unknown. More research is needed to unravel the pathophysiology of dental disease in guinea pigs.

### **3.4.2. General discussion and concluding remarks**

This study clearly demonstrates that satin guinea pigs lag behind their non-satin peers with regard to their health and vitality. The previous observations of a poor performance of satins have been verified in quantitative terms. The satin guinea pigs have a significantly shorter life expectancy than the non-satins; in the current experiment a difference of almost 2 years was found, which is a substantial timespan for rodents. The satin guinea pigs are also significantly lighter, suggesting that some hitherto unknown factors influence their ability to thrive. Certain disorders, such as motoric dysfunction and dental disease seem to be more common in satin guinea pigs than in other animals.

In the light of the above results one can state that the hypothesized satin syndrome (see Chapter 1, Section 1.2) is reality. The satin phenotype does have a negative impact on the two crucial vital parameters: the lifespan and the weight. However, based on these results one cannot fully elucidate the pathophysiology of the satin syndrome. There are relatively few characteristic features of disease in satin guinea pigs. Certain lameness patterns, such as progressive dysfunction of extremities, are predominantly observed in satins. In contrast, non-satin animals either display light symptoms and recover, or are immobilized in their terminal stage (Fig. 3.7). However, global associations of the satin factor with motoric problems appear not to be statistically verifiable. The same was valid for the acquired dental disease (Section 3.4.1).

The lack of statistical significance may be due to a limited scope of this study; on the other hand, the number of involved animals was sufficiently high to demonstrate other statistical associations (e.g. the gender-dependent predisposition to dental disease). Alternatively, one may argue that motoric and dental disorders are common in guinea pigs of any breed, and that it is plausible that satin guinea pigs

are not spared. In this sense, motoric and dental problems cannot be regarded as hallmarks of the the satin syndrome. This may have two important implications: i) the satin syndrome has other, not yet identified manifestations, and ii) the satin syndrome is not necessarily unique to satin guinea pigs, or at least there are other, not breed-specific pathologies that present in the same way.

The above ambiguities cannot be resolved without a profound understanding of the nature of the satin syndrome. Regarding the vagueness of its clinical manifestation, a multifactorial etiology and a complex pathophysiology can be expected. Previous studies (Chapter 2) indicate that a departure from homeostasis in calcium metabolism may be the underlying cause. In the following chapters (Chapters 4 and 5), mineral imbalances and other potential contributing factors will be discussed in detail.

## 4. CALCIUM HOMEOSTASIS

### 4.1. INORGANIC IONS IN THE ORGANISM

Mono- and bivalent cations: sodium, potassium, calcium and magnesium are present in large amounts in all organisms; they are involved in virtually all intra- and extracellular metabolic processes (Alberts et al., 1994). Calcium is by far the most abundant mineral in the vertebrate body: in humans, the average calcium content is 1 kg, of which 99% is stored in the bones as insoluble hydroxyapatite (HAP, pentacalcium hydroxytriphosphate,  $\text{Ca}_5(\text{PO}_4)_3(\text{OH})$ ). Soluble calcium is mainly found in the extracellular space – serum and to a lesser extent in interstitial fluids. In serum, calcium is present both in the free ionized form ( $\text{Ca}^{2+}$ ) and bound to proteins (mainly albumin). It is generally accepted that only the free ionized fraction is metabolically active. Free calcium plays a pivotal role in physiological processes such as neuronal impulse transmission, muscle contraction, blood clotting, hormone release and numerous cell signaling pathways. To adequately fulfil these tasks, serum calcium must be maintained in a narrow concentration range. Normal levels in humans are 2.2-2.6 mmol/l (8.8-10.4 mg/dl), of which 1.1-1.4 mmol/l as free  $\text{Ca}^{2+}$ ; even small deviations in either direction cause severe disturbances (Rubin and Farber, 1999). Therefore, serum calcium concentration is subject to rigorous control and involves a number of physicochemical and endocrine feedback systems (Guyton and Hall, 2000).

Chlorine ( $\text{Cl}^-$ ) is the most abundant anion in the extracellular physiological fluid; in homeostatic balance its concentrations parallel the sodium concentrations (135-145 mmol/l). The second important anion is the inorganic phosphate ( $\text{H}_x\text{PO}_4^{(3-x)-}$ ). The physiological roles of phosphate are diverse. Organic phosphate compounds are structural components of cell membranes, nucleic acids and many proteins. Phosphate is also the key participant in the cellular energy storage and release system. Other functions include intracellular buffering, regulation of protein activity (phosphorylation) and participation in all basic chemical processes that involve energy transfer: glucose and fatty acid metabolism, ureum cyclus and many others (Alberts et al., 1994).

As will be discussed in this chapter, calcium and phosphate levels are inherently linked by the solubility of calcium phosphate salts. Consequently, both minerals are stored together and mobilized together. Moreover, the regulatory mechanisms that maintain homeostatic calcium and phosphate concentrations overlap. The only difference is that serum phosphate levels are not as closely regulated as calcium levels. In fact, phosphate regulation can be seen as a “side effect” of calcium regulation. As a result, serum phosphate concentrations can vary substantially in a healthy organism, and the normal range (0.8-1.6 mmol/l or 2.5-5.0 mg/dl in humans) is much broader than the one for calcium (2.2-2.6 mmol/l) (Bugg and Jones, 1998; Barrett et al., 2010).

The following sections (Sections 4.2 and 4.3) review various systems involved in maintaining mineral homeostasis. The key component in calcium regulation, the kidney, is treated separately in Section 4.4 and the impact of compromised kidney function on mineral balances is discussed. A kinetic model that describes renal calcium handling and interactions between calcium and other filtrate components such as sodium and protein was developed. Theoretical considerations and results are

presented in Section 4.5. This model will be employed further in this work to elucidate excessive calcium losses (“calcium wasting”) in renal insufficiency.

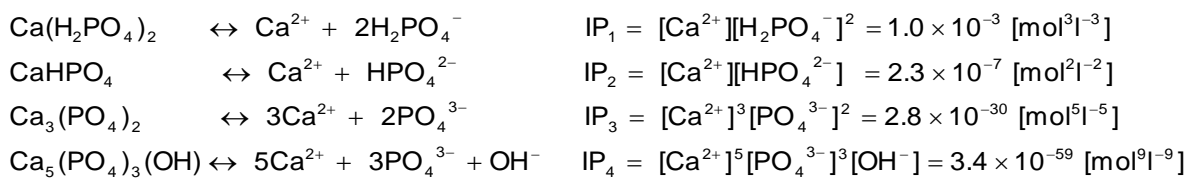
## 4.2. REGULATION OF CALCIUM AND PHOSPHATE LEVELS

Calcium and phosphate concentrations in serum and interstitial fluids are regulated at many levels. Physicochemical factors, such as calcium salt solubility, play a role at the primary tissue level and provide fine shifts in mineral concentrations. Secondly, calcium and phosphate levels are adjusted according to the demand by the variation in rates of absorption from the intestine and excretion by the kidney. Finally, the largest reservoir – the bone – is addressed when other mechanisms fail to maintain the adequate mineral supply. In steady state conditions, calcium and phosphate regulation occurs at all three levels simultaneously; however, these levels have their characteristic time scales and buffering capacities. The physicochemical tissue level provides the fastest response (milliseconds to seconds), but the magnitude of this response is very limited. Activation of kidney and gut-related mechanisms requires more time (hours to days) and allows adjustment in a broader range. The response of the bone is even slower: it may take weeks to months before the cellular processes have reached their maximum rates (Kearns and Kallmes, 2008). The bone has virtually an unlimited capacity to buffer calcium and phosphate levels. When bone resorption processes are timely activated, the necessary mineral supply is warranted even in presence of dramatic losses (“calcium wasting”, see Section 4.4). Homeostasis at the kidney, intestine and bone levels is assured by the concerted action of endocrine agents: parathyroid hormone, vitamin D and calcitonin. This system is called the renal-bone axis (Guyton and Hall, 2000).

### 4.2.1. Solubility in physiological fluids

Not all calcium salts are readily dissolved in aqueous media. The main calcium storage forms, calcium phosphate and hydroxyapatite (see above), are highly insoluble. Since free phosphate anions are present in blood, the thermodynamic equilibrium of calcium phosphate solubility forms the primary regulation system of tissue calcium levels. The equilibrium concentrations are strongly affected by the pH value. To illustrate the accurate functioning of this physicochemical regulatory mechanism, the equilibrium equations are solved for typical physiological conditions in blood serum.

The concentrations of calcium and phosphate in a saturated solution obey the solubility principle:



where  $\text{IP}_{1,2,3,4}$  refer to the solubility products of monocalcium diphosphate, monocalcium phosphate, tricalcium diphosphate and hydroxyapatite (HAP), respectively (McDowell et al., 1977). The corresponding phosphate anion concentrations are given by the Henderson-Hasselbach relations:

$$\text{pH} = \text{pK}_a^{4-x} + \log \frac{[\text{H}_{x-1}\text{PO}_4^{(4-x)-}]}{[\text{H}_x\text{PO}_4^{(3-x)-}]}; \quad x = 1, 2, 3; \quad \text{pK}_a^1 = 2.11, \text{pK}_a^2 = 7.05, \text{pK}_a^3 = 12.30$$

where  $\text{pK}_a$  values were calculated for  $T = 37^\circ\text{C}$  with the thermodynamic data provided by Dawson et al. (1987).

The values of  $[\text{H}_x\text{PO}_4^{(3-x)-}]$  and  $[\text{Ca}^{2+}]$  in a saturated solution at a total inorganic phosphate concentration of 1 mmol/l are given in Figs 4.1 and 4.2, respectively. It follows immediately from Fig. 4.2 that the solubility product of HAP sets the limit to the maximum free calcium concentration in serum or tissue. Naturally, this limit changes with changing pH and phosphate level, as depicted in Figs 4.3 and 4.4. In either case,  $\text{Ca}^{2+}$  and  $\text{PO}_4^{3-}$  follow opposite trends. Two important conclusions follow from Figs 4.1 – 4.4: i) pH has a strong influence on serum calcium levels: in acidosis calcium levels are directly raised, while in alkalosis the opposite occurs; this effect is additionally modulated by

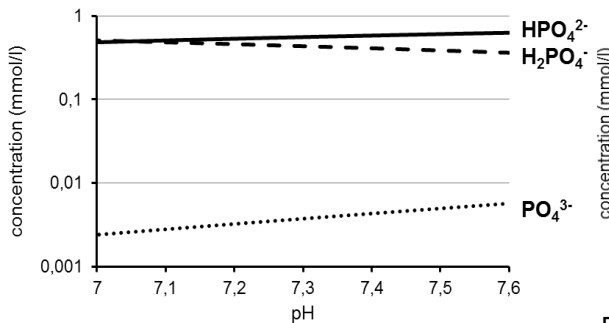


Fig. 4.1: Concentrations of phosphate anions in serum at a total inorganic phosphate concentration of 1 mmol/l, as a function of pH.

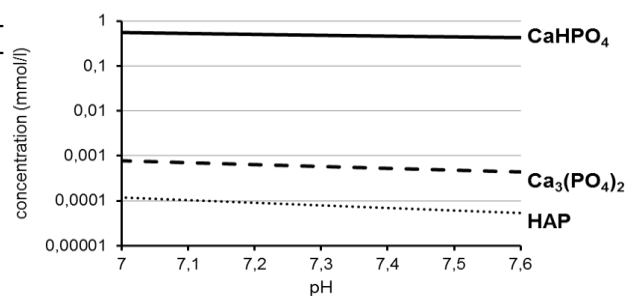


Fig. 4.2: Maximum concentrations of free ionized calcium, as determined from the solubility products of  $\text{CaHPO}_4$ ,  $\text{Ca}_3(\text{PO}_4)_2$  and hydroxyapatite, as a function of pH. The limit imposed by  $\text{Ca}(\text{H}_2\text{PO}_4)_2$  is much higher (not given here). Total phosphate concentration is 1 mmol/l.

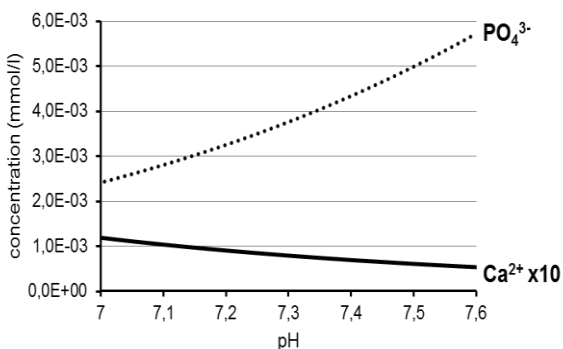


Fig. 4.3: Concentrations of  $\text{PO}_4^{3-}$  as a function of pH, and the corresponding maximum calcium concentrations governed by the solubility product of HAP. Total phosphate concentration is 1 mmol/l.

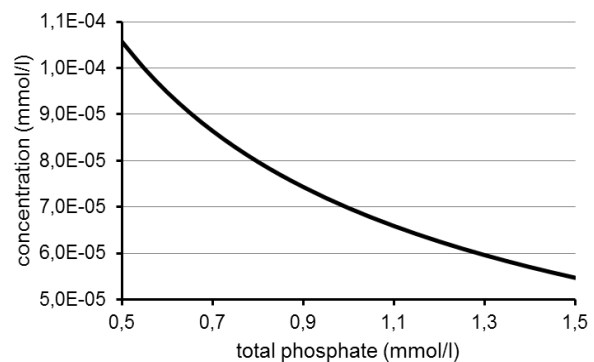


Fig. 4.4: Maximum concentration of calcium at  $\text{pH} = 7.4$ , governed by the solubility product of HAP, as a function of the total phosphate concentration.

equilibrium shifts in pH-dependent calcium-albumin binding – the negative charge on albumin decreases with decreasing pH, so that calcium is released (Portale, 1999), and ii) when calcium and phosphate concentrations are in the physiological range, serum is supersaturated so that HAP and other salts would precipitate in absence of inhibitory factors. In other words, calcification is a passive process that has to be actively prevented by specific reagents present in healthy tissues. Conversely,

calcium salts deposit in necrotic tissues; this phenomenon is known as dystrophic calcification (Rubin and Farber, 1999).

#### 4.2.2. Intermezzo: tissue calcification inhibitors

As shown in the previous section, calcium and phosphate coexist in a supersaturated solution, which is essentially a thermodynamically unstable system. The delicate balance is sustained by specific tissue- and bone-related calcification inhibitors; any alteration in this balance would inevitably cause soft tissue mineralization. Many calcification inhibitors have been identified: fetuin-A, matrix Gla protein, osteoprotegerin (Moe et al., 2005; Shroff et al., 2008), plasma cell membrane glycoprotein-1 (Hessle et al., 2002), and perhaps the most potent one – pyrophosphate  $P_2O_7^{4-}$  or  $PP_i$  (Harmey et al., 2004; O’Neill et al., 2009). The mechanisms of action are complex and diverse; moreover, there are tight interactions between various inhibitor molecules. Protein-based inhibitors such as the vitamin K-dependent matrix Gla protein (MGP) and fetuin-A bind calcium and sterically prevent HAP crystal growth. Osteoprotegerin (OPG) inhibits osteoclast activation by binding RANKL (see Chapter 5). MGP, fetuin-A and OPG knock-out mice develop arterial calcification (Luo et al., 1997; Bucay et al., 1998; Schafer et al., 2003). Cell membrane glycoprotein-1 (PC-1) displays a nucleoside triphosphate pyrophosphohydrolase (NTPPPH) activity, producing pyrophosphate. The mechanism of pyrophosphate action is the direct inhibition of hydroxyapatite crystal formation by preventing incorporation of phosphate ions into the solid matrix (Meyer, 1984). Pyrophosphate is in turn destroyed by alkaline phosphatase. NTPPPH enzymes and alkaline phosphatase are antagonists in regulation of tissue and bone mineralization.

Mineral precipitation in soft tissues has been recognized as one of the major complications in homeostatic imbalance of calcium and phosphate in humans. Calcification of the arterial tunica media (arteriosclerosis) has possibly the gravest impacts (Witteman et al., 1986; Foley et al., 1998). Vascular calcification is the most important contributing factor to morbidity and mortality in patients with disturbed calcium metabolism, such as in chronic kidney disease (CKD), osteoporosis, diabetes and Paget’s disease of bone (Rubin and Farber, 1999). Pathogenesis of these diseases involves higher levels of calcium and phosphate regulation, namely the renal-bone axis. However, abnormalities in local tissue calcification inhibitors are also present in patients (e.g. pyrophosphate, O’Neill et al., 2009), and have been found to aggravate the pathology (Sigrist et al., 2007).

An empirical method to evaluate the risk of soft tissue mineralization involves the so-called calcium-phosphorus product (Cozzolino et al., 2001, Dhingra et al., 2007):

$$Ca \times P = [Ca^{2+}] \times \sum [H_xPO_4^{(3-x)-}] \quad [mg^2/dl^2]$$

The product of total calcium (corrected for albumin) and total phosphate is not a physical magnitude such as the solubility product, but an empirical indicator of the total mineral load in serum.  $Ca \times P$  in normal individuals usually does not exceed  $50 \text{ mg}^2/\text{dl}^2$ . One of the markers of CKD is phosphate retention (see Section 4.4) leading to increased serum phosphate levels ( $> 2 \text{ mmol/l}$ ); therefore, elevated  $Ca \times P$  is often seen in chronic renal failure patients. When  $Ca \times P$  exceeds 70

mg<sup>2</sup>/dl<sup>2</sup> the risk of mortality due to cardiovascular complications is substantially increased (Block et al., 2004). The calcium-phosphorus product in satin syndrome will be discussed in Chapter 7.

In analogy to serum and interstitial fluids, urine of healthy individuals contains its own calcification inhibitors. Deficiencies in these factors predispose to crystalluria, or crystal precipitation in renal filtrate. The attendant nephrolithiasis and urolithiasis are widespread in humans (Rubin and Farber 1999) and in various animal species, including guinea pigs (Peng et al., 1990; Richardson 2000). The most important calcification inhibitors in urine are: citrate, glycosaminoglycans, Tamm-Horsfall protein (uromodulin) and osteopontin (Schlieper et al., 2007); their concentrations are strongly affected by urinary and systemic parameters. For example, citrate levels are subject to strong variations in function of systemic pH. In acidosis, urinary citrate is markedly reduced; this effect together with activation of the renal-bone axis (see Section 4.3) contributes to formation of urinary calculi (Simpson, 1983).

#### 4.3. THE RENAL-BONE AXIS

The renal-bone axis is the central regulatory system that handles the time-varying demand for calcium and phosphate. The processes governed by this system are the intestinal absorption, renal elimination and mobilization of the bone resources. The renal-bone axis is a master-slave type circuit

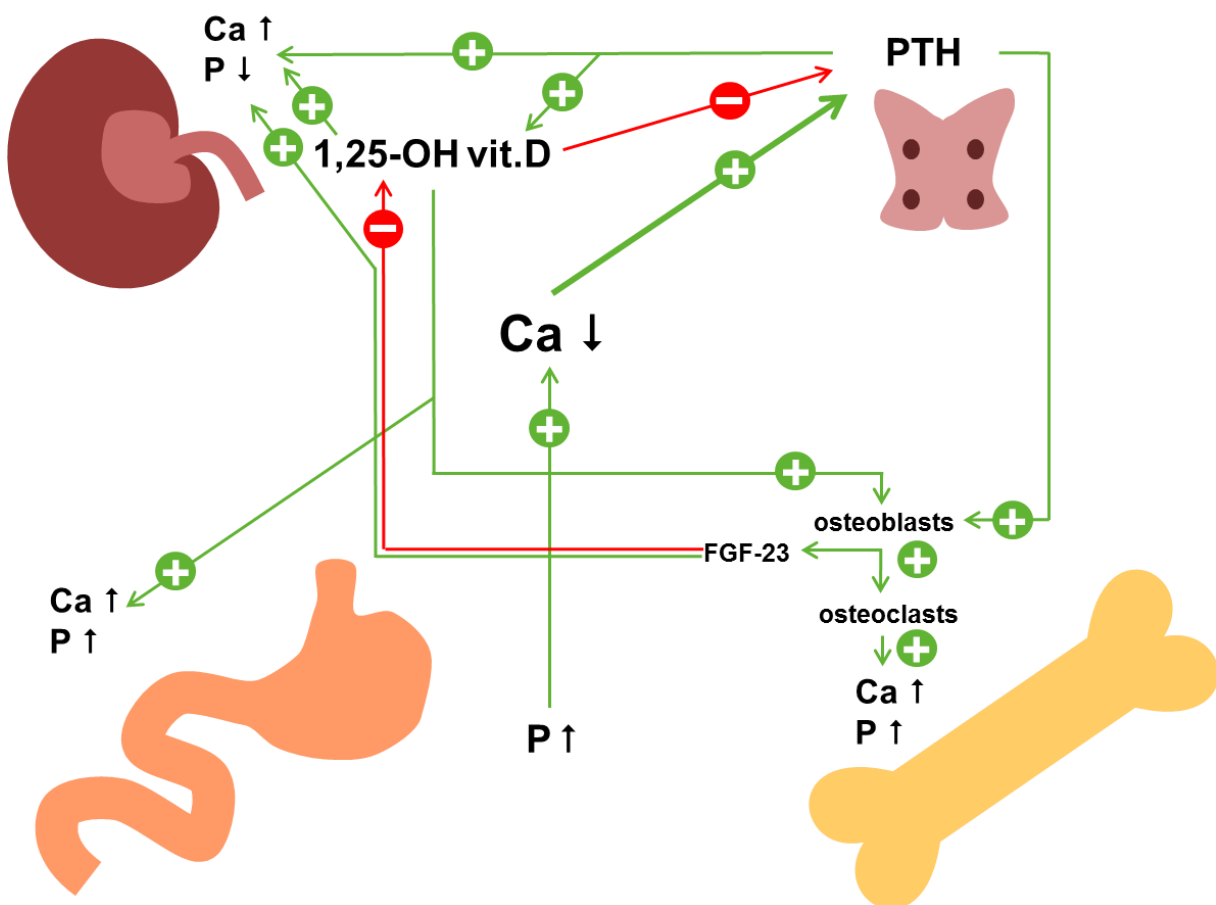


Fig. 4.5: The renal-bone axis, from upper left corner clockwise: kidney, parathyroid gland, bone, intestine. The humoral response to hypocalcaemia is shown. Ca, P – calcium and phosphate, PTH – parathyroid hormone, 1,25-OH vit. D – calcitriol, FGF-23 – fibroblast growth factor 23.

with numerous feedbacks. The parathyroid gland plays the central role. The major endocrine regulatory factors are the parathyroid hormone and vitamin D. The kidney is a vital part of the renal-bone axis, being simultaneously the site of hormone synthesis and hormone response, and participating in a number of related processes such as acid-base regulation. A general scheme is depicted in Fig. 4.5.

#### 4.3.1. The parathyroid gland and hormone

In most animal species, the parathyroid consists of four small, sharply delineated spherical glands embedded in the thyroid, symmetrically at both sides of the trachea. The parathyroid gland in guinea pigs has an atypical anatomy (Walter and Baldwin, 1963). It comprises a nodular part (*pars compacta*) consisting of about 10 scattered glands with a sub-millimeter size, and a diffuse part (*pars diffusa*) with small groups of cells spread through the thyroid interfollicular space. Microscopically, the parenchyma contains two types of cells: chief cells and oxyphil cells arranged in typical strings, lobuli or acini (Fig. 4.6). Normal parathyroid glands contain large amounts of fat cells (Rubin and Farber, 1999).

Oxyphil cells have no endocrine function. Chief cells secrete the parathyroid hormone (PTH), an 84 amino acid peptide that controls calcium, magnesium and phosphate metabolism. The primary function of PTH is increasing serum calcium levels in hypocalcaemia. Elevated serum phosphate also elicits a PTH response (Slatopolsky et al., 1996). This effect is partly due to a decrease in tissue calcium concentration controlled by the solubility products, as described in Section 4.2.1. However, phosphate can also stimulate the parathyroid gland in a calcium-independent way. PTH secretion increases in systemic acidosis (Lopez et al., 2002); this effect together with the influence of tissue pH (Fig. 4.3) is responsible for hypercalcaemia and calciuria of acidosis (Greenspan, 1949).

The direct response sites of PTH are kidneys and bones. In the kidney, PTH increases calcium and magnesium uptake, and blocks phosphate reabsorption. Furthermore, it stimulates biosynthesis of the active form of vitamin D (calcitriol) in proximal tubular cells. Calcitriol creates a negative feedback mechanism by downregulating PTH secretion. In the bone, PTH stimulates bone resorption by indirect activation of osteoclasts; bone resorption leads to release of both calcium and phosphate into serum.



Fig. 4.6: Guinea pig: a normal parathyroid gland, located next to a thyroid gland. Insert: chief cells (basophilic nuclei and little cytoplasm), oxyphil cells (large pale cytoplasm). H&E stain.

Serum calcium levels are detected by the parathyroid calcium sensing receptor CaSR, which is a trans-membrane G-protein coupled receptor (Slatopolsky et al., 1999). Other bivalent cations, in particular magnesium, also display affinity for CaSR.

Therefore, hypomagnesaemia can activate the parathyroid gland in a similar way to hypocalcaemia, causing mobilization of large amounts of calcium and phosphate from the bone. In normocalcaemic subjects

with chronic magnesium deficiency, the elicited parathyroid response may lead to hypercalcaemia, elevation of the calcium-phosphorus product (see Section 4.2.2) and soft tissue mineralization. Indeed, low-magnesium diets were implicated to induce metastatic calcification in guinea pigs (O'Dell et al., 1957).

Pathology of the parathyroid gland, especially hyperparathyroidism, is common in humans and animals (Rubin and Farber 1999; McGavin and Zachary 2007). Briefly, three types of hyperparathyroidism can be distinguished. Primary hyperparathyroidism is typical for humans and is usually caused by benign tumors or idiopathic hyperplasia of the gland, and exceptionally by carcinomas (Lack et al., 1999). Secondary hyperparathyroidism is induced in response to hypocalcaemia in disturbed calcium and phosphate metabolism. The most common causes are insufficient alimentary calcium uptake due to low calcium or low calcium to phosphate ratios (secondary nutritional hyperparathyroidism), vitamin D deficiency (osteomalacia or rickets) or intestinal malabsorption, and increased calcium losses in renal failure (secondary renal hyperparathyroidism). These forms of hyperparathyroidism (nutritional and renal) have been frequently diagnosed in animal species (McGavin and Zachary 2007; Bandarra et al., 2011; Vanbrugghe et al., 2011). Tertiary hyperparathyroidism is specific to humans and may be induced by benign hyperplasia of the gland after long-term overstimulation, such as in CKD. Tertiary hyperparathyroidism does not regress after removal of the causative agent (e.g. after kidney transplantation, Lack et al., 1999).

Renal hyperparathyroidism is often a sequel to CKD, but the response of the gland is often complex. In CKD the parathyroid is primarily activated due to a higher calcium demand caused by renal calcium wasting. Indeed, hyperplastic parathyroid glands were observed in rats with kidney insufficiency (Ritter *et al.*, 2001). However, as the disease progresses, the parathyroid response is modulated by two antagonistic processes. It can be enhanced when the negative feedback exerted by calcitriol is lifted due to downregulation of the vitamin D receptor, or due to reduced synthesis of calcitriol in damaged kidneys (Fukuda et al., 1993; Jennette and Spargo, 1999). This may result in hypercalcaemia. On the other hand, it can be quenched due to downregulation of CaSR (Gogusev et al., 1997; Slatopolsky et al., 1999), which in turn causes hypocalcaemia and phosphate retention. Hyperphosphataemia often but not always accompanies renal failure (Hruska et al., 2008). Desensitisation of the parathyroid is one of the important factors responsible for hyperphosphataemia, the other one is an inadequate response to PTH in damaged tubules (Jennette and Spargo, 1999).

Dependent on which process prevails, the net result can be either hyperplasia or quiescence of the gland. Because of the unpredictable behavior of the parathyroid gland, neither serum calcium nor PTH levels are reliable markers for hyperparathyroidism in CKD. Another reason is degradation of the intact hormone (i-PTH) into fragments that influence the immunoassay results (Lepage et al., 1998).

Parathyroid calcium receptor is a target of calcimimetic drugs. CaSR antagonists such as cinacalcet are used to control hyperparathyroidism, hypercalcaemia and bone loss (Veighey and Cunningham, 2011).

### 4.3.2. Calcitonin

Calcitonin is the functional opponent of PTH. Calcitonin is a peptide hormone secreted by parafollicular cells of the thyroid gland in response to elevated serum calcium. Relatively little is known on mechanisms of action of calcitonin. The hormone appears to be less important in mineral regulation; calcitonin deprivation after thyroidectomy does not cause symptoms in humans (Pérez et al., 2008). The main actions of calcitonin are: inhibition of intestinal calcium and phosphate uptake, probably by downregulation of transporters (Lafont et al., 2011), direct stimulation of osteoblasts and inhibition of osteoclasts in the bone (Lerner 2006; De Schutter, 2012) and inhibition of renal calcium and phosphate reabsorption. Note that although calcitonin and PTH are functional antagonists, they act in a similar way on renal phosphate excretion. The global effect of calcitonin on mineral handling in the kidney is considered to be minor (Guyton and Hall, 2000).

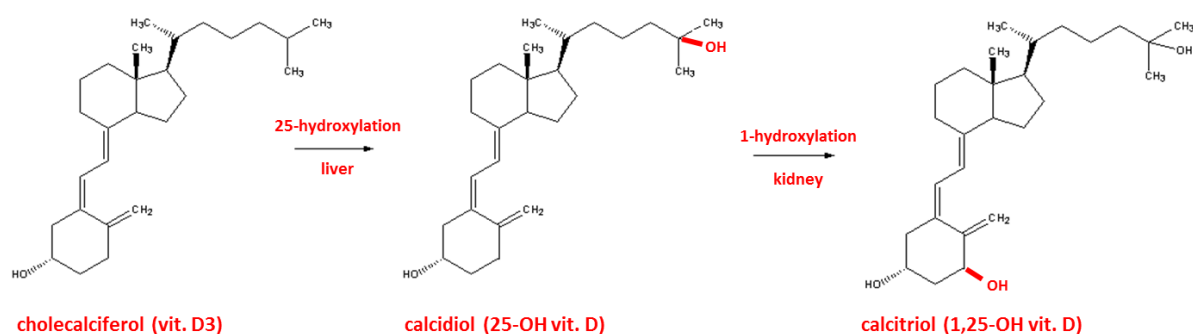


Fig. 4.7: Biotransformation of vitamin D3 (cholecalciferol) into 1,25-OH vitamin D (calcitriol). Source: Wikipedia Commons.

### 4.3.3. The biochemistry of vitamin D

Vitamin D is a group of lipophilic steroid hormones produced by animal and plant cells. Cholecalciferol (vitamin D3) is the inactive precursor in animals. It is synthesized in the skin under the influence of UV radiation. Vitamin D3 undergoes biochemical transformations in the liver and kidneys. The final activating step, 1-hydroxylation of 25-hydroxycholecalciferol, takes place in proximal tubular cells of the kidney and is enhanced by the parathyroid hormone. The resulting 1,25-dihydroxycholecalciferol (1,25-OH vitamin D, calcitriol) is the active form of vitamin D. At low PTH levels, kidneys convert the substrate into a biologically inactive 24,25-dihydroxycholecalciferol. The summary of pathways is given in Fig. 4.7.

Calcitriol is a versatile hormone. Its receptor, also called vitamin D receptor or VDR, is present in many cells: osteoblasts, keratinocytes, intestinal and kidney epithelial cells, hepatocytes, cells of the parathyroid gland and T cells of the immune system (Makishima et al., 2002; Nagpal et al., 2005; Han et al., 2010). VDR is a nuclear receptor. After binding its ligand, VDR undergoes conformational changes by heterodimerization with the retinoid X receptor (RXR) belonging to the vitamin A receptor family. The product binds to the hormone responsive element (HRE) at a gene's promoter site and modulates transcription of this gene. Expression of the following genes is upregulated by the calcitriol-VDR complex (the list is not exhaustive): osteocalcin (bone mineralization promotor), osteopontin and

RANKL (osteoclast activating factors), calcium-binding proteins that facilitate transcellular Ca transport (calbindin) in kidneys and intestine, carbonic anhydrase in bone and kidney, transforming growth factors TGF- $\alpha$  and  $\beta$ , regulatory and anti-inflammatory cytokines IL-10 and IL-4, and several liver enzymes (McMahon et al., 2001; Nagpal et al., 2005). The inhibited genes include: parathyroid hormone, pro-inflammatory cytokines TNF- $\alpha$  and IL-2, prostaglandins (PGE<sub>2</sub>), some matrix metalloproteinases and IFN- $\gamma$ . Therefore, the action of calcitriol is multisystemic and complex.

The primary function of calcitriol is maintaining calcium homeostasis. In the kidney, the action of vitamin D is twofold: enhancement of calcium reabsorption (directly) and phosphate excretion (indirectly), in concert with the parathyroid hormone. Transcellular calcium transport in kidney cells is mediated by upregulation of cytosolic calcium binding proteins (CaBP) and membrane transport proteins: the luminal epithelial calcium channel EcaC and the basolateral Ca<sup>+</sup>-Na<sup>+</sup> antiporter and calcium ATPase (PMCA) (Hoenderop et al., 2001). Suppression of phosphate reabsorption is due to expression of fibroblast growth factor 23 (FGF-23), a phosphaturic protein secreted by osteoblasts in response to calcitriol (Gutierrez et al., 2005; Kolek et al., 2005). In the intestine, calcitriol promotes calcium uptake by upregulating calcium transporters and binding proteins, in an analogous way to the kidney.

The influence of 1,25-OH vitamin D on the bone is most complex and dosis-dependent (Guyton and Hall 2000). Calcitriol facilitates bone mineralization by upregulating osteocalcin and suppressing pro-osteolytic inflammatory cytokines (TNF- $\alpha$ ). This occurs at low to normal circulating levels of the hormone. However, at higher levels calcitriol promotes bone resorption by stimulating osteoclasts via upregulation of osteopontin, RANKL and carbonic anhydrase (Nagpal et al., 2005; Riihonen et al., 2007). In renal disease, circulating levels of calcitriol are difficult to predict: they may be low in tubulo-interstitial nephropathy with declined 1-hydroxylase activity or normal to high in renal hyperparathyroidism with a normal tubular function. The osteoprotective action of calcitriol can be easily outweighed by its adverse effects. The resulting mobilization of calcium from the bone contributes to soft tissue mineralization, as confirmed in guinea pigs fed high vitamin D diets (Richardson, 2000) and in rats with kidney disease (De Schutter, 2012). Vitamin D is in fact the key mediator in the calcification paradox of renal failure. Calcification paradox refers to the apparent discrepancy between calcium wasting and deficiency on one hand, and calcium deposition in soft tissues on the other hand. Hypercalcaemia and soft tissue calcification in renal disease have been implicated to be driven by calcitriol (De Schutter, 2012). Another adverse effect of calcitriol is the induction of adynamic bone disease (Toussaint et al., 2006), see Chapter 5. Therefore, supplementation of exogenic vitamin D3 or its activated analogues such as  $\alpha$ -calcidol (1-OH cholecalciferol) to CKD patients is controversial and requires the greatest caution. Especially  $\alpha$ -calcidol should be administered under strict control, because its influence on bone resorption is greater than on intestinal uptake of calcium (Nagpal et al., 2005).

1,25-OH vitamin D and its receptor participate in a number of non-calcaemic processes. An important function is immunomodulation, which proceeds mainly via VDR in T cells. Calcitriol promotes differentiation of Th0 (null cells) into Th2 and Th3 (regulatory) helper cells (Verstuyf, 2010) thus tempering immune reactions and directing the immune response towards the humoral type. This is of

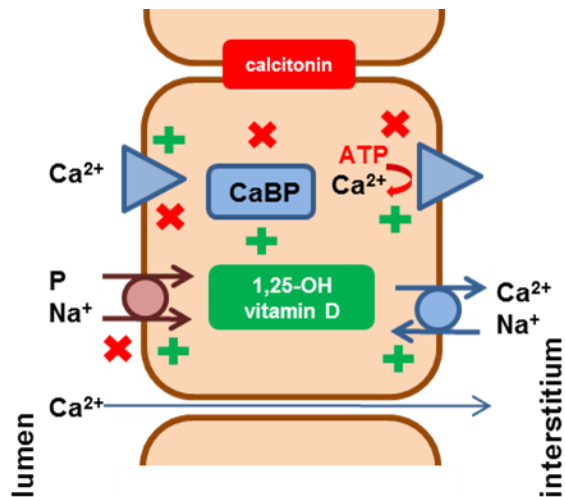


Fig. 4.8: Uptake of calcium and phosphate by enterocytes. CaBP – calbindin. **X** – hormone inhibits the transport mechanism, **+** – hormone enhances the mechanism.

bone mineralization causing osteomalacia or rickets (Berry et al., 2002), but are also associated with autoimmune diseases, alopecia and skin ailments, and cancer. Conversely, hypervitaminosis of vitamin D induces hypercalcaemia and soft tissue calcification, which has grave impacts on cardiovascular function (Witteaman *et al.*, 1986; De Schutter 2012.), see also Section 4.2.2.

#### 4.3.4. The intestine

Alimentary calcium and phosphate are absorbed in the small intestine. An overview of mechanisms is depicted in Fig. 4.8. In calcium transport, there is a transcellular (active) and a paracellular (passive) component. The relative importance of these two transport mechanisms is strongly dependent on animal species and on dietary calcium supply.

Transcellular absorption is a saturable process that is determined by the activity of transport proteins. The active pathway is regulated by calcitriol at three levels. Firstly, calcitriol increases the expression of the apical calcium membrane channels TRPV5 and 6. Further it upregulates calbindin, which in turn creates a  $\text{Ca}^{2+}$  concentration gradient by binding calcium, and facilitates its intracellular transport towards the basolateral membrane. Finally, calcitriol stimulates basolateral transport by upregulating the  $\text{Ca}^{2+}$ - $\text{Na}^{+}$  antiporter (NCX) and the  $\text{Ca}^{2+}$  ATPase (PMCA) (Saddoris, 2007). About 80-90% of active absorption takes place in the ileum (Pérez et al., 2008). Calcitonin has the opposite effect.

The paracellular pathway is gradient-driven and plays a role only at high calcium concentrations in ingesta. Calcium is absorbed passively throughout the whole length of the small intestine. It is a nonsaturable process, which implies that there is virtually no limit to calcium uptake. Passive calcium transport is of particular significance in humans, rabbits, rats and guinea pigs (Bronner 1987; Rosenthal, 2006). Therefore, in these species a high-calcium diet is more likely to induce hypercalcaemia, urolithiasis and related disorders than in species that control their calcium uptake by vitamin D solely (dogs, Schedl et al., 1968). This also suggests that dietary calcium supplementation

particular importance in controlling autoimmune diseases such as systemic lupus erythematosus (SLE) and rheumatoid arthritis (Nagpal et al., 2005). Furthermore, VDR in the skin is important in controlling the hair cycle (Li et al., 1998) and VDR in the liver is capable of regulating detoxification of potentially carcinogenic substances (Makishima et al., 2002; Han et al., 2010).

In the light of the above, it can be understood that disturbed vitamin D metabolism has a spectrum of systemic implications. The circulating active form of vitamin D concentration must be sustained in a very narrow range. Too low levels of this hormone not only impair bone

could normalize calcium levels in satin guinea pigs, but simultaneously it could increase the risk of urinary calculi.

Absorption of dietary phosphate is an active process, controlled by the apical  $\text{Na}^+$ -phosphate symporter (Berner et al., 1976; Karsenty et al., 1985; Cross et al., 1990). The expression of this transporter is upregulated by calcitriol (Cross et al., 1990). Thus, at low calcium supply and/or when no paracellular Ca uptake is possible, absorption rates of calcium and phosphate are coupled. Note that this codependence produces a vicious circle in phosphate-rich and calcium-deficient diets. Low calcium and high phosphate activate the bone-renal axis resulting in secondary nutritional hyperparathyroidism and increased circulating calcitriol levels (Gilka and Sugden, 1984). When calcium is scarce, calcitriol-induced phosphate uptake becomes relatively higher, causing a larger deviation from the equilibrium. This results in bone resorption and nutritional osteodystrophy (Bandarra et al., 2011). To protect the bone, the alimentary calcium to phosphate ratio should be about 1.5-1.7 (Richardson, 2000); this corresponds to the stoichiometry of bone minerals: calcium phosphate and hydroxyapatite.

Intestinal uptake of calcium and phosphate is enhanced in high-lactose diets; this has been implicated to play a role in soft tissue calcification (Debiec et al., 1988, Kawata et al., 2008).

#### 4.3.5. The bone

Bone is the major storage site of minerals and one of the key elements in maintaining calcium homeostasis. Bone is designed to buffer substantial homeostatic imbalances. Therefore, it is a metabolically active structure that continuously undergoes remodeling.

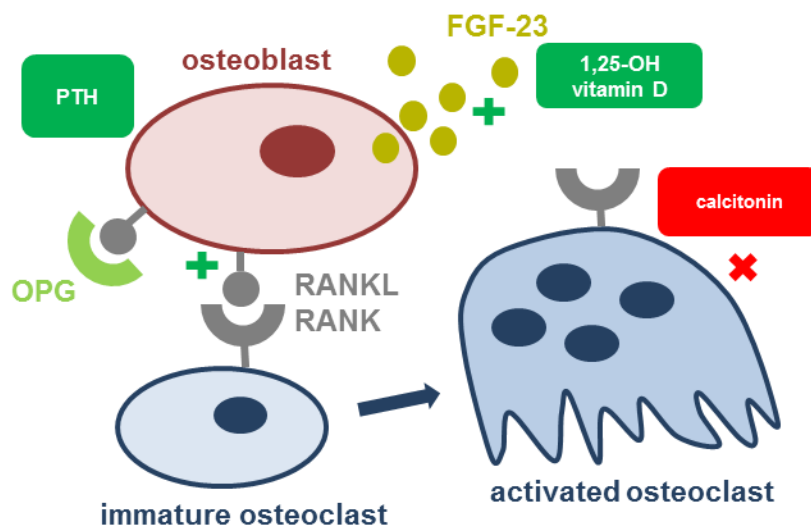


Fig. 4.9: Bone resorption by active osteoclasts is promoted by PTH and calcitriol via RANKL on osteoblasts. FGF-23 – fibroblast growth factor 23, OPG – osteoprotegerin.

remodelling will be treated in detail in Chapter 5. Shortly, upon increased calcium demand bone resorption by osteoclasts is enhanced. Osteoclasts (macrophage family) are large syncytial cells that are capable of osteolysis by secreting acids and proteolytic enzymes. The activation of osteoclasts is indirect and proceeds via the RANK-RANKL pathway with participation of osteoblasts (Suda et al., 1999). PTH and calcitriol bind to their receptors on osteoblasts and induce expression of the receptor activator of the nuclear factor  $\kappa\text{B}$  (RANK) ligand. RANK ligand (RANKL) binds to RANK on osteoclasts and initiates osteoclast maturation. Furthermore, osteoblasts secrete other pro-osteolytic factors, such as osteopontin that anchors osteoclasts to the bone matrix (Crosby et al., 1995). The action of RANKL is moderated by a RANKL decoy receptor - osteoprotegerin (OPG), which is also secreted by

osteoblasts. A summary of pathways is shown in Fig. 4.9. Note that since osteoblasts but not osteoclasts are primary targets for PTH and calcitriol, low levels of these hormones have osteoprotective rather than osteolytic effects (Brouwers et al., 2009). The situation is reversed at high PTH and calcitriol levels (Fukugawa et al., 2002).

#### 4.4. THE KIDNEY

##### 4.4.1. Anatomy

Guinea pig kidneys are bean-shaped organs with typical dimensions of 2-2.5 x 1.5-2 cm and a weight of 3-3.5 g (Chevalier, 1982). Kidneys are located in the retroperitoneal space at both sides of the vertebral column, approximately at the level of L1-L2; the right kidney lies more cranially. Kidneys are not palpable in a healthy animal.

The structure of the guinea pig kidney is simple (unipapillary) with one single calyx; the cortex-medulla length ratio is approximately 1:1.5. The functional unit of the kidney is the nephron (Fig. 4.10)

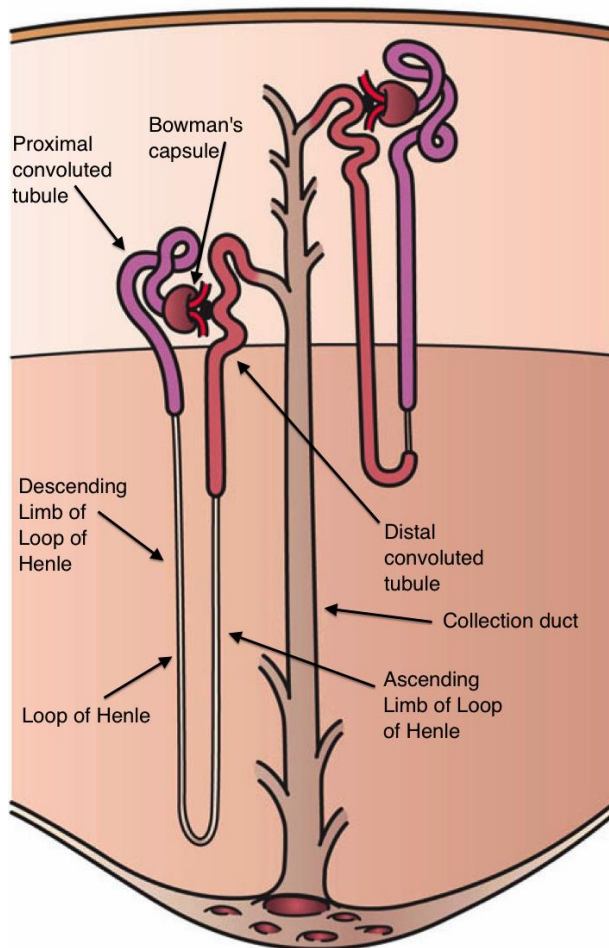


Fig. 4.10: A scheme of a nephron, with its proximal convoluted tubule (PCT), thick ascending limb of the loop of Henle (TAL) and distal convoluted tubule (DCT). Source: Wikipedia Commons.

consisting of the glomerulus and its tubule terminating in the collecting duct in renal medulla. An adult guinea pig has about 40-80 thousand nephrons per kidney (Spitzer and Brandis, 1974; Chevalier, 1982). The tubule consists of four distinct regions, each with its specific physiological functions: the proximal convoluted tubule (PCT), the loop of Henle with its thin descending limb (TDL) followed by the thick ascending limb (TAL) and the distal convoluted tubule (DCT).

##### 4.4.2. Glomerular filtration

Glomerulus is the filtration apparatus. A schematic view of a glomerulus is depicted in Fig. 4.11. A normal guinea pig glomerulus, with its Bowman capsule and space, mesangial cells and capillaries is shown in Figs 4.12. Afferent arterioles originating from renal arcuate arteries form a complex capillary network within the glomerulus. Their endothelium is fenestrated and adherent to the basal membrane (Fig. 4.11). The basal membrane (BM) carries a negative charge and prevents filtration of large negatively charged molecules (e.g. proteins). Podocytes

reside at the other side of the membrane. These large epithelial cells reinforce the function of the basal membrane. With their cytoplasmic extensions (foot processes), podocytes wrap around

capillaries. The junctions between podocyte foot processes, termed slit diaphragms (SD) prevent passage of large molecules (proteins) into the Bowman space. Massive proteinuria occurs after damage to slit diaphragms, detachment of podocytes from the BM or disruption of the BM (Tojo and Kinugasa, 2012). This condition is also termed nephrotic syndrome (Jennette and Spargo, 1999).

Filtration through BM and podocyte junctions is described by the Starling filtration equation:

$$GFR = K_f [(P_C - P_B) + (\pi_B - \pi_C)] = SNGFR * N_n \quad (4.1)$$

In the above, GFR is the glomerular filtration rate (ml/min),  $P_{C,B}$  and  $\pi_{C,B}$  are hydrostatic and osmotic (oncotic) pressures in the capillaries and the Bowman space, respectively,  $K_f$  is the filtration coefficient, normally about 12 ml/min/mmHg. GFR can be also expressed as the single nephron glomerular filtration rate (SNGFR) times the number of nephrons ( $N_n$ ). In guinea pigs, SNGFR is about 20 nl/min and GFR is about 2 ml/min (Spitzer and Brandis, 1974). GFR is about 20% of the total renal blood flow, which in turn amounts to 20% of the cardiac output (Guyton and Hall, 2000). From eq. 4.1 follows directly that GFR increases with increasing arterial pressure. The latter may result from expanded blood volume or vasoconstriction of the efferent arteriole (sympathetic activity or angiotensin). Also an increased oncotic pressure of the filtrate, such as in proteinuria, gives rise to a higher GFR. Conversely, hypovolaemia, hypotension and loss of functional glomeruli lead to a decrease in GFR. Experimentally, GFR is determined from the clearance rate of a molecule that is filtered by the glomerulus, but neither resorbed nor secreted in the tubules, e.g. creatinine or for a more accurate determination, inulin. The clearance rate equals the urine volume output per unit time multiplied by the ratio of urine to serum concentrations

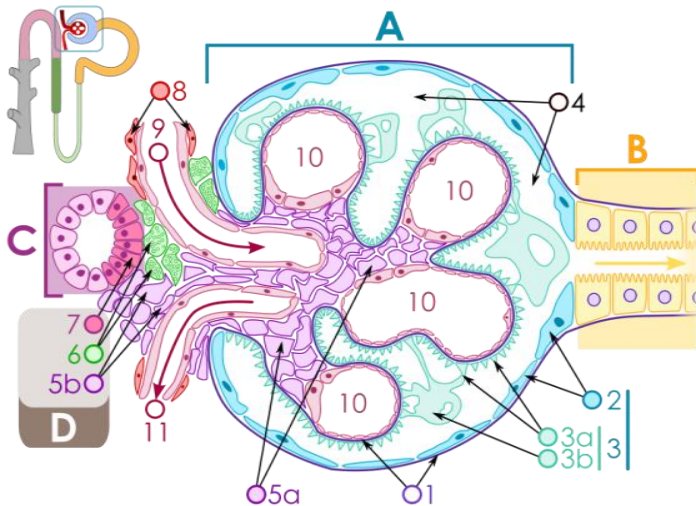


Fig. 4.11: A schematic view of a glomerulus (A) and a proximal tubule (B). 1 – parietal and visceral BM, 2 – epithelial cells of the parietal Bowman capsule, 3 – podocytes, 4 – Bowman space, 5a,b – mesangial cells, 6 – juxtaglomerular cells, 7 – macula densa, 8 – capillary wall, 9 – afferent capillary, 10 – capillaries, 11 – afferent capillary. Source: Wikipedia Commons.

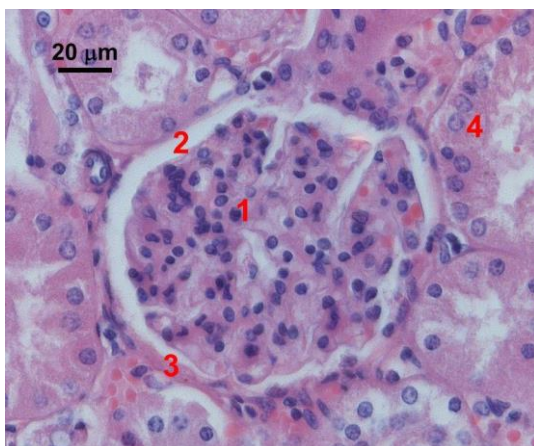


Fig. 4.12: A normal glomerulus of a guinea pig. 1 – mesangium and capillary loops, 2 – Bowman space, 3 – parietal Bowman capsule (basal membrane), 4 – proximal convoluted tubules. H&E stain.

of the test molecule:

$$GFR = \frac{V_{urine} C_{urine}}{t C_{blood}}$$

To validate the GFR value of a guinea pig, one can estimate the daily urine output. In guinea pigs, the average creatinine concentration is  $33 \pm 21$  mg/dl in

urine and  $1.07 \pm 0.41$  mg/dl in blood (see Chapter 7). Thus, the total urine output per 24 h is about 90 ml. This is in a very good agreement with the author's experimental observations.

The ultrafiltrate that exits the Bowman space is isotonic but not isoosmotic with blood serum. In a healthy kidney, the filtrate contains inorganic ions, glucose and aminoacids at the same concentrations as in serum, but it does not contain significant amounts of protein. Small amounts of mainly low molecular weight proteins (albumin) can be filtered: the normal ratio of filtrate to serum protein concentration, also called the sieving coefficient, is about  $10^{-4}$ - $10^{-5}$  (Tojo and Kinugasa, 2012). Protein-bound serum components are not filtered. Thus, only free  $\text{Ca}^{2+}$  (about 50% of total calcium) can pass into filtrate. In nephrotic animals the sieving coefficient can become as high as 0.06 or 6% (Tencer et al., 1998) and protein bound calcium is lost into urine.

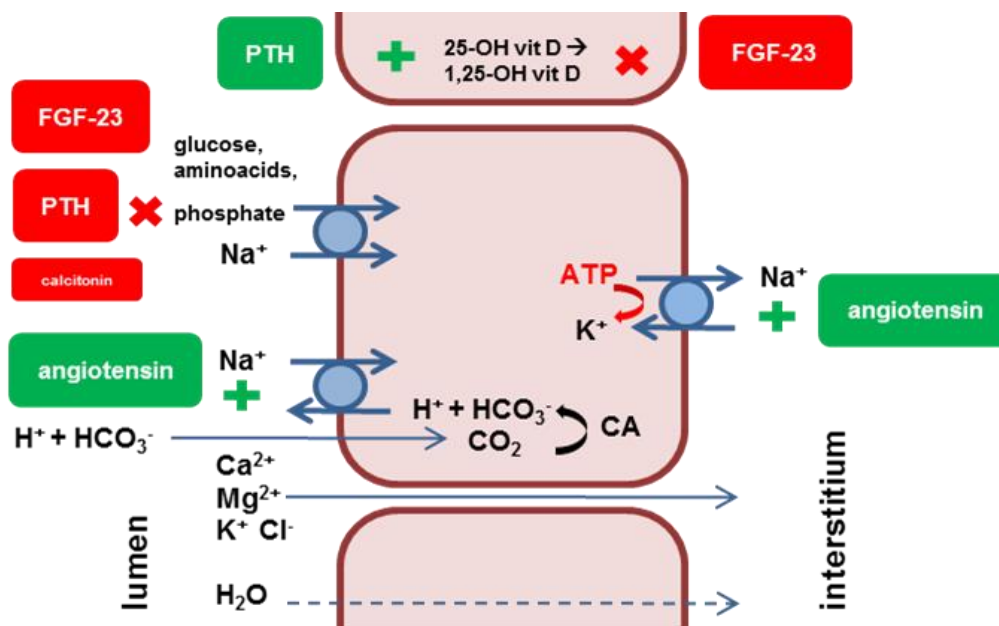


Fig. 4.13: Physiological functions of the proximal tubules. PTH – parathyroid hormone, FGF-23 – fibroblast growth factor 23, CA – carbonic anhydrase.

#### 4.4.3 Proximal tubule

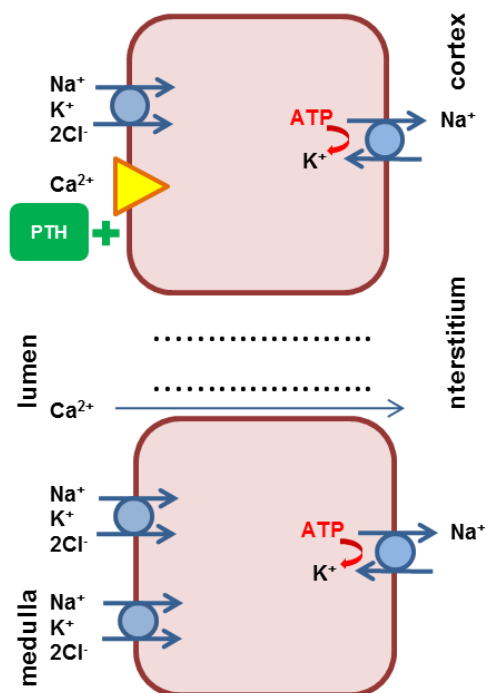
The proximal convoluted tubule (PCT) is the site of bulk reabsorption of water and electrolytes. A general scheme of solute flows through the epithelium is shown in Fig. 4.13. Reabsorption in the proximal tubule is isoosmotic: the filtrate is not concentrated. The most important process is sodium uptake via apical transporters. The largest part of sodium is exchanged for protons via a  $\text{Na}^+$ - $\text{H}^+$  antiporter (Thomas and Dagher, 1994). Protons excreted into the lumen recombine with bicarbonate. The resulting carbon dioxide diffuses into cells and is transformed back into bicarbonate by carbonic anhydrase. This is the major mechanism of bicarbonate reabsorption: about 80% of bicarbonate is reabsorbed in the PCT. The  $\text{Na}^+$ - $\text{H}^+$  antiporter is enhanced by angiotensin (Liu and Cogan, 1988; Cogan, 1990). Sodium is reabsorbed together with aminoacids, glucose and phosphate via other transport molecules.  $\text{Na}^+$ -phosphate symporter is inhibited by PTH and FGF-23 (Gutierrez et al., 2005; Kolek et al., 2005). In damaged proximal tubules, there is no adequate response to these hormones which leads to phosphate retention. A basolateral ATPase pumps sodium into the interstitium; this is followed by sodium transport to vasa recta. Vasa recta are arteries that run parallel to tubules; filtrate

in tubules and blood in arteries flow in opposite directions. This creates conditions for efficient solute transport - the counter current exchange system well-known to engineers (Guyton and Hall, 2000). Efficient removal of sodium from the interstitium prevents its backward diffusion into the tubules.

Because sodium is the major osmogenic component in the normal primary filtrate, its tubular uptake causes water to shift passively into the interstitium. Ions such as chlorine, calcium, potassium and magnesium can diffuse freely via the paracellular route following concentration gradients. In a steady state situation their concentrations in the lumen are the same as in the interstitium. This implies that these ions are reabsorbed in an equal proportion to sodium. On average, 55-65% of sodium and total fluid are reabsorbed in the PCT, but large variations are possible in function of dietary sodium intake, blood pressure and many other factors (Guyton and Hall, 2000). These variations have a major impact on reabsorption of other ions. Sodium and calcium uptake is coupled in the PCT, and only to some extent dissociated in distal nephron segments (Duarte and Watson, 1967; Sutton et al., 1979). Any disorder that affects proximal sodium reabsorption will directly translate into abnormal calcium losses.

#### 4.4.4. Loop of Henle

A corticomedullary osmolarity gradient, necessary for the concentration of urine, is sustained: the renal medulla is hyperosmotic, while the cortex is isoosmotic. The loop of Henle passes through both regions. Its thin descending limb (TDL) is permeable to water but not to salts. The filtrate is temporarily



concentrated while the TDL passes through medulla. Epithelium of the thick ascending limb (TAL) is impermeable to water, and contains numerous sodium-potassium-chlorine cotransporters (NaKCC2) that pump these ions into the interstitium (Fig. 4.14). Ion transporters in the TAL create the osmolarity gradient; this is termed *counter current multiplier system*. About 30% of total sodium reabsorption takes place in the TAL. No humoral regulation of uptake rates has been described.

In the TAL, calcium can be still resorbed via the paracellular way, in analogy to the PTC. However, since almost no water is resorbed, the process is not isoosmotic anymore: filtrate osmolarity decreases as the fluid moves through the TAL. Therefore, passive calcium diffusion is possible only in the proximal (medullary) segment of the TAL. Hence, sodium and calcium reabsorption are still coupled in the medulla, but dissociated in the cortical segment of the TAL.

In the cortical part, PTH-stimulated active calcium reabsorption takes place (Suki et al., 1980). The estimated capacity of the TAL with regard to calcium reabsorption is about 20% (Guyton and Hall, 2000), which is lower than that of PCT (55-65%). Active transport accounts for about 50% of total reabsorption in the TAL (Evangelista et al., 2004).

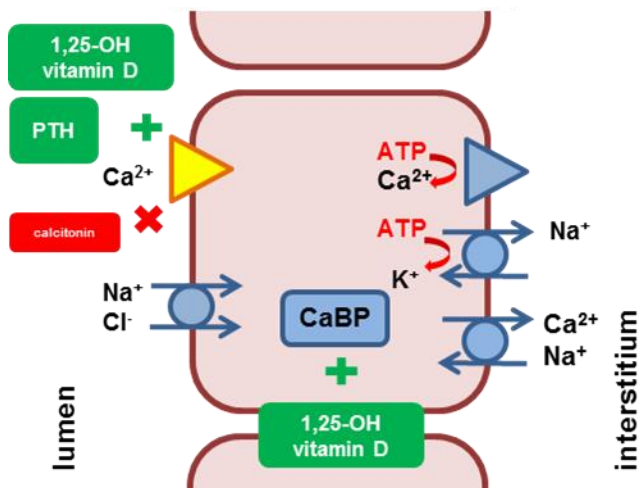


Fig. 4.15: Ion transport in the distal convoluted tubule.

A tubulo-interstitial pattern of nephropathy with damage to distal tubules could lead to impaired calcium reabsorption and secondary renal hyperparathyroidism (Cooke and Kleeman, 1950). Tubular pathology in satin guinea pigs will be evaluated in Chapter 7.

#### 4.4.6. Renin-angiotensin-aldosterone system

The renin-angiotensin-aldosterone system (RAAS) provides a mechanism of GFR and blood pressure regulation by the kidney. RAAS is activated in response to hypovolaemia, hyponatraemia, sympathetic stimulation (Guyton and Hall 2000) and raised serum potassium levels (Pratt 1982). Its main function is to restore blood volume and cardiac function by saving sodium and eliminating excess of potassium.

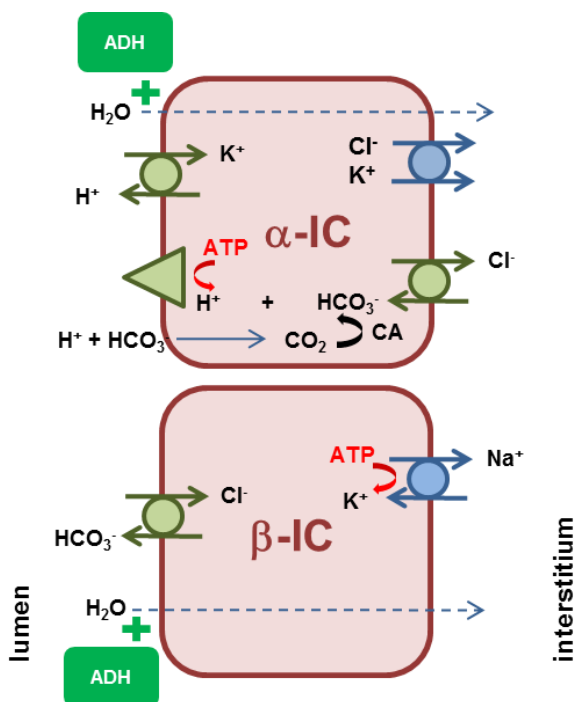


Fig. 4.16: Processes in the collecting duct.  $\alpha, \beta$ -IC –  $\alpha$  and  $\beta$  intercalated cells, CA – carbonic anhydrase, ADH – antidiuretic hormone.

#### 4.4.5. Distal tubule

A general scheme of ion flows in the distal convoluted tubule (DCT) is shown in Fig. 4.15. About 5% of total calcium is reabsorbed here, exclusively by transcellular (active) mechanisms involving the epithelial calcium channel (ECaC). The ECaC is controlled by PTH and calcitriol; both hormones upregulate its expression. There is no evidence of humoral regulation of basolateral calcium pumps (Hoenderop et al., 2001; Hoenderop et al., 2002).

The central element of this system is the juxtaglomerular apparatus (JGA), consisting of juxtaglomerular cells (JGC) and the sensory part - macula densa (Fig. 4.11), which is a contact spot between the DCT and glomerular arterioles. JGC secrete renin, an enzyme that converts liver angiotensinogen to angiotensin I. Angiotensin I is subsequently converted by angiotensin-converting enzyme (ACE) in the lung to angiotensin II (A II), the most potent vasoconstrictor in the organism. A II constricts both afferent and efferent glomerular vessels, however, its has a greater effect on the efferent arteriole (Ito et al., 1993), resulting in an increase in GFR. The secretion level of renin is tempered by feedback from distal tubules: when macula densa cells detect an increase in sodium or other solute concentration in the DCT, they inhibit the JGC.

Although associations between RAAS and calcium regulation may seem distant, numerous experimental data showed positive correlations between high A II levels and calcium reabsorption in the kidney (McCarron et al., 1980; Pratt, 1982; Sellmeyer, 2002). Some direct effects of angiotensin on calcium transporters in the kidney have been reported (Pratt, 1982); however, sodium provides the most important link between angiotensin and the renal calcium handling. Angiotensin increases proximal sodium reabsorption via its effect on both apical (Cogan, 1990) and basolateral (Shah and Hussain, 2006)  $\text{Na}^+$  transporters. This results in an increased calcium uptake by passive mechanisms described in Section 4.2.3. Conversely, low A II levels reduce sodium reabsorption and contribute to renal calcium wasting. RAAS is affected by any disorder that compromises the function of the juxtaglomerular apparatus. Thus, tubulo-interstitial nephropathy could exert its influence via this mechanism.

#### **4.4.7. Acid-base regulation**

Systemic pH enhances renal calcium excretion through a spectrum of different mechanisms. The primary effect is due to fluctuations of free calcium levels in function of pH, regulated by local solubility equilibria and calcium-protein binding. In systemic acidosis, free calcium levels rise and consequently more calcium is filtered. Secondly, there is a calcium-independent positive effect of low pH on PTH secretion (Lopez et al., 2002). Acidosis reduces calcium reabsorption by influencing calcium channels (ECaC) in the distal tubules (Hoenderop et al., 2002). Finally, the kidney itself, with its powerful acid-base regulation system, provides an important contribution.

Kidneys play an eminent role in controlling the acid-base balance of blood. Disruption of this control leads to renal tubular acidosis (Soriano, 2002). As discussed in Section 4.4.3, the proximal  $\text{Na}^+$ - $\text{H}^+$  exchange accounts for more than 80% of bicarbonate reabsorption. Defective transporter function causes type II or proximal renal tubular acidosis (pRTA). Proximal RTA manifests often as part of the more general Fanconi syndrome, which is a type of renal insufficiency characterized by dysfunction of all uptake mechanisms in the PCT (Laing et al., 2005; Quigley 2006). Typical features are natriuria, glycosuria and phosphate wasting. Failure to activate the bone-renal axis because of low serum phosphate levels is responsible for Fanconi syndrome-associated bone disease; osteomalacia or rickets are common findings (Rao et al., 1987). Fanconi syndrome has been described in animals; in particular, Basenji dogs are predisposed (Bovee et al., 1978). A Fanconi-like renal transport defect is a potential candidate for the underlying pathology of bone disease in satin guinea pigs.

Distal segments of a nephron control blood pH via several different mechanisms. Intercalated cells of the collecting duct regulate proton flows, as depicted in Fig. 4.16. The  $\alpha$ -intercalated cells secrete protons via the apical  $\text{K}^+$ - $\text{H}^+$  antiporter and the proton ATPase, providing an important route for potassium reabsorption and acid excretion. The  $\beta$ -intercalated cells secrete bicarbonate and are mainly involved in managing alkalosis (Guyton and Hall, 2000). The distal pathways appear to be more powerful than the effects of proximal bicarbonate reabsorption. In patients with Fanconi syndrome and normal distal nephron function, the kidneys can still compensate the proximal dysfunction and eliminate the excess of acids. Dysfunction of the distal system, termed type I or distal renal tubular acidosis (dRTA) has more severe, potentially life-threatening consequences. Distal RTA causes hyperchloraemic hypokalaemic acidosis that cannot be compensated by other mechanisms.

Note that hypokalaemia in dRTA tends to lower angiotensin levels by suppressing the RAAS. This inhibits proximal sodium-bicarbonate exchange and exacerbates acidosis as well as calcium wasting. Indeed, dRTA is associated with increased urinary calcium losses, secondary hyperparathyroidism and metabolic bone disease (Simpson, 1983; Lopez et al., 2002; Stover et al., 2002; Laing et al., 2005). Since dRTA is often fatal in humans and extremely rare in domestic animals, it has not been considered as a possible cause of the satin syndrome.

## 4.5 CALCIUM, SODIUM AND PROTEIN INTERACTIONS

### 4.5.1 Modeling tubular ion flows

As shown in the previous section, renal elimination of various anorganic ions does not occur independently. In particular, calcium losses are subject to strong variations in function of concentrations of other molecules in the proximal renal tubule. Since the proximal tubule is responsible for reabsorption of the majority of filtered calcium, altered transport and interactions at this site may have a dramatic influence on the eventual urinary calcium output. To understand abnormal calcium elimination in renal failure, it is essential to elucidate the kinetics of coupled ion transport.

Because of the complexity of renal mineral handling, an accurate prediction of calcium losses cannot be readily made. The complicating factors include uncertainties in hormone-regulated activities of ion transporters, abnormalities caused by partial renal dysfunction, e.g. in presence of renal tubular acidosis (see Section 4.4.7), and individual variations. However, simplified models allow estimating the magnitude and trends in mineral excretion.

Modeling of tubular ion flows and resorption was pioneered by Thomas and coworkers (Thomas and Mikulecky, 1978; Oken et al., 1981; Thomas and Dagher, 1994; Thomas et al., 2006). A reabsorption-transport model for sodium, potassium, chlorine and bicarbonate in rat proximal tubules was developed to calculate ion flows through apical and basolateral cell membranes, ion concentration profiles along the tubules and pH changes. Calcium transport was not included in this model.

Experimental efforts preceded the models and allowed determining rate constants necessary for kinetic calculations. Ion transport through renal membranes was studied *in vitro* using isolated membrane vesicles (Kinne and Schwartz, 1978; Kinsella and Aronson, 1980; Aronson et al., 1982), isolated perfused kidneys (Spring and Giebisch, 1977), kidney homogenates and cultured tubular epithelial cells (Friedman et al., 1981; Friedman and Gesek, 1995; Friedman, 2000). *In vivo* measurements involving micropuncture sampling of the filtrate were performed for various animal species (Tojo and Kinugasa, 2012), including guinea pigs (Spitzer and Brandis, 1974).

A few general features of reabsorption kinetics can be deduced from the literature data. The most important one is that sodium is the only actively reabsorbed ion in the proximal tubule. The uptake process consists of a saturable transport step through the apical cell membrane, dominated by the  $\text{Na}^+\text{-H}^+$  exchange (Thomas and Dagher, 1994) and an unsaturated basolateral active transport step driven by the  $\text{Na}^+\text{-K}^+$  ATPase (Spring and Giebisch, 1977). The kinetic constants are often uncertain and species-dependent, so that no extrapolations can be made. However, it is accepted that under physiological perfusion conditions, the apical transport is the rate-limiting step for sodium uptake in the

proximal tubule. Reabsorption of sodium, water and electrolytes along the tubule is thus governed by the balance between the volume flow of the filtrate ( $V$ ) and the apical  $\text{Na}^+$  uptake (mainly via the  $\text{Na}^+$ - $\text{H}^+$  antiporter). Sodium and chloride are the main inorganic ions in the primary filtrate ( $C_{\text{Na}} \approx C_{\text{Cl}} \approx 140$  mmol/l), and the electroneutrality requires that their fluxes be equal. The process is isoosmotic, which implies that water follows  $\text{Na}^+$  and  $\text{Cl}^-$  passively. The volume flow in the beginning of the tubule is given by the single nephron glomerular filtration rate (SNGFR). Volume depletion is proportional to the amount of reabsorbed sodium, and limited by the capacity of sodium transporters. Under typical physiological conditions NaCl is the main osmogenic component of the filtrate, and the normal volume depletion at the end of the proximal tubule is higher than 50% of SNGFR (Spitzer and Brandis, 1974).

Ionic species that are capable of paracellular diffusion, such as calcium, equilibrate between the lumen and the interstitium. Thus, the end volume of the filtrate that leaves the proximal tubule determines roughly the amount of calcium that is lost to urine. The eventual excretion is modulated by processes in distal tubules; however, the limited capacity of distal regulation systems cannot buffer bulk losses (see Section 4.4).

Any process that expands the end filtrate volume will inevitably lead to increased calcium excretion. Increased end filtrate volumes may result from deficient sodium reabsorption due to dysfunction of proximal transporters, e.g. Fanconi syndrome and proximal renal tubular acidosis (Greenspan, 1949; Quigley, 2006), diuresis induced by carbonic anhydrase inhibitors and increased filtration rates due to blood volume expansion or high salt intake (McCarron et al., 1980). There is however another mechanism that may be of equal importance: osmotic diuresis. When NaCl is no longer the only significant osmogenic species in the filtrate, volume depletion is partially decoupled from sodium reabsorption. The end volume depends on the total concentration of (unresorbed) osmogenic filtrate components. An evident cause of osmotic diuresis is proteinuria. In principle, proteins are capable of exerting high colloid osmotic pressures and may contribute to calcium wasting. In the following paragraphs this effect will be evaluated.

In the present work the model of Thomas and coworkers (Thomas and Dagher, 1994) was adapted to establish a semi-quantitative relation between renal sodium, calcium and protein excretion. Firstly, the equations were formally derived, the assumptions were revised and several simplifications were introduced to the original model. Furthermore, kinetic reaction constants for guinea pigs were determined. Finally, the filtrate volume at the end of the proximal tubule was calculated and calcium losses were estimated in function of sodium and protein concentrations and SNGFR.

Water and solute (e.g.  $\text{Na}^+$ ) flow through a tubule can be generally described by the mass transfer (continuity) equation with source and sink terms:

$$\frac{\partial c}{\partial t} + \vec{V} \cdot (\vec{v}c) = D\vec{\nabla}^2 c + J \quad (4.2)$$

where  $c$  is the concentration of the solute,  $\vec{V}$  is the flow velocity (convection term),  $D$  is the diffusion coefficient (diffusion term) and  $J$  represents the sources and sinks (production and destruction terms). A steady-state situation ( $\partial c/\partial t = 0$ ) is assumed, and diffusion terms are neglected as being much smaller than convection and reaction terms (Stoffels and Stoffels, 1994). Assuming unidirectional flows

and only longitudinal and no radial variations in the solute concentration, eq. 4.2 can be reduced to a simple one-dimensional flow conservation equation:

$$\frac{\partial(vc)}{\partial x} = -J(c, x) \quad (4.3)$$

where  $J$  (the sink term) is the solute uptake rate through the apical cell membrane. Now, the kinetic equation describes the changes of the solute flux ( $vc$ ) in function of the longitudinal coordinate ( $x$  – the distance along the tubule axis). The sink term ( $J$ ) obeys the Michaelis-Menten kinetics:

$$J = J_{\max} \frac{c}{K_m + c}$$

where  $K_m$  is the Michaelis-Menten constant and  $J_{\max}$  is the maximum reaction rate. Further, the flow velocity can be expressed as:

$$v = \frac{1}{S} \frac{\partial V(x, t)}{\partial t} = \frac{V_t(x)}{S}$$

where  $V_t(x)$  is the volume flow and  $S$  is the cross-sectional area of the tubule (it is assumed that this area remains constant throughout the tubule). Note that  $V_t(0) = \text{SNGFR}$ . The volume flow at the end of the proximal tubule is the magnitude that needs to be estimated. After introducing  $\phi_{\max} = SJ_{\max}$  (the flux gradient along the tubule, mol/mm/min), eq. 4.3 becomes:

$$\frac{\partial(V_t c)}{\partial x} = \phi_{\max} \frac{c}{K_m + c} \quad (4.4)$$

The isoosmotic requirement at the position  $x$  can be expressed as:

$$\pi = \text{const} \Rightarrow \pi(x) = \pi_p(x) + RT \sum i_k c_k(x) = \pi_p(0) + RT \sum i_k c_k(0) \quad (4.5)$$

The total osmotic pressure  $\pi$  is determined by the sum of all (ionized and non-ionized) solute concentrations  $c_k$  times their Van't Hoff factors ( $i_k$ ). Usually  $i$  is equal to the total charge of the ion; for non-ionized species  $i = 1$ . In kidney filtrate, sodium and chlorine are the dominant inorganic ions, and their contribution is  $2RTc_{\text{Na}}$ . The additional term  $\pi_p$  in eq. 4.5 is due to oncotic pressure, or colloid osmotic pressure exerted by filtrate proteins (mainly albumin). The Van't Hoff factor for proteins is difficult to determine, but is substantially larger than 1. Proteins carry multiple charges and are capable of cation retention. This provides the so-called Gibbs-Donnan extra pressure, so that  $\pi_p \gg RTc_p$  (Guyton and Hall, 2000). The dependence of  $\pi_p$  on the protein concentration at physiological pH can be approximated by  $\pi_p [\text{mmHg}] \approx 5c_p [\text{g/dl}]$  (Canaan-Kühl et al., 1993). Oncotic pressure is pH dependent; however, in the current model pH variations in function of  $x$  are neglected. It is assumed that bicarbonate is efficiently reabsorbed in the proximal tubule, i.e. that protons excreted via the  $\text{Na}^+/\text{H}^+$  antiporter recombine immediately with  $\text{HCO}_3^-$  in the lumen and do not alter the filtrate pH. The results for rats (Thomas and Dagher, 1994) showed only small pH variations along the proximal tubule. Furthermore, reabsorption of proteins is not taken into account. Although endocytosis of albumin is possible (Amsellem et al., 2010), this mechanism is insufficient in essential proteinuria. Therefore:

$$\pi_p(x) = \pi_p(0) \frac{\text{SNGFR}}{V_t(x)}$$

and the final set of equations describing the volume flow in function of the longitudinal coordinate becomes:

$$\frac{\partial V_t(x) c_{\text{Na}}(x)}{\partial x} = \phi_{\text{max}} \frac{c_{\text{Na}}(x)}{K_m + c_{\text{Na}}(x)}; \quad c_{\text{Na}}(x) = c_{\text{Na}}(0) - \frac{\pi_p(0)}{2RT} \left[ \frac{\text{SNGFR}}{V_t(x)} - 1 \right] \quad (4.6)$$

Since no exact kinetic data are available for guinea pigs, the model had to be calibrated using the experimental values for healthy animals. In guinea pigs, the normal SNGFR was found to be 20 nl/min, the length of proximal tubules was 6 mm, and the reabsorbed part of SNGFR at  $x = 6$  mm was 11.3 nl/min (Spitzer and Brandis, 1974).  $K_m$  was assumed to be 80 mmol/l, as determined in rabbits (Laradi et al., 1986). In healthy animals there is no proteinuria ( $\pi_p = 0$ ) and  $c_{\text{Na}}(0) = 140$  mmol/l. This resulted in  $\phi_{\text{max}} \approx 400$  pmol/mm/min, similar to the one found in rabbits (Schafer et al., 1974). The values of  $\phi_{\text{max}}$  and SNGFR in rats: 2100 pmol/mm/min and 40 nl/min respectively (Thomas and Dagher, 1994) were substantially higher.

#### 4.5.2. Calcium-sodium interaction

Codependence of calcium and sodium excretion has been the most frequently studied interaction (Friedman, 1981; Friedman, 1998); this is because its clinical implications are of major importance in humans. Various studies show that increased calcium excretion due to excessive salt intake poses a risk of developing secondary hyperparathyroidism, bone disease and urinary tract stones (McCarron et al., 1980; Cappuccio et al., 2000; Sellmeyer et al., 2002). Urinary calcium wasting in high salt diets is

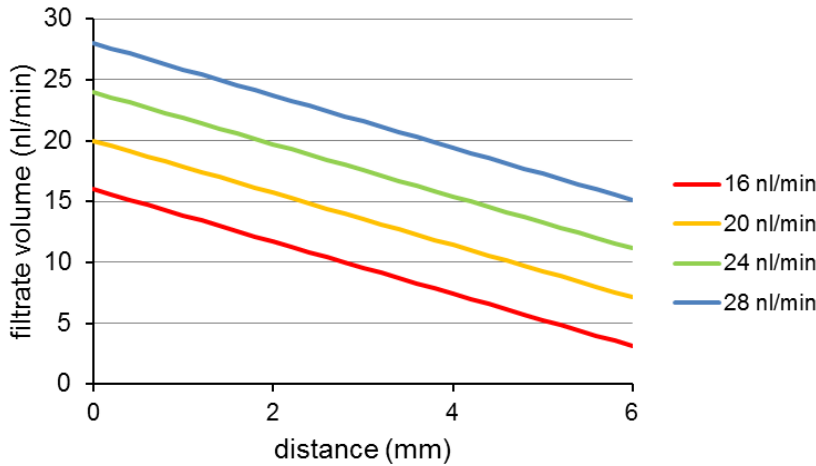


Fig. 4.17: Filtrate volume in function of the longitudinal coordinate in the proximale tubule (total length = 6 mm), for different SNGFR values (16-28 nl/min).

not related to any kind of renal dysfunction: the fundamental mechanisms that govern renal calcium and sodium excretion are responsible for this phenomenon. Obviously, impaired tubular reabsorption in renal pathology would contribute to calcium wasting.

Estimates of calcium losses and calcium-sodium codependence were obtained by solving eqs 4.6 for  $\pi_p = 0$ . In this case, isoosmocity (eq. 4.5) reduced to isotonicity:  $c_{\text{Na}}(x) = c_{\text{Na}}(0)$  and the equations could be solved analytically:

$$V_t(x) = \text{SNGFR} - \frac{\phi_{\text{max}}}{K_m + c_{\text{Na}}(0)} x \quad (4.7)$$

In the calculations,  $c_{Na}(0)$  was assumed to be 140 mmol/l. Serum calcium level was 2.5 mmol/l, of which 50% was filtered. Daily sodium and calcium excretion was estimated by calculating losses in the PCT (eq. 4.7) and taking into account reabsorption in distal nephron segments (TAL and DCT). It was assumed that distal reabsorption systems work at their maximum capacity, which is about 40% of total sodium and 25% of total calcium (Guyton and Hall, 2000). It was assumed that an adult guinea pig has 80000 functional nephrons (40000/kidney). Humoral regulation of GFR and reabsorption rates was not incorporated in this model.

Volume flow in function of the longitudinal coordinate  $x$  is plotted in Fig. 4.17 for various SNGFR values. Fig. 4.18 depicts the total end volume of the filtrate exiting the proximal tubule in function of GRF and the corresponding sodium and calcium flows. Finally, the relation between sodium and calcium excretion is given in

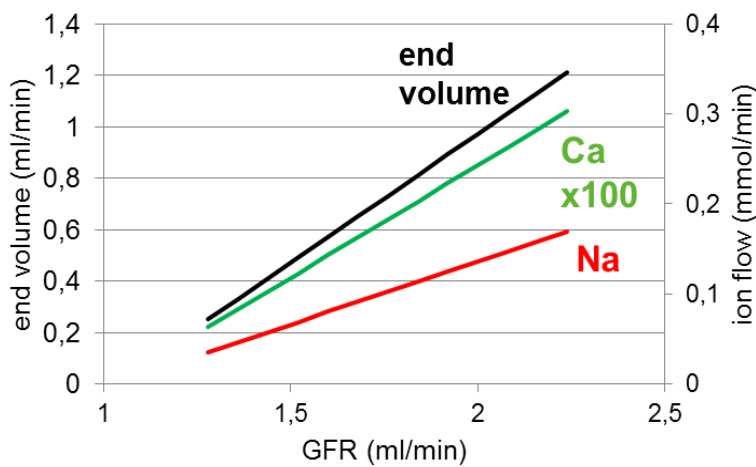


Fig. 4.18: Filtrate volume, sodium and calcium flows at the end of the proximal tubule. Serum  $Na^+$  is 140 mmol/l. Serum  $Ca^{2+}$  is 2.5 mmol/l, 50% is filtered.

Fig. 4.19.

The model demonstrates the codependence of urinary sodium and calcium losses under normal physiological conditions. Note that the amounts of excreted sodium presented in Fig. 4.19 (a few hundreds mg per day) may seem unrealistically high. However, a guinea pig consumes daily about 50 g of commercial dry chow with 6 to

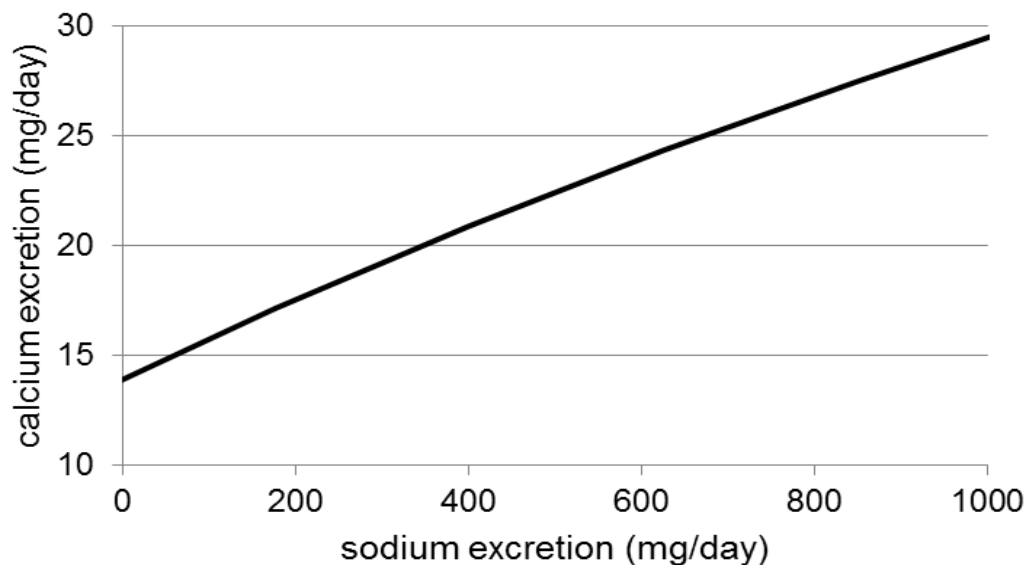


Fig. 4.19: Codependence of sodium and calcium excretion, assuming variable  $Na^+$  and  $Ca^{2+}$  reabsorption in PCT (in function of GFR) and maximum reabsorption in distal nephron.

8% crude ash content and 0.3 to 0.5% sodium. This corresponds to 150-250 mg sodium per day. Providing salt lick stones would further increase sodium consumption and excretion. The additional presence of tubular nephropathy would reduce the efficiency of mineral reabsorption and exacerbate sodium as well as calcium wasting. It is known that satin guinea pigs develop more severe symptoms when fed an all-pellet diet without fresh vegetables.

Under physiological conditions, the reabsorption rates are subject to humoral regulation. However, it is difficult to describe this effect in quantitative terms. The influence of RAAS and angiotensin has been demonstrated by many authors (Liu and Cogan, 1988; Geibel et al., 1990). The RAAS is activated at low glomerular filtration rates. Angiotensin II reduces sodium losses by enhancing the reabsorption rate ( $\phi_{max}$ ). The effect on  $\phi_{max}$  is substantial in rats: sodium reabsorption in the PCT increased by about 50% after administration of intravenous angiotensin at 20 ng/min/kg body weight (Geibel et al., 1990). At high GFR values, RAAS is suppressed and angiotensin levels are low. This implies that calcium losses may increase more drastically with increasing GFR than predicted by the current model. Unfortunately, there is no data on circulating levels of angiotensin in relation to GFR and  $\phi_{max}$  in guinea pigs.

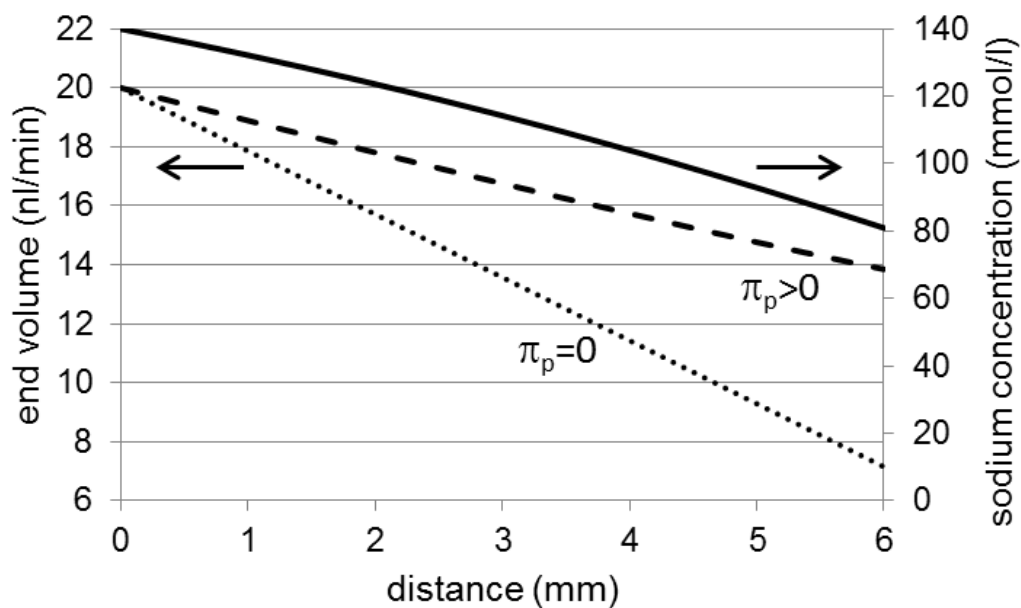


Fig. 4.20: Sodium concentration (solid line) and filtrate volume (dashed line) as a function of the longitudinal coordinate in the proximal tubule (total length = 6 mm), for SNGFR = 20 nl/min. The protein concentration in the filtrate is 1 g/dl (sieving coefficient of 25%). The reabsorption curve in absence of protein ( $\pi_p = 0$ ) is given for comparison (dotted line).

#### 4.5.3. Calcium-protein interaction

Correlations between proteinuria and calciuria have been widely recognized. Regardless of its background – glomerular nephropathy (Adams et al., 1969) or high dietary protein intake (Kerstetter et al., 2003) – proteinuria has been implicated as one of important causes of calcium losses, hyperparathyroidism and formation of urinary tract calculi in humans.

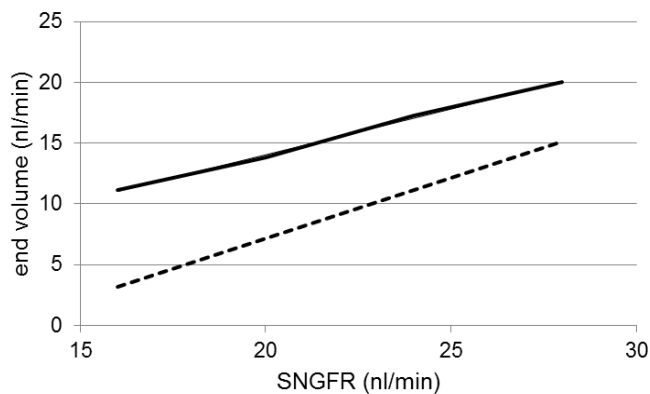


Fig. 4.21: Filtrate volume at the end of PCT as a function SNGFR, at sieving coefficient of 25% (solid line) and 0% (no proteinuria, dashed line).

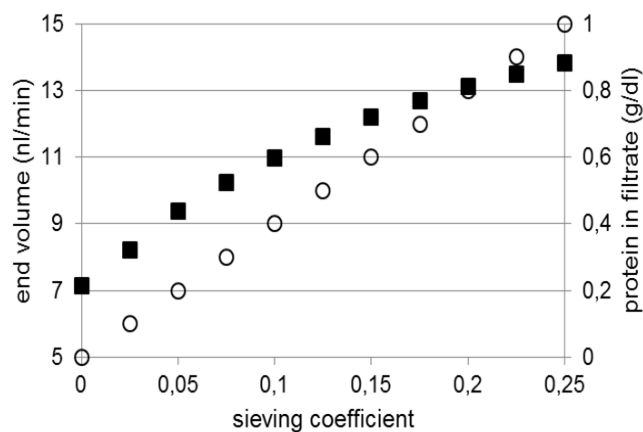


Fig. 4.22: Filtrate volume (squares) at the end of PCT in function of the sieving coefficient at SNGFR = 20 nl/min. Open circles: protein concentration.

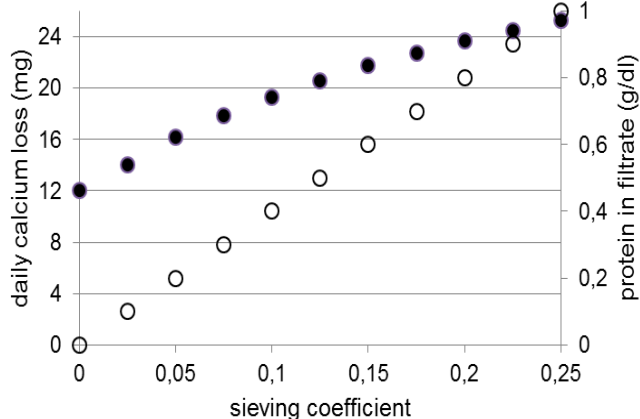


Fig. 4.23: Daily calcium loss (solid circles) in function of the sieving coefficient at SNGFR = 20 nl/min. Serum Ca is 2.5 mmol/l, 50% is filtered. Open circles: protein concentration.

For  $\pi_p \neq 0$  eqs 4.6 were integrated numerically. To visualize the effect of oncotic pressure on longitudinal profiles of filtrate volume and sodium concentration, the equations were solved for a very high protein concentration (1 g/dl), corresponding to a glomerular sieving coefficient of 25%. In further calculations, end filtrate volume and daily calcium losses were determined for more realistic (lower) sieving coefficients. As in Section 4.5.2, sodium and calcium concentrations were assumed to be 140 mmol/l and 2.5 mmol/l, respectively. In calculating total calcium losses, calcium bound to albumin was taken into account. In the relevant albumin concentration range, the  $\text{Ca}^{2+}$  binding coefficient is about 2 mg/g albumin (Besarab and Caro, 1981). An average urine output was assumed to be 100 ml/day.

The results are shown in Figs 20-23. Fig. 20 depicts the longitudinal variations in filtrate volume and sodium concentration in the PCT. The end volume after passage through the PCT in function of SNGFR is displayed in Fig. 21. Fig. 4.22 shows the end volume, and Fig. 4.23 the corresponding daily calcium excretion as a function of the sieving coefficient.

It can be deduced from Fig. 4.20 that the filtrate volume is markedly expanded in presence of a non-resorbable osmogenic solute. Simultaneously, sodium concentration is reduced because of sodium reabsorption without passive water reabsorption. The effect of expanded

filtrate volume due to oncotic pressure becomes particularly pronounced at low GFR values (Fig. 4.21). Volume expansion of the filtrate leads to a substantial increase in urinary calcium excretion

(Figs 4.22-23), also at sieving coefficients of the order of a few percent. The contribution of protein-bound calcium to total calcium losses is relatively small.

#### **4.5.4. Conclusion**

Modeling results of calcium-sodium and calcium-protein interactions show that both inadequate tubular sodium reabsorption and proteinuria can significantly increase urinary calcium losses. Intuitively, one might expect that tubular nephropathy with impaired mineral reabsorption is more likely to cause renal calcium wasting than glomerular disease. However, nephrotic syndrome attendant to glomerular damage may also provide an important underlying mechanism.

## 5. RENAL OSTEODYSTROPHY

In this chapter, renal osteodystrophy is reviewed in the context of contemporary kidney research. First, commonly used animal models of renal disease are described and their properties are discussed. Furthermore, the physiology of bone remodeling with its molecular regulation systems is presented. Finally, types of metabolic bone disease in humans and animal models, and the corresponding pathological findings are described.

### 5.1. CKD IN ANIMAL MODELS

Chronic kidney disease (CKD) has a broad spectrum of systemic sequelae in humans. Examples include soft tissue calcification with concomitant arteriosclerosis and hypertension, osteodystrophy, gout, urolithiasis and other urinary tract diseases (Rubin and Farber, 1999). Cardiovascular complications of renal failure have by far the gravest implications in humans; therefore, the majority of studies focuses on resolving the pathophysiology of soft tissue calcification (Moe et al., 2005; Shobeiri et al., 2010; Neven and D'Haese, 2011; De Schutter, 2012), see also Chapter 4, Section 4.3.3. The second area of intensive investigations is renal osteodystrophy (Wada et al., 1998; Moe et al., 2006). For the purpose of gaining insight in the human disease, animal models must be developed that adequately reproduce the disease in humans. However, there are many different pathologic processes that underlie CKD in humans (e.g. diabetes, infections and autoimmune diseases) and produce their specific clinical pictures (Jennette and Spargo, 1999). It is not always possible to obtain a representative model for each type of disorder. Besides, not all pathophysiological features of CKD in humans may have their counterparts in animals (Neven and D'Haese, 2011). Therefore, developing animal models poses a scientific and technical challenge.

Despite the high degree of complexity of CKD-related disorders, certain phenotypic parallels exist between human and animal kidney failure, namely: increased plasma creatinine and blood urea nitrogen, hyperparathyroidism and hyperphosphatemia (Shobeiri et al., 2010). The least requirement for an animal CKD model is a well-defined reduction of the glomerular filtration rate (GFR) that would result in a reproducible uraemic environment without any additional physiological changes. Such a model, termed 5/6 nephrectomy (5/6Nx) or the remnant kidney model was developed in the first decades of the XXth century (Chanutin and Ferris, 1932). Many trial-and-error experiments had to be carried out to obtain a stable model. Initially, CKD was induced by partial nephrectomy in dogs, rats and mice, but the mortality in animals undergoing this procedure was high, especially in dogs (Bradford, 1899). Eventually, the rat has proven to be the most suitable species (Chanutin and Ferris, 1932). The procedure is carried out in two steps: first, two of three branches of the renal artery are ligated to create an ischemic infarction in approximately 2/3 of the kidney tissue. One week later, after recovery from this surgery, the contralateral kidney is removed. Since GFR is drastically suppressed, 5/6Nx procedure produces inherently uraemic animals. Post-operative changes to the remnant kidney include proliferation of mesangial and (to a lesser degree) endothelial cells, followed by infiltration of monocytes and macrophages and focal sclerosis, as determined in rats (Floege et al., 1992). Progressive glomerulosclerosis accounts for proteinuria in 5/6Nx animals. Similar features present in common human kidney diseases, such as membranous and membranoproliferative (immune-mediated) glomerulopathy (Jennette and Spargo, 1999) or hypertensive kidney damage (Kopp et al.,

2008). Therefore, the remnant kidney rat is still state of the art and the “gold standard” in kidney research (Chow et al., 2003). 5/6Nx rats develop hyperparathyroidism and are widely used in studies of metabolic bone disease and vascular calcification (Neven and D’Haese, 2011; De Schutter, 2012). However, induction of vascular calcification that would mimic arteriosclerotic lesions in human CKD patients cannot be achieved spontaneously in 5/6Nx rats. Therefore, surgery is often combined with administration of mineralization-accelerating supplements such as phosphate (Shobeiri et al., 2010) or lactose (Debiec et al., 1988; Kawata et al., 2008).

In 1983, another CKD model was developed by surface electrocautery of mice kidneys (Gagnon and Duguid, 1983). This model is also based on a two-step procedure of ablation of the superficial cortex, followed by contralateral nephrectomy. The performance is similar to that of 5/6Nx, and often disappointing with regard to soft tissue calcification. Both surgical procedures are time-consuming and associated with loss of animals. Electrocautery has a poor survival rate as compared with 5/6Nx: it can result in mortality as high as 30% in mice (Shobeiri et al., 2010).

A different concept was introduced by Yokozawa and coworkers (Yokozawa et al., 1982) and further elaborated by Okada et al. (1999). It was observed that dietary supplementation of purines (adenine) induced renal failure in rats. The mechanism of kidney damage is based on a disruption of the normal pathways of nucleobase metabolism, which results in production of nephrotoxic metabolites (2,8-OH-adenine) that precipitate in tubules (Wyngaarden and Dunn, 1957). A tubulo-interstitial pattern of renal failure is induced, with pronounced tubular obstruction and interstitial fibrosis (De Schutter, 2012). Rats fed 0.75% adenine for 4 weeks develop irreversible kidney damage (Okada et al., 1999) and fairly reproducible vascular calcification (Shobeiri et al., 2010). The major advantage of the adenine rat model is that it does not require surgery, which reduces the work load and costs, and improves the survival of animals (Shobeiri et al., 2010).

Development of spontaneous CKD models was also pursued (Cowley et al., 1993). To date, the best documented spontaneous renal failure in laboratory animals is the Cy/+ rat, in which an autosomal dominant mutation produces a polycystic kidney syndrome (Moe et al., 2009). Heterozygous Cy/+ rats develop uraemia, hyperparathyroidism and bone disease at about 40 weeks of age, but soft tissue calcification is less pronounced than in other models. The applicability of Cy/+ rats in cardiovascular research is thus limited (Shobeiri et al., 2010).

Alternatively, the genetic basis of CKD was investigated and correlations were sought after by analyzing quantitative trait loci (QTL) in uraemic humans and animals. High degrees of concordance between human and animal kidney failure loci were demonstrated in rats and mice (Korstanje and DiPetrillo, 2004). This research line is exceptionally promising, because of its high potential of producing refined animal models that are faithful replicas of different human pathologies (Watson et al., 1992; Remuzzi et al., 2006). With the introduction of transgenic animal technology, a breakthrough was made in research on CKD (Kerjaschki, 2001; Chen and Moe, 2004; Nakagawa et al., 2007). Knock-out mice are nowadays indispensable in detailed studies of pathways and interactions. The usage of gene deletion techniques in kidney research allowed visualising the role of tissue calcification inhibitors, nitric oxide synthase and fibroblast growth factor 23 (Chen and Moe, 2004; Kurosu et al.,

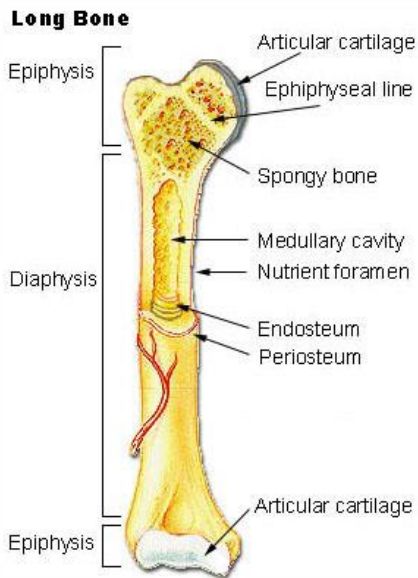


Fig. 5.1: A schematic view of a long bone. Source: Wikipedia Commons.

2006; Nakagawa et al., 2007). Knock-out technology is often combined with 5/6 nephrectomy or electrocauterization.

In summary, a large variety of animal models for CKD is available, each with its benefits and drawbacks. Most of the currently used models rely on gross surgical intervention to the kidney and are inevitably followed by major systemic changes. The research on spontaneous CKD and its genetic background in animals may result in development of new, refined models with tailored pathophysiological features.

## 5.2. BONE REMODELING

As indicated in the previous section, much research effort is invested in understanding bone disease in human renal insufficiency (Moe et al., 2006; De Schutter 2012). Before discussing bone changes in kidney disease more profoundly, some basic facts of bone physiology are presented.

The bone is a cell-rich and physiologically active structure that has, next to its mechanical and haematopoietic functions, an important task of storing inorganic salts and regulating the mineral balance. A general scheme of a long bone is depicted in Fig. 5.1.

### 5.2.1. Bone matrix and cells

Bone is a highly mineralized tissue that consists of 60% hydroxyapatite (HAP) and 30% organic matrix, in which the cellular component amounts up to 10%. The organic matrix contains mainly type I collagen (88%), about 10% other proteins and a small amount of lipids and glycosaminoglycans (Schiller and Teitelbaum, 1999). The cellular component is represented by osteoprogenitor cells (stem cells), osteoblasts (osteogenic cells), osteocytes (maintenance cells) and osteoclasts (osteolytic cells).

Osteoprogenitor cells are resident marrow stromal cells derived from pluripotent mesenchymal stem cells. Osteoprogenitor cells are mainly found in the periosteum and the marrow cavity, and may differentiate into chondrocytes, adipocytes, or muscle cells, as well as osteoblasts and further into osteocytes (Raggatt and Partridge, 2010).

Osteoblasts are ontogenetically and functionally related to fibroblasts. These cubic mononuclear cells line the bone surface and deposit the organic matrix (osteoid or osteoid seam) which is mineralized at later instances (the so-called mineralization lag time). Osteoblasts secrete alkaline phosphatase (ALP), which releases phosphate and accelerates mineralization of osteoid (Schiller and Teitelbaum, 1999). Other factors that influence mineralization are pH, availability of calcium and presence of calcification inhibitors (Cochran and Wilkinson, 1975; Mocetti et al., 2000; Hesse et al., 2002). Besides ALP and bone collagen, osteoblasts secrete other matrix proteins such as osteocalcin, an important factor in the mineralization process and a biomarker for bone formation, and osteopontin and sialoproteins, which are integrins (Schiller and Teitelbaum, 1999). Osteopontin is an integrin that facilitates osteoclast anchoring to the bone surface in bone resorption processes (Crosby et al., 1995).

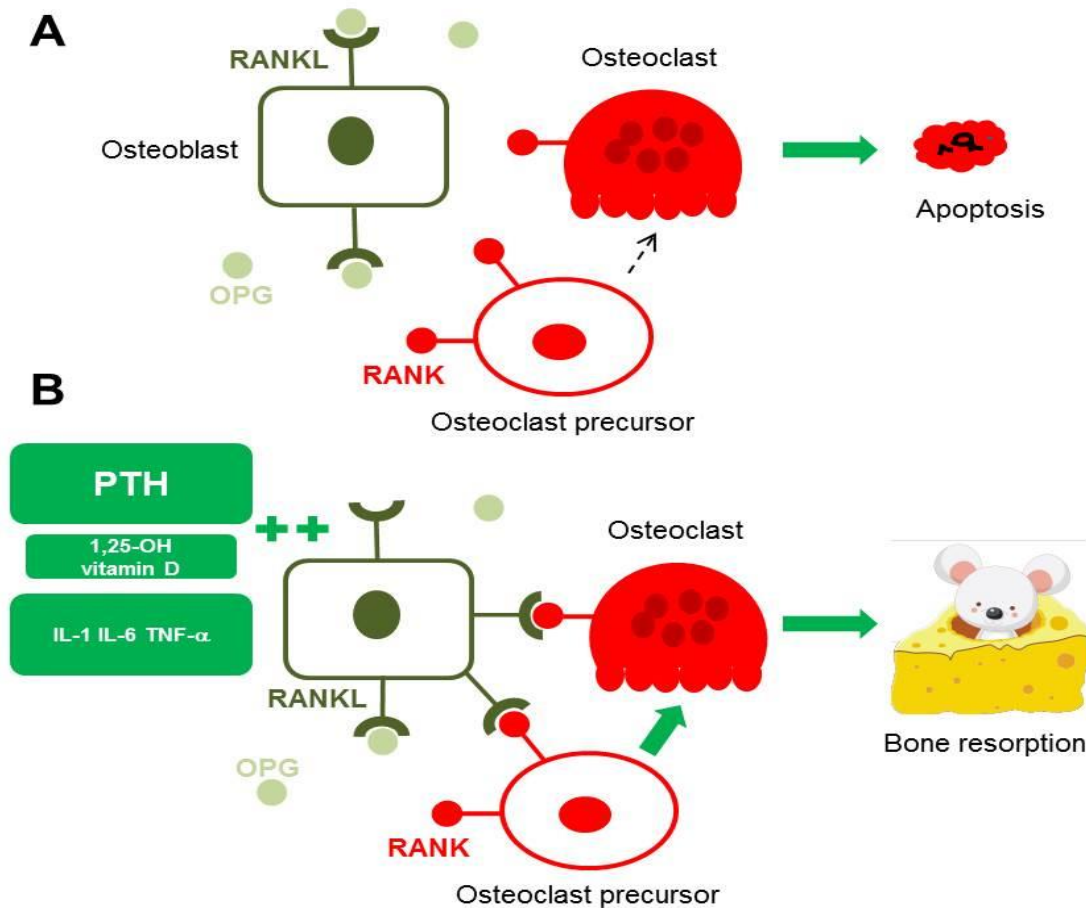


Fig. 5.2: A scheme of the RANKL-RANK signaling pathway. A – low levels of PTH. RANKL is largely occupied by osteoprotegerin (OPG). Differentiation of osteoclast precursors is maintained at a low level, osteoclasts undergo apoptosis. B – high levels of PTH, calcitriol or inflammatory cytokines. RANKL expression is increased beyond the capacity of OPG. Due to RANKL-RANK interactions osteoclast differentiation is enhanced and apoptosis is suppressed. After Fukugawa et al. (2002).

Osteoblasts also produce the fibroblast growth factor 23 that increases urinary phosphate excretion (Gutierrez et al., 2005; Kolek et al., 2005; Kurosui et al., 2006).

Osteoblasts are the only bone cells expressing PTH and calcitriol receptors, and thus being direct targets of humoral regulation of bone turnover. In response to PTH and calcitriol, osteoblasts upregulate the receptor activator of the nuclear factor  $\kappa$ B ligand (RANKL), a tumor necrosis factor (TNF) related cytokine that causes maturation and activation of osteoclasts. Besides RANKL, osteoblasts express osteoprotegerin, a soluble decoy receptor for RANKL. Osteoprotegerin tempers the osteoclastic response under normal conditions (Theoleyre et al., 2004); however, this pathway is disrupted in hyperparathyroidism (Fukugawa et al., 2002).

Other factors that regulate osteoclast activity are: growth factors such as transforming growth factor beta (TGF- $\beta$ ) and the insulin-like growth factor family (Chen et al., 2012), and inflammatory cytokines (IL-1, TNF- $\alpha$ ). Growth factors enhance osteoblast activity and bone formation, whereas inflammatory cytokines inhibit osteoblast differentiation simultaneously enhancing RANKL expression. This is the mechanism that underlies osteolysis in inflammation (Gilbert et al., 2000; Steeve et al., 2004).

Osteocytes can be seen as mature or fully differentiated osteoblasts. These cells are embedded in the osteoid, but remain in contact with surface osteoblasts by the cytoplasmic processes that osteoblasts extend into osteoid (Schiller and Teitelbaum, 1999). They have been implicated to play a role in signaling pathways in bone resorption (Hruska and Teitelbaum, 1995).

Osteoclasts belong to a different cell family: they have a haematopoietic origin and are related to monocytes/macrophages. These large multinucleated cells usually rest within small depressions in the bone surface, called Howship's lacunae. A characteristic feature of an osteoclast is its multiply folded cytoplasmic membrane, termed "ruffled border". With their ruffled borders osteoclasts attach to the mineralized bone surface by means of integrins (osteopontin), and acidify the local environment by pumping protons into the gaps formed by their membrane folds and the bone. Acidic medium dissolves hydroxyapatite and exposes organic matrix. Subsequently, osteoclasts degrade the organic matrix by secreting proteases. Osteoclasts cannot attach to unmineralized osteoid (Schiller and Teitelbaum, 1999).

The chief regulatory mechanism of osteoclast maturation and activation is the RANKL-RANK pathway. Osteoclasts express a surface receptor RANK – the receptor activator of the nuclear factor  $\kappa$ B, which is a member of the TNF receptor superfamily. Upon binding RANKL expressed by osteoblasts in response to humoral (e.g. PTH) stimulation, immature osteoclasts form syncytia and commence bone resorption. There is no feedback mechanism from osteoclasts. Instead, osteoclastic activity is inhibited by osteoblast-derived osteoprotegerin that binds RANKL. An overview of pathways is schematically depicted in Fig. 5.2 (Fukugawa et al., 2002).

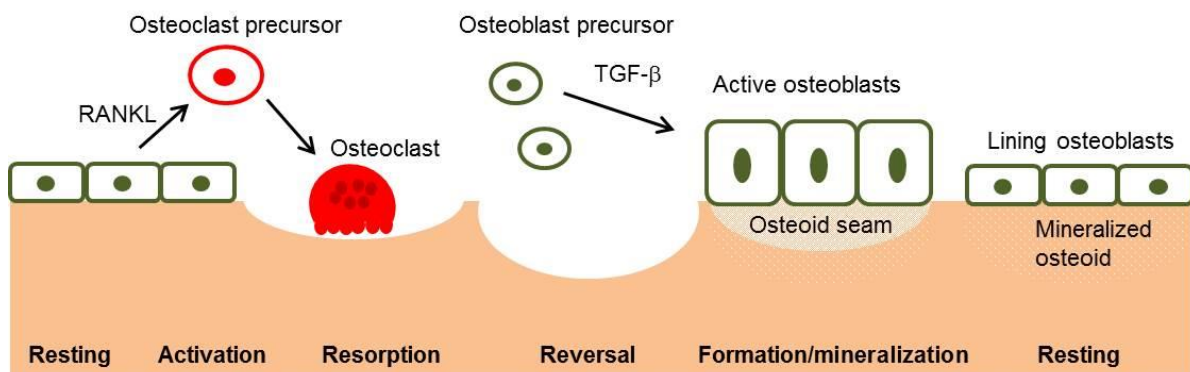


Fig. 5.3: The bone remodeling cycle. After Kearns and Kallmes 2008.

### 5.2.2. Bone remodeling

Bone is a dynamic medium that constantly undergoes microscopical changes. The remodeling cycle consists of five stages: resting, activation, resorption, reversal, formation and mineralization (Raggatt and Partridge, 2010). In the resting phase, the bone is quiescent and its surface is lined by flattened osteoblasts. In the activation phase that follows humoral (PTH, calcitriol) stimulation, osteoblasts retract and expose the surface, while expressing RANKL that promotes osteoclast differentiation and maturation. In the resorption phase, osteoclasts erode both mineral and organic matter, but the latter process is slower. During the degradation process, osteoclasts form

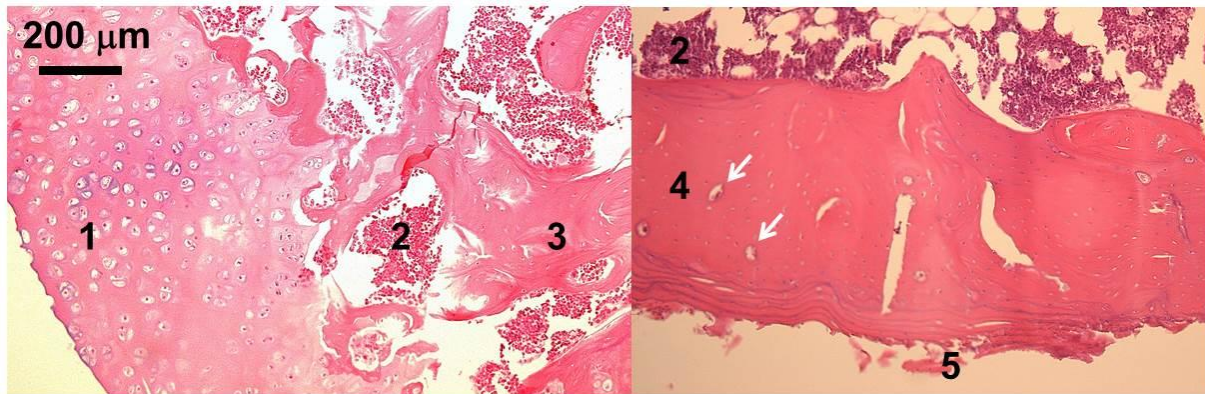


Fig. 5.4: Guinea pig bones. Left – trabecular bone and cartilage (rib), right – compact bone (femur). 1 – chondrocytes, 2 – red marrow, 3 – trabeculae, 4 – compact bone (arrows: Haversian canals), 5 – periosteum with circumferential lamellae. H&E stain.

characteristic resorption lacunae. When the layer of demineralized osteoid becomes too thick, osteoclasts cease their activity, detach and undergo apoptosis. Another type of cell, a specialized tissue macrophage or “osteomac” has been implicated in removing the remaining osteoid (Raggatt and Partridge, 2010), but the signaling pathways are not yet clear. The following phase is the reversal phase, in which new osteoblasts are recruited. The mechanisms of osteoblast differentiation and activation are not completely resolved. Bone matrix-derived TGF- $\beta$  may play a role, but other chemotactic signals have been implicated as well (Raggatt and Partridge, 2010). In the commencing formation phase, activated (cubic) osteoblasts secrete new osteoid until the lacunae are filled. The termination signals are largely unknown. The last step, mineralization, is a passive process and its kinetics (mineralization lag time) depends mainly on local biochemical factors (see Section 5.2.1). After mineralization, osteoblasts can return to their quiescent state, undergo apoptosis or differentiate to osteocytes embedded in bone matrix. A graphic presentation of the various phases is given in Fig. 5.3 (Kearns and Kallmes, 2008; Raggatt and Partridge, 2010).

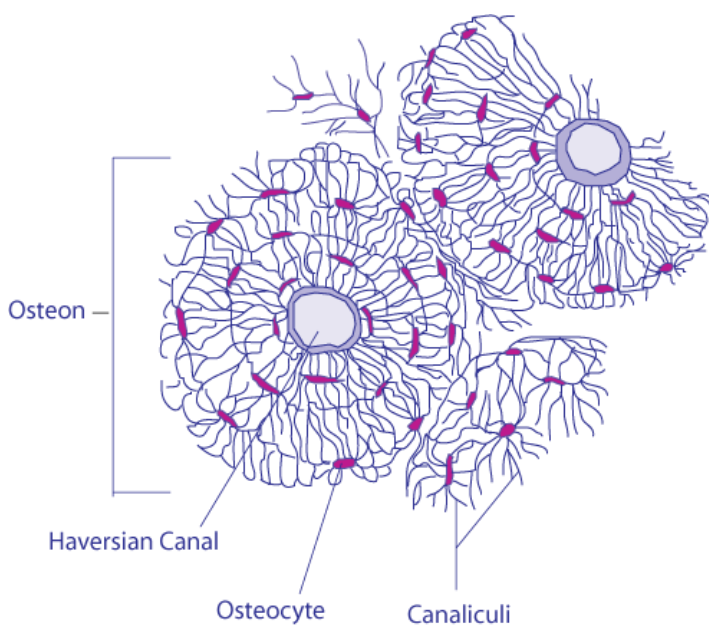


Fig. 5.5: A scheme of an osteon (Haversian system). Source: Wikipedia Commons.

A typical time scale of the remodeling cycle in adult humans is of the order of several months (Kearns and Kallmes, 2008). However, certain not necessarily pathological factors may accelerate bone turnover, such as bone growth at young age and mechanical or exercise-induced stress (Brouwers, 2008).

### 5.2.3. Bone morphology

The total of bone formation and remodeling processes determine the eventual macroscopic and microscopic bone structure. Morphologically, two types of bone can be distinguished:

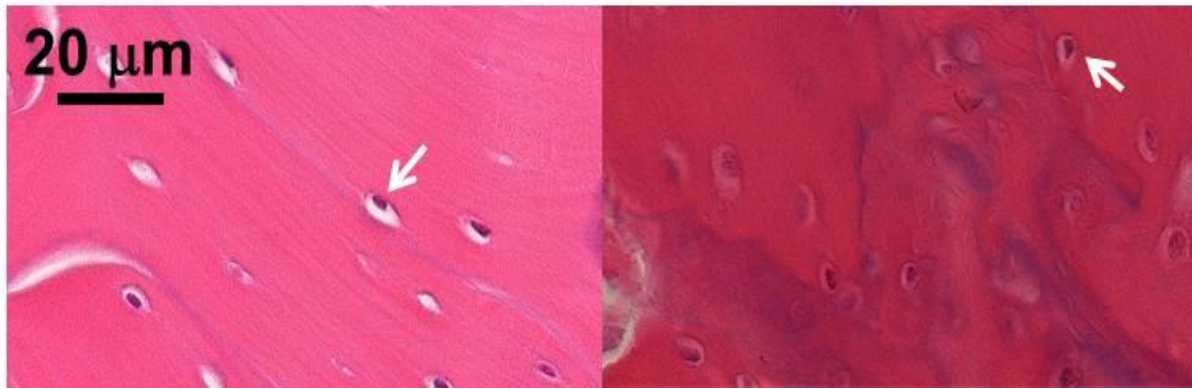


Fig. 5.6: Guinea pig bones (femur cortex). Left – normal lamellar bone. Right – pathological woven bone with pronounced reversal lines. Arrows – osteocytes. H&E stain.

trabecular or cancellous bone, and cortical or compact bone (Fig. 5.4). Trabecular bone is typically located in the metaphyseal (growth plate) and epiphyseal regions of long bones, and in the skull, ribs and vertebrae. It represents the young or growing bone that undergoes the most intensive metabolic changes. Compact bone is present in the diaphyseal region of long bones and in cortical (superficial) portions of other bones. This is the mature type of bone that stores large mineral masses, but does not display such high levels of cellular activity as the trabecular bone (Schiller and Teitelbaum, 1999).

Trabecular and cortical bones have different microscopic architectures. Compact bone has a characteristic structure consisting of osteons (Fig. 5.5) with a central Haversian canal, surrounded by concentric bony lamellae with embedded osteoblasts. Haversian canals contain blood vessels and serve to supply nutrients and cells needed for bone growth and remodeling. No osteons are present at the cortical and medullary peripheries; instead, lamellae are arranged parallel to the bone surface, forming circumferential (outer) and endosteal (inner) lamellae (McGavin and Zachary, 2007).

Regardless of the type of bone (trabecular versus compact), healthy bone always displays a lamellar structure (Schiller and Teitelbaum, 1999). Lamellae result from the bone remodeling activity and represent bone layers deposited by osteoblasts. Under normal conditions, osteoblasts form well-aligned collagen fibers (Fig. 5.6). When the osteoblast activity is temporarily halted, a thin collagen-deficient demarcation line is created (a cement line). This line appears basophilic in haematoxylin-eosin (H&E) stain. Cement lines are also formed when osteoblasts resume osteoid deposition after the reversal phase of bone remodeling (McGavin and Zachary, 2007). The so-called reversal lines reflect the resorption lacunae created by osteoclasts and are normally unapparent.

The microscopic appearance of lamellae and cement lines are highly informative of the pathophysiological state of the bone. Particularly, the loss of lamellar structure is indicative of an (abnormally) increased bone turnover. The resulting woven bone displays chaotically arranged collagen fibers and usually thick and fringed reversal lines (Fig. 5.6). Woven bone can be physiological in young growing individuals or as a temporary structure in healing fractures, but abundant formation of woven bone in the adult is considered pathognomonic of bone disease (Schiller and Teitelbaum, 1999). In the compact (cortical) bone portions, the presence of woven bone, randomly scattered osteocytes, broad reversal lines and expanded Haversian canals are highly suggestive of pathologically enhanced resorption (Jaffe and Bodansky, 1930).

The morphology of the calcification front (osteoid seam) at the bone surface is also of high diagnostic relevance in bone pathology, because it yields information about osteoblastic activity as well as the chemical properties of the bone environment. For example, in acidosis or calcium deficiency-induced bone disease (rickets, osteomalacia and fibrous osteodystrophy) the osteoblast activity is high but mineralization fails. This results in a pronounced osteoid seam. In bone quiescence (osteoporosis), the opposite is true (Hruska and Teitelbaum, 1995; Schiller and Teitelbaum, 1999).

### 5.3. BONE IN SECONDARY RENAL HYPERPARATHYROIDISM

Calcium deficit ("calcium wasting", see Chapter 4) accompanied by phosphate retention are often the primary systemic consequences of chronic kidney disease (Hruska et al., 2008). When calcium and phosphate imbalances exceed a certain limit above which no local compensation is possible, a systemic response is elicited by activation of the bone-renal axis. As a result of an increased parathyroid hormone secretion, molecular pathways are upregulated resulting in a release of calcium from bone resources (see Section 5.2) so as to cover the systemic deficit. Note that this compensatory mechanism is intrinsically defective. Bone resorption results in a release of both calcium and phosphate, in the proportion of 5 to 3 (as in hydroxyapatite). Thus, bone resorption yields calcium, but simultaneously exacerbates hyperphosphataemia (Schiller and Teitelbaum, 1999).

Further evolution of parathyroid hormone, calcium and phosphate levels in CKD is modulated by many additional factors and mechanisms, and depends on the type of renal defects (tubular versus glomerular nephropathy), dietary patterns and the presence of other systemic disorders such as diabetes mellitus (Pei et al., 1993; Hruska and Teitelbaum, 1995; Krakauer et al., 1995; Slatopolsky et al., 1999; Toussaint et al., 2006). The concerted action of these factors determines the final histopathological appearance of the bone. In humans, three major types of histological manifestations of renal bone disease have been described, of which only one (fibrous osteodystrophy) can be characterized as a high-turnover disease.

#### 5.3.1. Fibrous osteodystrophy

Fibrous osteodystrophy can be considered as the classic or primary presentation of bone disease in secondary hyperparathyroidism. The general feature is an abnormally high bone turnover. Increased bone resorption is reflected by a large number of osteoclasts that are recruited from bone marrow and the periosteal regions. Microscopically, so-called tunneling resorption, also termed *osteitis dissecans* is observed (Schiller and Teitelbaum, 1999). Since osteoclasts cannot attach to unmineralized osteoid (e.g. osteoid seam), they seek mineralized zones to form resorption lacunae. Thus, osteoclastic activity produces numerous indentations and irregularly shaped channels in the bone. Simultaneously, bone formation is increased which is reflected by an increase in the numbers of active (cubic) osteoblasts and unmineralized osteoid (Christiansen, 2001; Parfitt, 2003). The resulting structure may roughly resemble normal trabeculae, but in *osteitis dissecans*, these pseudo-trabeculae consist mainly of woven bone (Hruska and Teitelbaum, 1995).

Fibrous osteodystrophy affects primarily trabecular (epiphyseal) bone. Structural changes in compact bones occur in advanced pathology. Interestingly, bone loss in the epiphyseal (trabecular) regions may be unapparent, and bone mass may be even increased with respect to the normal

situation. Mixed osteolytic and osteosclerotic lesions are often seen in radiography (Jevtic, 2003). This is caused by accumulation of woven bone due to enhanced osteoblast activity. The situation is different in diaphyseal portions of long bones. In cortical bone, abnormal remodeling results in bone loss and increased bone porosity. Such bones become prone to fractures and deformations (Hruska and Teitelbaum, 1995).

Other features of fibrous osteodystrophy are: enhanced angiogenesis and progressive fibrosis of peritrabecular spaces, reflected by an increase in the proportions of fibroblasts and vascular cells. Fibrosis of bone marrow is also one of the hallmarks of fibrous osteodystrophy. Without intervention, *osteitis dissecans* evolves in *osteitis fibrosa* and eventually in *osteitis cystica fibrosa*. In *osteitis fibrosa*, bone marrow cells are largely phagocytosed; the medullary cavity contains reactive woven bone, numerous haemorrhages, hemosiderin-laden macrophages and large amounts of fibrous tissue. In the end stage – *osteitis cystica fibrosa* – large, often nodular lesions containing macrophages, giant cells (osteoclasts) and abundant fibrous material are formed. Due to their radiolucence, these lesions are termed “brown tumors” in radiography (Chew and Huang-Hellinger, 1993; Schiller and Teitelbaum, 1999).

Fibrous osteodystrophy is the most common form of renal bone disease in humans, and the only spontaneous form in animals (McGavin and Zachary, 2007; Bandarra et al., 2011).

### **5.3.2. Osteomalacia**

Osteomalacia is another presentation of bone disease in renal hyperparathyroidism. This type is associated with depletion of circulating levels of calcitriol (the active form of vitamin D) or downregulation of the vitamin D receptor (VDR). Biochemical pathways are described in detail in Chapter 4, Section 4.3.3. The disorder is characterized by low bone turnover, impaired mineralization and accumulation of unmineralized osteoid. In histology sections of trabecular bone, osteomalacia is characterized by thin trabeculae and pronounced osteoid seam.

Osteomalacia is seen in end-stage renal disease in humans, when kidneys fail to produce adequate amounts of calcitriol. Phosphate depletion due to excessive usage of phosphate binders can also cause this condition, because low serum phosphate inhibits the renal-bone axis. Besides, phosphate is necessary for mineralization (De Schutter, 2012). Alternatively, hindered osteoblast differentiation due to aluminum intoxication has been implicated (Hruska and Teitelbaum, 1995; Malluche, 2002). Aluminum was formerly used in oral phosphate binders to control hyperphosphataemia in CKD patients. Nowadays, aluminum toxicity has been widely recognized and phosphate binders do not contain aluminum anymore. Consequently, osteomalacia in renal failure has become less frequent (Schiller and Teitelbaum, 1999). Osteomalacia may affect animals fed low vitamin D diet (McGavin and Zachary, 2007).

### **5.3.3. Adynamic bone disease**

Adynamic bone disease (ABD) is a relatively uncommon presentation in CKD, and the underlying mechanisms are poorly understood. This condition is characterized by drastically decreased bone turnover. As a result, the bone is hypocellular, trabeculae are thin and unapparent, and the osteoid seam is practically absent (De Schutter, 2012). ABD may be caused by excessive calcium intake in

combination with phosphate depletion (calcium-based phosphate binders), or by supplementation of vitamin D and its analogues (Toussaint et al., 2006). This type of bone disease is also seen in diabetes mellitus (Krakauer et al., 1995).

Adynamic bone disease does not have its counterpart in animals. However, it can be reproduced in animal models. Lund and coworkers developed an ABD mouse model by combining electrocautery of the kidney, restriction of dietary phosphate and supplementation of calcitriol (Lund et al., 2004).

Finally, mixed uraemic osteodystrophy, featuring both *osteitis fibrosa* and osteomalacia, has been identified in humans (De Schutter, 2012). This type of bone disease is not of importance in animals.

With this knowledge, interpretation of radiographic and histopathological bone features in satin guinea pigs can be attempted (Chapters 6 and 7).

## 6. COMPUTED TOMOGRAPHY AND BONE DENSITY MEASUREMENTS

### 6.1. INTRODUCTION

Computed tomography (CT) is a medical imaging technique that combines standard X-ray radiography with numerical deconvolution procedures to create two- and three-dimensional images of objects. CT is the technique of choice in studying bone pathology, with focus on alterations in the spatial structure and mineral densities. CT is widely applied in human healthcare to diagnose and characterize complex fractures, tumors and other lesions, osteomalacia, osteoporosis and many other conditions (Genant et al., 1987; Boutrouy et al., 2005). Applications in veterinary medicine are less common, mainly due to the high cost and the necessity of prolonged anaesthesia. The latter becomes an issue in small animals, such as rodents and rabbits where anaesthesia negatively interferes with physiological processes in the organism. *In vivo* CT imaging of rodents is frequently applied in biomedical research (Rummens 2003; Brouwers 2008; Brouwers et al., 2008), but not as a routine diagnostic in pet animals (Capello and Lennox, 2008).

Metabolic bone diseases are followed by changes in fine trabecular structure and mineral density. In evaluation of bone lesions, the parameters of interest are bone mineral content (BMC, in g), bone mineral density (BMD, in  $\text{g}/\text{cm}^3$ ) and bone volume/total volume ratio reflecting the trabecular bone volume (BV/TV, dimensionless). Standard radiographic methods of determining these parameters are DXA (dual-energy X-ray absorptiometry) and QCT (quantitative computed tomography). The major advantage of QCT is its high resolution (10-20  $\mu\text{m}$ ), which allows visualizing minor lesions and alterations of trabecular patterns (Brouwers, 2008).

In this chapter the outcome of a limited-scale CT imaging study in guinea pigs is presented. Global bone morphology, microstructural changes and dental pathology were studied. No absolute bone density measurements (QCT) could be performed; however, a simple semi-quantitative method was developed to assess the degree of bone decalcification in satin guinea pigs. Bone densities in satins were compared with those in non-satin animals, the latter group comprising guinea pigs with normal kidney function and with post-mortally diagnosed kidney disease.

### 6.2. MATERIALS AND METHODS

Experiments were conducted at two locations: Department of Biomedical Engineering, Eindhoven University of Technology, The Netherlands using a high-resolution *in vivo* micro-CT scanner VivaCT 40, Scanco Medical AG, Brüttsellen, Switzerland (Brouwers, 2008), and Veterinary Clinic Causus, Oudenburg, Belgium, using a Philips Mx8000 Dual CT Scanner. CT imaging of guinea pigs was performed after euthanasia or spontaneous death of the animal. In the first experiment, two satin guinea pigs (aged 2.5 and 4 years) and two controls (aged 4 years) were examined. These satin animals had severe symptoms of lameness and were euthanized because of prolonged anorexia secondary to dental disease. The controls deceased spontaneously and no remarkable changes were found at necropsy. In the second experiment, three satin guinea pig from another case study (cases 3, 4, and 5 from Chapter 7) and one spontaneously deceased satin animal (N=4), five non-satin controls (N=5) and three non-satin guinea pigs with gross kidney lesions at necropsy (N=3, referred to as CKD) were examined. An overview of the animal vital data is given in Table 6.1.

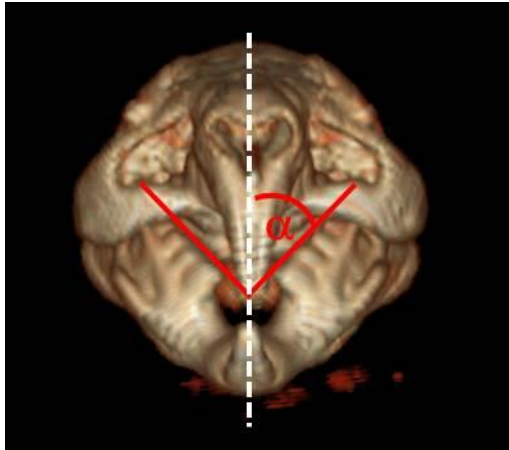


Fig. 6.1: Measurements of the inclination angle of the tooth arcade. A rostrocaudal view of CKD 1 with normal dentition.

The scanned bones were skulls and hind legs. The following conditions were used: 70 mV, 85  $\mu$ A, 1000 projections/180<sup>0</sup>, 350 ms integration time and steps of 15  $\mu$ m for VivaCT, and 120 kV, 150 mAs, 510 steps of 1 mm per scan, total scanned area of 242 mm in diameter for Philips Mx8000 Dual. Three-dimensional reconstructions of the skulls were made to visualize the ventral surface of the lower jaw (ventrodorsal view), mandibular branches (lateral and ventrodorsal views) and the occlusal plane (rostrocaudal view). This allowed evaluating the degree of dental malformation. Molar occlusion was evaluated by measuring the angle between the mandibular molar arcade and the vertical

(sagittal) line, as explained in Fig. 6.1.

Evaluation of bone mineral density was performed by analyzing the images with the ImageJ software. Measurements were carried out for the group of satin, CKD and control animals examined using the Philips Mx8000 Dual scanner. Average grayscale density was determined by integration of bone cross-sectional slices over a circular sampling area with a diameter of 1 mm. In diaphyses of long bones, only the cortex region was evaluated. Three measurements were performed per slice and an average value was calculated. Note that this method of evaluation was informative only when the X-ray absorption resulted in grayscale density lower than 230 (maximum: 255). At high absorptions and high grayscale densities the signals were saturated and could not be compared. The following bones were examined: diaphyseal femur and tibia (mid-diaphyseal cortical bone), epiphyseal femur and tibia (distal femur and proximal tibia) and skull: calvarium, *bulla tympanica*, incisors, premolars, *ramus mandibulae*. The radiopacity of soft tissues was noted, too.

To evaluate the relative cortex and medulla radiopacity in long bones, density profiles were plotted in function of the radial coordinate of the bone. In long bones, bone diameter and cortex to medulla density ratios were determined.

This procedure did not provide absolute bone mineral densities (in  $g/cm^3$ ) but only relative numbers (arbitrary units). Nevertheless, comparison of satin, CKD and control groups was possible. The control group was taken as a reference.

The differences were analyzed by means of one-way ANOVA and pairwise Student t-tests with Bonferroni correction using the R 3.0.2 software package;  $p < 0.05$  was considered significant.

Animal ID	Age (yr)	Sex	Clinical findings	Necropsy findings
Case 3	2	♂	Dental disease	Kidney lesions
Case 4	2	♂	Severe dental disease	Kidney lesions
Case 5	5.5	♂	Severe dental disease	Kidney lesions
Satin 1	2	♀	Anorexia (dental disease?)	Kidney lesions
CKD 1	3	♀	-	Kidney lesions
CKD 2	1.5	♀	Abortion	Kidney lesions

CKD 3	6	♂	Moderate dental disease	Kidney lesions
Control 1	4	♀	Respiratory tract disease	Lung lesions
Control 2	2	♀	-	-
Control 3	1.5	♀	Retentio secundinarum	Necrotizing placentitis
Control 4	1	♀	-	-
Control 5	4	♀	Acute death	Haemothorax

Table 6.1: An overview of the participating animals. Case 3-5 – satin guinea pigs taking part in clinical and histopathology investigations (see Chapter 7), Satin 1 – satin guinea pig found dead after a period of anorexia, CKD 1-3 – non-satin animals with gross kidney lesions at necropsy, Control 1-5 – non-satin animals.

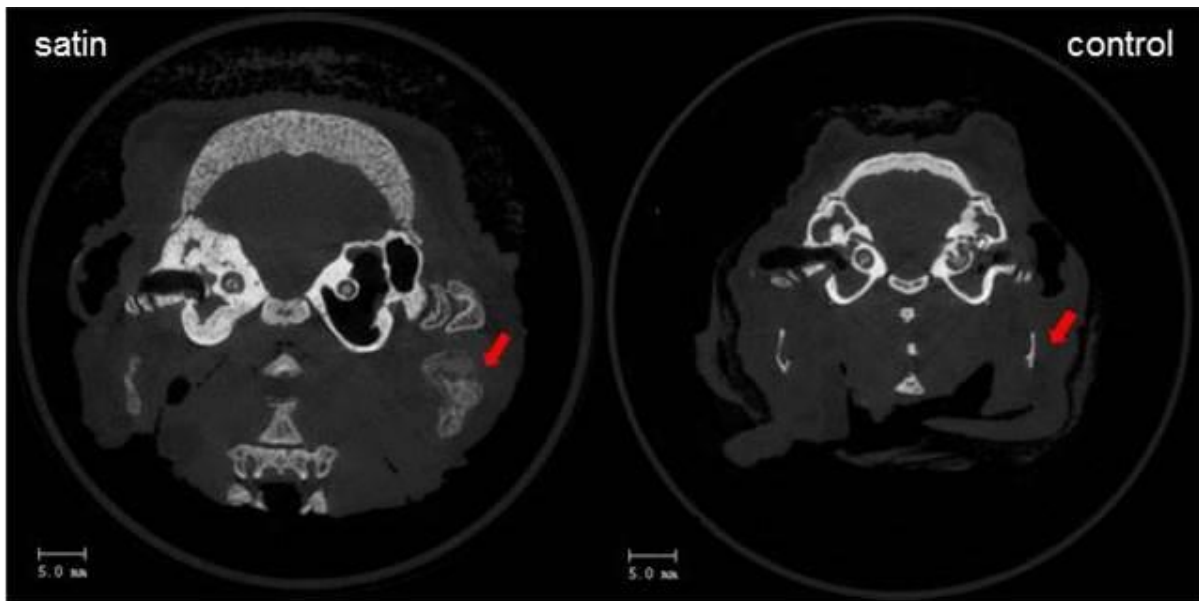


Fig. 6.2: Transversal slices of guinea pig skulls at the level of *bulla tympanica*. Left – satin (2.5 year old), right – non-satin (4 year old). Note the changes to the *ramus mandibulae* (arrows), calvarium and *bullae* in the satin animal.

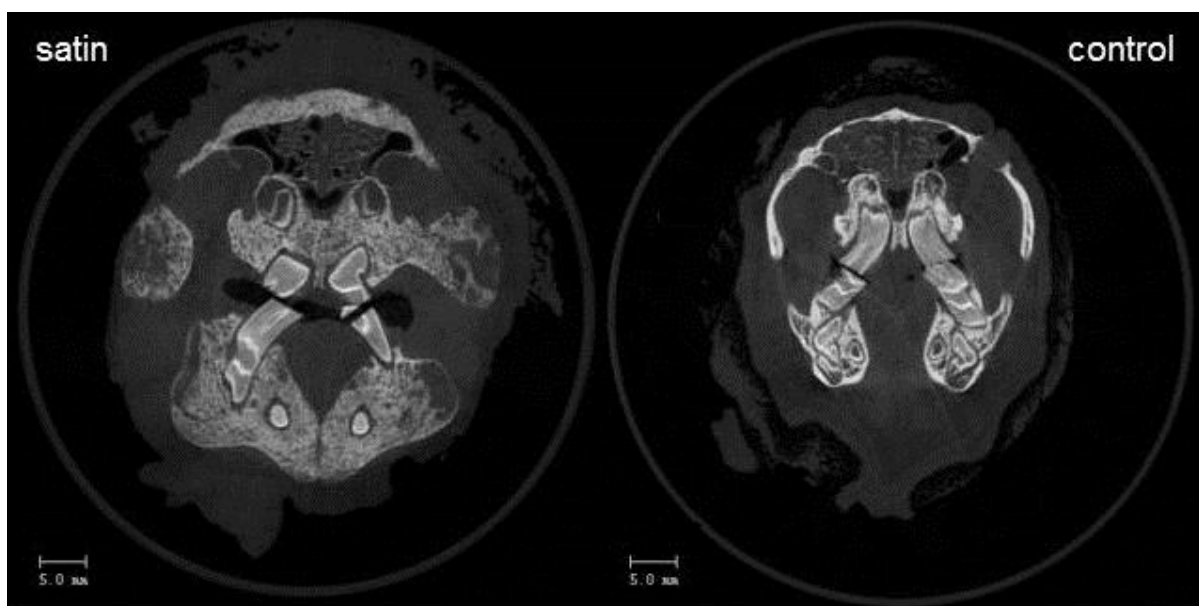


Fig. 6.3: Transversal slices of guinea pig skulls at the level of premolars. Left – satin (2.5 year old), right – non-satin (4 year old). Note cystic lesions in the bone and unaltered molars in the satin animal.

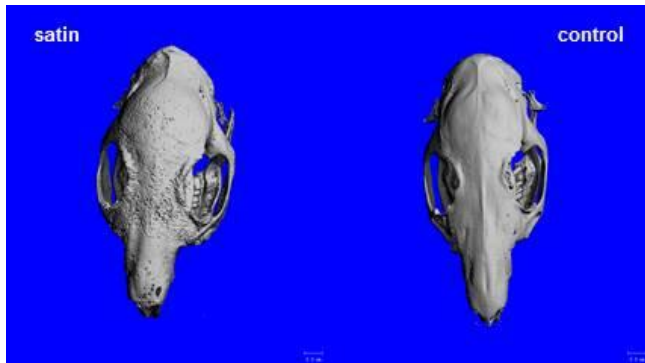


Fig. 6.4: Dorsoventral views of guinea pig skulls. Left – satin (4 year old), right – non-satin (4 year old).

## 6.3. RESULTS

### 6.3.1. General bone morphology

The VivaCT 40 scanner had a very good resolution and provided insight in the fine structure of the bone. Gross deviations were found in all examined bones. Figures 6.2 and 6.3 depict typical pathological features in the skull: thickening of calvarium and (unilaterally) *bulla tympanica*, degeneration

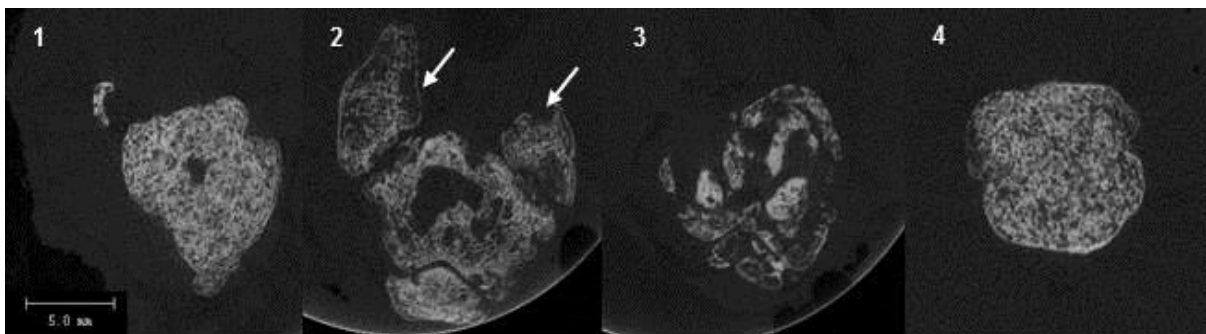


Fig. 6.5: Cross-sectional images of satin guinea pig (age 2.5 years) tibia and femur. 1 – tibia, proximal 1/3 diaphysis; 2 – proximal tibia, at the level of fabellae (arrows); 3 – tibia, epiphysis; 4 – femur, mid-diaphysis.

of mandibular branches, large cystic lesions in the alveolar bone and zygomatic arch. The bone had a characteristic fine patchy structure; areas of increased radiolucency were intermingled with radiopaque zones. Three-dimensional reconstructions revealed numerous indentations in the periosteum of the skull (Fig. 6.4). Despite drastic changes to bones, teeth of satin guinea pigs had a normal radiographic appearance.

The whole hind extremity was affected (Fig. 6.5). The mid-diaphyseal sections showed expansion of cortex and suppression of the bone marrow cavity; in the femur, the medullary cavity was not present anymore. Cortical bone was replaced by a meshwork of radiolucent and radiopaque spots, as was the case in the skull. The metaphyseal portion of tibia and fabellae contained numerous radiolucent zones (cysts). Radiopaque and radiolucent patches were found in the epiphysis.

### 6.3.2. Dental disease

Fig. 6.6 displays several views of satin (case 4) and non-satin guinea pig skulls, obtained with the Philips Mx8000 Dual scanner. No large cystic lesions, such as in Fig. 6.3, were found. The resolution was insufficient to visualize fine structural details of the bone surface. Nevertheless, striking differences between the control and satin groups could be observed. In control animals, the mandibula had a solid and smooth ventral surface, and pronounced radiopaque branches (*rami mandibulae*). Zygomatic arches appeared solid. In the rostrocaudal view, the molar arcade was symmetric with the normal dorsobuccal to ventrolingual inclination of the occlusal planes (at an angle of 50-52° with respect to the sagittal plane). In satin guinea pigs, the mandibular branches had a radiopacity close to that of soft tissues. Various grades of dental disease were observed. Cases 3-5 had markedly

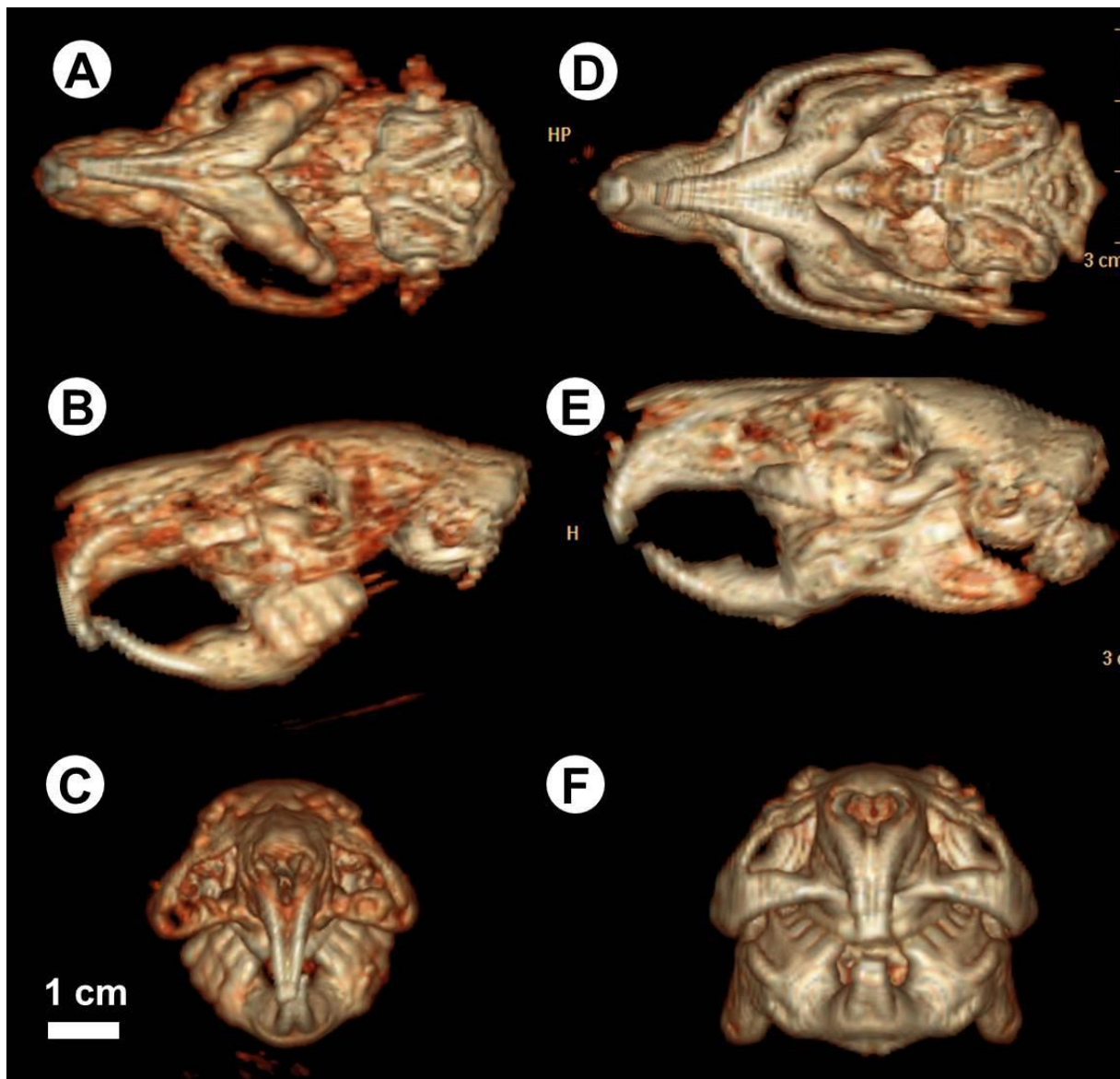


Fig. 6.6: Three-dimensional reconstructions of skulls: A-C – satin (case 4) and D-F – non-satin (control 2). Note the absence of mandibular branches and the presence of nodules in the ventral aspect of mandibula in A-C, caused by deformed molar apices.

thickened mandibulae (Figs 6.6-6.8) with clearly visible nodules in their ventral aspects. The nodules were due to hypertrophic molar apices (“bulging”). In case 3, a “spike” – buccal deviation of the left maxillar M2 crown was present (Fig. 6.7). Case 5 displayed severe deformities in the reserve crowns of mandibular molars. To visualize the reserve crowns and to accentuate the deformities, a three-dimensional image of deep bone layers was computed using the Philips Mx8000 Dual software and superimposed on the lateral oblique view of the skull. The right mandibular M2 was thickened and its apex protruded beyond the jaw margin (Fig. 6.8). The lesions in the other satin guinea pig (satin 1) were less prominent (Fig. 6.9). The CKD group had a normal bone morphology and molar alignment, except CKD 3 where ruffling of the ventral aspect of the mandibula and steepening of the occlusal plane was observed (Fig. 6.10). The measured inclination angles of the occlusal planes are listed in Table 6.2. In animals with pre-mortally documented dental disease, the inclination angle was smaller. This means that the occlusal plane was steeper.

	Satin (N=4)				CKD (N=3)			Control (N=5)				
ID	C3	C4	C5	S1	Ck1	Ck2	Ck3	C1	C2	C3	C4	C5
$\alpha$ ( $^{\circ}$ )	46.2	38.6	44.7	43.0	50.1	52.8	40.5	49.8	53.1	51.3	53.4	53.1
<b>Av.</b>	<b>*43.1<math>\pm</math> 3.3</b>				<b>47.8<math>\pm</math> 6.5</b>			<b>52.1<math>\pm</math> 1.6</b>				

Table VI.2: Inclination angle of the occlusal plane with respect to the sagittal plane. C3-5 – satin cases 3-5, S1 – satin 1, Ck1-3 – chronic kidney disease 1-3, C1-5 – controls (non-satin). \*  $p < 0.05$ .

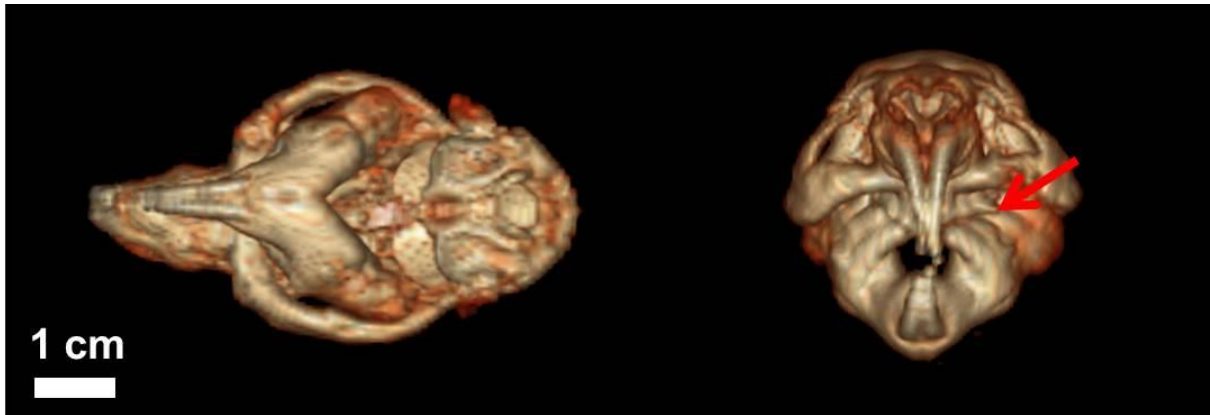


Fig. 6.7: Case 3 – thickening of the lower jaw at ventrodorsal view, asymmetry and molar malocclusion with buccal diversion (“spike”) of maxillary M2 crown (arrow).

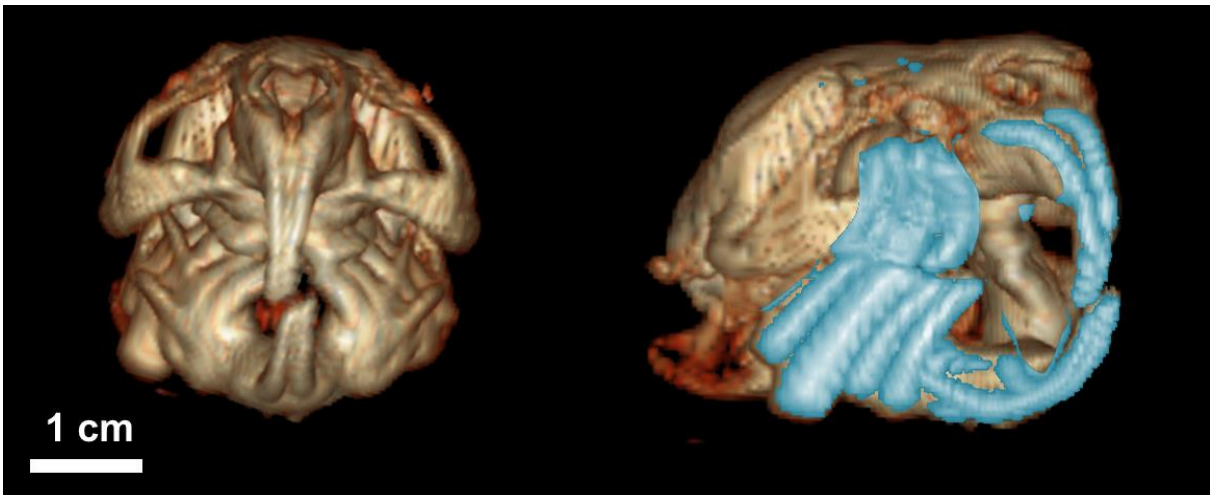


Fig. 6.8: Case 5 – jaw asymmetry and malocclusion of molars and incisors. Right image: computed reconstruction of molars superimposed on the lateral oblique view of the skull reveals a severely malformed mandibular M2.

### 6.3.3. Bone density measurements

Relative magnitudes of bone mineral density were determined for the satin, CKD and control groups. Average numbers per group are given in Table 6.3.

Rel. density (A.U.)	Satin (N=4)	CKD (N=3)	Control (N=5)	p Satin: Control	p Satin: CKD	p CKD: Control
Calvarium	125± 13	158± 6	161± 4	0.009	0.009	0.5
<i>Bulla tympanica</i>	237± 5 <sup>?</sup>	229± 38	251± 5 <sup>?</sup>	-	-	-
Alveolar bone	158± 19	226± 29	221± 22	0.003	0.03	0.8
<i>Ramus mandibulae</i>	58± 24	127± 31	137± 19	0.001	0.04	0.6
Molars	222± 15	207± 31	228± 23	0.5	0.6	0.5
Incisors	207± 19	234± 19 <sup>?</sup>	240± 10 <sup>?</sup>	-	-	-
Diaphysis femur	164± 28	181± 16	208± 16	0.04	0.4	0.08
Diaphysis tibia	146± 29	183± 7	204± 13	0.02	0.07	0.03
Epiphysis femur	113± 20	130± 5	142± 11	0.06	0.2	0.09
Epiphysis tibia	96± 27	129± 4	121± 19	0.2	0.09	0.5
Soft tissue (hind leg)	34± 2	28± 8	31± 2	0.06	0.3	0.5

Table 6.3: Relative mineral densities and p values for various bones in satin, CKD and control groups. A.U. – arbitrary units. In long bones, only the cortical density is given. ? signals were close to the saturation limit (255) and could not be compared.

The most prominent reduction of the mineral density in satin guinea pigs was observed in the skull bones: calvarium, *bulla tympanica* and jaws. In the hind extremities, significant differences with respect to the control group were found in mid-diaphyseal femurs and tibiae. In the CKD group, skull bones had no significantly altered density with respect to the controls. However, the mid-diaphyseal density of the tibia was lower than in control animals.

The radial density profiles of long bones, reflecting bone diameters and relative cortex en medulla radiopacities are shown in Figs 6.11 and 6.12, respectively. In non-satin guinea pigs, the medulla was radiolucent and the cortex to medulla density ratio was about 5:1. The radiopacity of the medulla was markedly increased in cases 3 and 4, and the density ratio was decreased to about 2:1, whereas the two other satin animals retained a fairly normal bone density profile. No remarkable deviations were observed in the CKD group. No large variations in bone diameter were seen in the examined animals.

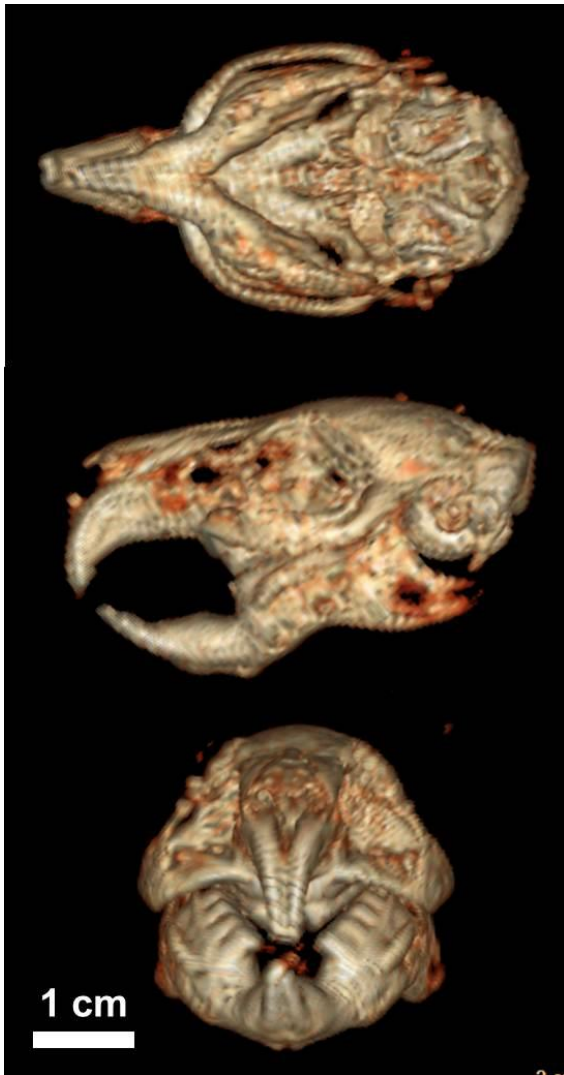


Fig. 6.9: Satin 1: less severe deformities: ruffled ventral aspect of the mandibular, mild malocclusion.

#### 6.4. DISCUSSION

High-resolution CT imaging demonstrated dramatic bone changes in satin guinea pigs. Abnormalities in trabecular bone of the skull and epiphyses, as well as in compact bone of extremities were observed. The normal bone structure was largely lost and replaced by a fine meshwork with alternating osteosclerotic and osteolytic zones. The bone surface contained numerous indentations. Large osteolytic lesions were present in the periosteal regions of the skull and long bones. Below, these features will be compared with typical bone changes in human hyperparathyroidism (Schiller and Teitelbaum, 1999).

In hyperparathyroidism, the porosity of the bone is increased and there is a characteristic “salt and pepper” pattern consisting of mixed osteolytic and osteosclerotic lesions (Jevtic, 2003). Skull bones are a predilection site for lesions (Lautenbach et al., 1968; Lee et al., 1996). The cortex of long bones is affected as well, and the bone marrow cavity is suppressed (Hruska and Teitelbaum, 1995). Characteristic indentations in the surface result from periosteal bone resorption where tunneling osteoclasts bore channels in the compact bone. These indentations eventually transform into large

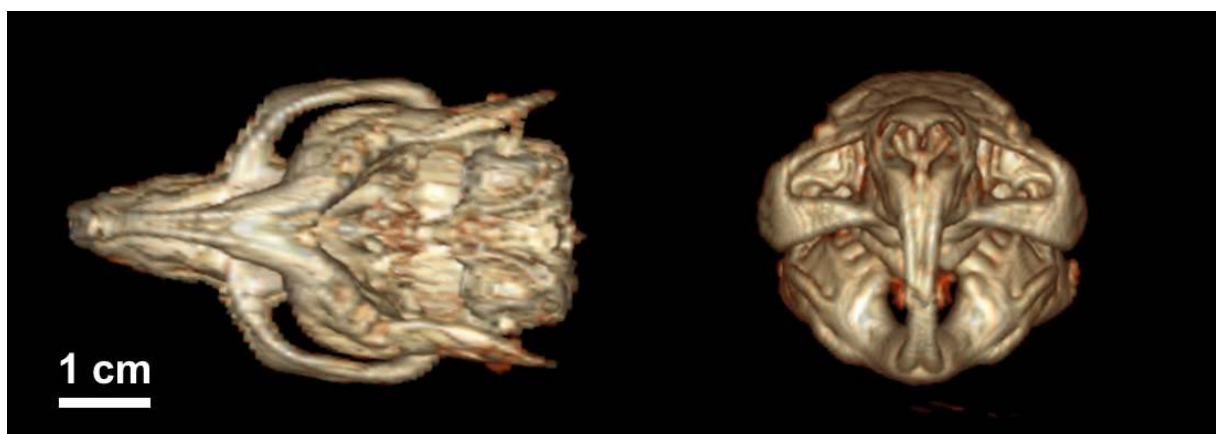


Fig. 6.10: A guinea pig with CKD (CKD 3): slight ruffling of the ventral mandibular margin and moderate malocclusion.

delineated cystic lesions (brown tumors, see Fig. 6.13 and Chapter 2, Fig. 2.4). Brown tumors are typical for of renal osteodystrophy in humans and often represent end-stage kidney and bone disease – *osteitis cystica fibrosa* (Chew and Huang-Hellinger, 1993; Schiller and Teitelbaum, 1999;

Triantafyllidou et al., 2006). The radiographic appearance of skulls and extremities in satin guinea pigs is strongly reminiscent of that of hyperparathyroidism in humans: “salt and pepper” like patterns and periosteal cysts are present in the skull bones, and suppression of the medulla in long bones is also clear (Jevtic, 2003).

The relationship between lesions and clinical symptoms may be difficult to quantify. Satin animals

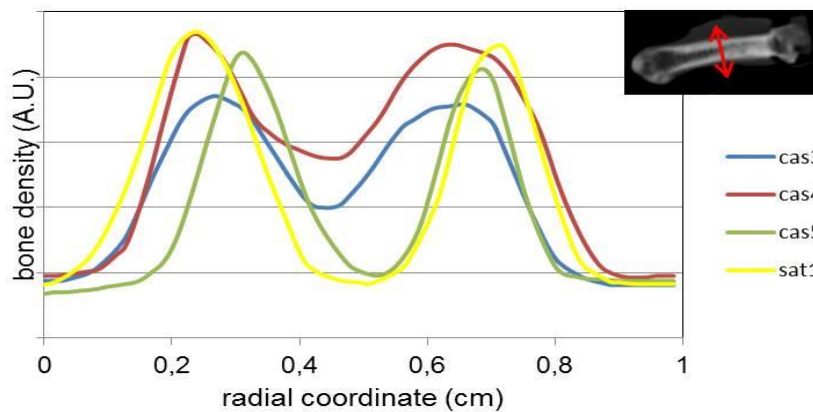


Fig. 6.11: Radial bone density profiles in satin guinea pigs. Note the increased radiopacity of medulla in case 3 and 4. Insert: longitudinal section through a femur, with the position and coordinate(x axis) indicated.

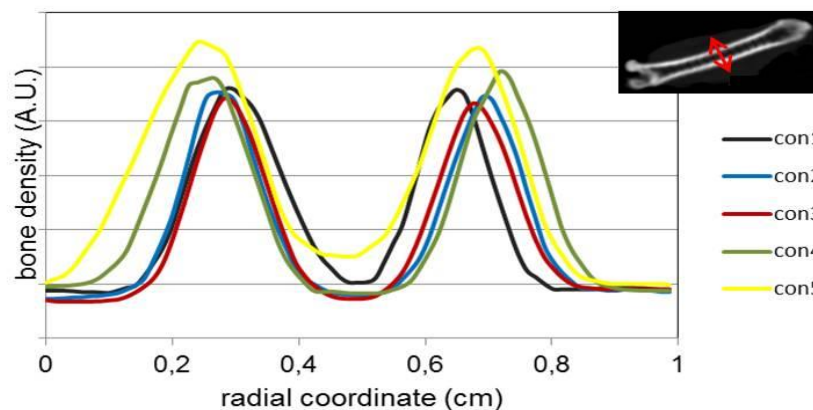


Fig. 6.12: Radial bone density profiles in control animals. Insert: longitudinal section through a femur, with the position and coordinate indicated.

There is too little data to establish statistically sound links between clinical symptoms and radiographic bone abnormalities. It can be however expected that an advanced degree of bone resorption such as displayed in Figs 6.2-5 will result in severe debilitation, anorexia and lameness.

Despite its practical limitations in studying living animals, CT imaging is a very efficient diagnostic method to describe dental pathology (Capello and Lennox, 2008). Radiographic signs of dental disease such as incisor and molar malocclusion, thickening and roughening of the alveolar bone of the mandibula were evident in all examined satin guinea pigs. Nodular jaw deformity caused by hypertrophic molar reserve crowns (“bulging”) was seen in advanced cases. Interestingly, the first sign of malocclusion was a change in the inclination angle between the occlusal and sagittal planes. In dental disease, also in absence of hypertrophic molars, the occlusal plane appeared steeper, which is

examined using VivaCT 40 were in an advanced stage of disease and had severe general (anorexia) and lameness symptoms. In these animals, end-stage lesions such as brown-tumor like cysts were observed in the skull as well as in epiphyseal portions of long bones. This radiographic presentation is compatible with *osteitis cystica fibrosa* (Chapter 5, Section 5.3). Animals scanned with Philips Mx8000 Dual displayed much milder general symptoms and no evident lameness. The resolution of the Philips apparatus would allow visualizing large features, such as cysts, but none were observed in this

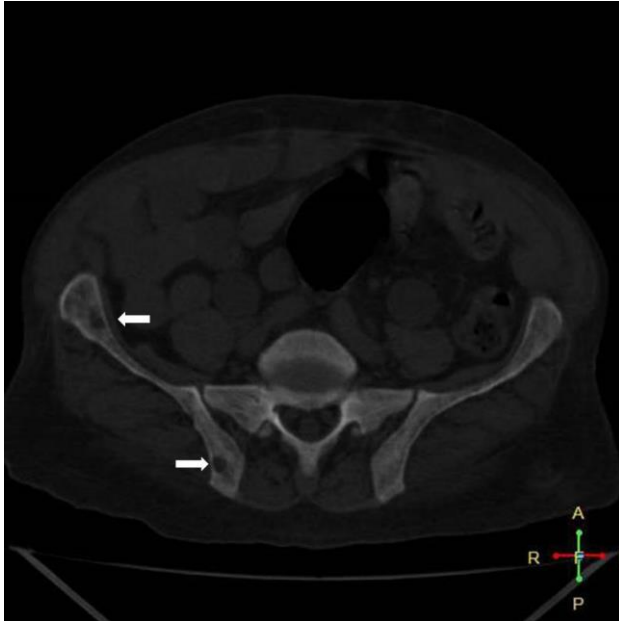


Fig. 6.13: A transverse CT section of human abdomen showing altered bone structure and osteolytic lesions (arrows) in pelvis and vertebrae in human renal hyperparathyroidism. Contributed by Dr A. Abd Rabou. Reproduced by courtesy of Dr. F. Gaillard, Editor, <http://radiopaedia.org>

likely to be caused by lateral deviation of the molar apices. This deformity might be caused by deteriorated mechanical properties (decreased hardness) of the alveolar bone. Lower jaw molars normally have an oblique dorso lingual to ventro buccal orientation. During mastication, their crowns are subjected to pressure, mainly in the dorsoventral direction, and may act as levers. When the alveolar bone rigidity is compromised, the bone cannot provide adequate support and the apices may be displaced buccally, resulting in a more horizontal positioning of molars.

Based on the results of the current study, it cannot be unambiguously decided whether satin guinea pigs are predisposed for dental disease. The statistical studies (Chapter 3) were also not conclusive. However, there may be an intrinsic correlation between dental disease and metabolic bone disease. Mineralization of dental tissue does not undergo the same hormonal regulation as bone remodeling. In rodents it is governed by other mechanisms than in humans (Bosshardt and Schroeder, 1996). In guinea pigs and rabbits, dental tissue mineralization is a complex process that is initiated by formation of so-called cementum pearls that are subsequently mineralized. For the latter step, osteoclastic resorption of alveolar bone is indispensable, because it delivers calcium (Jayawardena et al., 2002). In hyperparathyroidism there is enhanced osteoclastic activity, and jaws are a predilection site for bone resorption (Lautenbach et al., 1968). It is thus plausible to assume that such changes would also influence tooth formation. In particular, excessive mineralization of dental tissue and hypertrophy of reserve crowns may be expected. A correlation between acquired dental disease and metabolic disorders (hyperparathyroidism) in rabbits was hypothesized by Harcourt-Brown (2007). More research is needed to verify the coincidence of these conditions and to reveal their interactions and a potentially common pathological background.

Bone density measurements revealed large differences between satin and non-satin guinea pigs. The satin group had a significantly reduced bone density, especially in the trabecular bones of the skull: calvarium, alveolar bones and *rami mandibulae*. The latter were not visible in three-dimensional reconstruction images (Figs 6.6-7). The long bones were affected, too. In fact, largest deviations were observed in the diaphysis (compact bone). In the CKD group there was also a reduction in bone density, but its significance was lower. Only the diaphysis of tibia was markedly affected.

Bone resorption is a hallmark of secondary hyperparathyroidism. In renal hyperparathyroidism and bone disease, bone densitometry is an important diagnostic method to evaluate the stage of disease (Rix et al., 1999). As pointed out by Hruska and Teitelbaum (1995), in renal

hyperparathyroidism bone loss may be more pronounced in the diaphyseal than in epiphyseal regions of long bones. Epiphyses consist of trabecular bone. In the trabecular bone, accumulation of woven bone may result in an unchanged or even a higher than normal bone density (sclerotic lesions, Jevtic 2003). This is consistent with the current findings in the satin and CKD groups, where significant differences were found in diaphyses and not in epiphyses of long bones.

Although no gross bone lesions such as brown tumors were found in this group of satins, the animals had undeniable radiographic signs of bone pathology. The significant decreases of bone density provide sound evidence.

Note that the mineral density of the teeth was similar in all groups, regardless of the presence of the satin factor or dental disease. This is consistent with the fact that tooth mineralization is regulated by other processes than bone remodeling.

The radial density distributions showed a remarkable increase in the radiopacity of the medulla in two satin cases (Fig. 6.12). This feature corresponds to suppression of the medulla, which is consistent with other medical imaging findings (Fig. 6.5). Suppression of bone marrow cavity is a typical sign in hyperparathyroidism; it is readily demonstrated by means of radiography and histopathology. Microscopically, it reflects the second stage of renal bone disease – *osteitis fibrosa* (Schiller and Teitelbaum, 1999).

## 6.5. CONCLUSION

Computed tomography is a powerful tool to demonstrate bone and tooth pathology in guinea pigs. It allows visualizing the lesions and quantifying the degree of bone damage. Although it may be not practical as a diagnostic to monitor the disease progress in living guinea pigs, it yields insights that are helpful in resolving the pathophysiology of unknown disorders. In case of satin guinea pigs, bone lesions typical for hyperparathyroidism are present. Reduced bone mineral densities support this diagnosis. CT imaging alone does not yet allow identifying the cause of hyperparathyroidism. The observed lesions are suggestive of renal osteodystrophy in humans, but any interspecies extrapolations should be made with great reserve.

## 7. CLINICAL DIAGNOSTICS AND HISTOPATHOLOGY

### 7.1. INTRODUCTION

There are many unanswered questions concerning the pathophysiology of the satin syndrome. Studies performed in the past generated many indications and hypotheses; however, none of these hypotheses could be confirmed. Based on radiography and blood tests, several authors (Schwartz et al., 2001; Jordan, 2008; Rapsch-Dahinden et al., 2009; Jordan et al., 2009) suggested that satin cavies were afflicted by fibrous osteodystrophy of unknown origin. Interestingly, Jordan and coworkers reported macroscopic kidney lesions in the majority of animals subjected to post-mortem examination. Massop (2009) found cystic kidneys in one of two necropsied satin cavies. Preliminary computed tomography and histopathology data yielded hints for the underlying renal pathology, but this association was not elaborated.

Diagnosis of the satin disease was not evident in living animals. Blood tests, in particular serum biochemistry did reveal abnormalities (Jordan 2008), but specificity of such tests is limited. Moreover, blood tests usually do not provide new insights into pathophysiology of a disease. The same was valid for routine radiography. Although specific pathological conditions of the bone may translate into unique radiographic features in humans (Jevtic, 2003; Chang et al., 2007, see also Chapter 2 and VI), one cannot always extrapolate these findings to animals. Macroscopic patterns of bone loss are likely to be species-dependent.

To unravel the mechanisms responsible for bone and kidney disease in satin guinea pigs, one has to carry out a random survey and systematically record all abnormalities in affected individuals. This cannot be easily accomplished. The satin breed has become scarce and it is difficult to provide a statistically sound number of animals for the investigation. Therefore, it is particularly important to combine numerous *in vivo* and post-mortem diagnostic methods and to maximize the amount of information per animal.

In this chapter, seven cases of terminal satin guinea pigs are described. Blood and urine tests were carried out and potentially affected tissues and organs were analyzed upon necropsy. Kidney and bone lesions were evaluated. Microscopic features of affected kidneys were described quantitatively.

### 7.2. MATERIALS AND METHODS

Seven satin guinea pig cases were elaborated in this study. Three animals deceased spontaneously, and four were examined clinically ante-mortem. Blood samples were collected via cardiac puncture in animals deeply anaesthetized with an overdose of medetomidine (5 mg/kg) en ketamine (50 mg/kg), immediately followed by intracardiac injection of T-61. Standard hematology and serum biochemical data were obtained (Medvet Laboratories, Belgium). In evaluating blood values and performing statistical analyses, retrospective data (Massop, 2009) were included. The total number of screened satin animals was 15 (N=15). Control data for blood (N=9) were provided by veterinary practitioners (Dr. Frank Verstappen, Veterinary Clinic Hoofdstraat, Driebergen, The Netherlands). When feasible, urine was collected and submitted for biochemical analysis. Control samples were obtained by collecting urine from four healthy guinea pigs sheltered by the author.

In three of the submitted satin animals, computed tomography scans of skull and hind extremity were recorded (Chapter 6).

Histopathology was carried out on seven satin guinea pigs (N=7, see above) and one non-satin animal (case 8) with symptoms of chronic kidney disease (CKD) and gross morphological kidney lesions upon necropsy. Four Dunkin-Hartley guinea pigs (N=4) of about 4 years of age were used as controls. The cadavers were dissected within approximately 2 hours after sacrifice. Gross morphological features were evaluated and cytology of caecum (Hemacolor) was performed. The following tissues and organs were harvested: skin from the lateral aspect of the hind extremity, kidneys, parathyroid glands and long bones (femur and tibia). Samples were fixed using 10% buffered formaldehyde and after 3-4 days transferred to 70% ethanol. Bones were prepared by soaking overnight in a decalcification buffer (8% HCl), according to standard protocols (Verdenius and Alma, 1958). The following histopathology stains were used: haematoxylin-eosin (H&E) for all tissues, and periodic acid Schiff base (PAS), Von Kossa, Van Gieson, and Kongo red for the kidneys.

Histological specimens were examined using a Leica light microscope equipped with a camera. Quantitative measurements of tissue properties (dimensions and areas of structures) were performed using the Leica Suite 3.8 software package. For each individual, 5 to 10 data points on skin thickness, cross-sectional area of the parathyroid gland, glomerular area, glomerular basal membrane thickness, Bowman space gap length and the area of proximal tubule cells were collected. To assess renal calcinosis, Von Kossa stained kidney sections were processed using ImageJ software, and relative surface areas of stained (calcified) zones were calculated. Measurement points were spread uniformly through various zones of the tissue. Statistical analyses were performed using the R 3.0.2 software package. Significance was tested by means of pairwise Student t-tests with Bonferroni correction and one-way ANOVA with linear contrasts (cell means model);  $p < 0.05$  was considered significant.

## 7.3. RESULTS

### 7.3.1. Anamneses and necropsy findings

Table 7.1 summarizes the medical history and clinical findings in the screened animals. In general, satin guinea pigs submitted to clinical examination had an extremely low body condition score (cachexia), were lethargic and reluctant to move. Three of them had a history of dental disease. Necropsy did not reveal any lesions that would be suggestive of infection. There were no significant changes to heart, lungs, liver (except case 6), spleen and intestines. Numerous yeast cells were found in caeca of two satin animals. The most striking necropsy findings were related to bones and kidneys. The bones of satin animals were extremely soft and elastic. Even the cortex of long bones such as femur and tibia could be easily cut with a scalpel. The gross appearance of the kidneys was aberrant. The organs were darker and visibly smaller than in controls and had indentated surfaces (pitting of the cortex). In two satin animals cystic kidney lesions were found. Bladder walls were markedly thickened. Large casts, composed of gelatinous protein-rich substance, were recovered from the bladders.



Fig. 7.1: Macroscopic appearance of a satina guinea pig kidney (case 1). Note the irregular surface with numerous indentations.

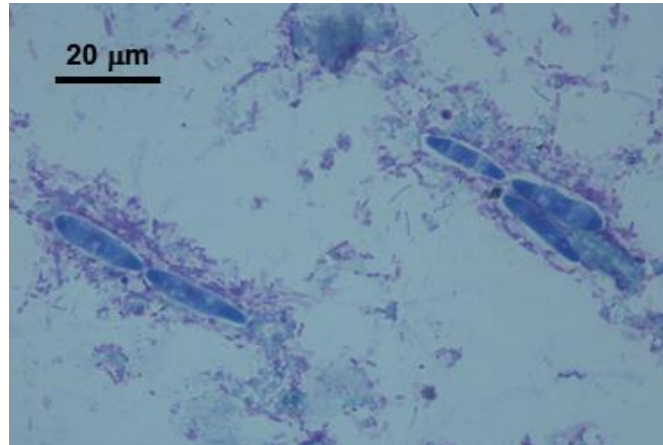


Fig. 7.2: Caecum cytology of case 2 (Hemacolor). The large basophilic cells bear a morphological resemblance to yeasts of the genus *Candida*.

Animal ID	Age (yr)	Sex	Weight (g)	Symptoms	Main post-mortem findings	Remarks
1	3	♂	870	Severe lameness (score 4, see Chapter 3), cachexia.	Gross kidney lesions: indentations (Fig. 7.1), cortex-medulla ratio <1:1.5. Swollen knee joints. Yeasts (compatible with <i>Candida</i> spp.) in caecum.	
2	4	♀	690	Profuse diarrhoea followed by shock.	Distended caecum with microorganisms (Fig. 7.2), serohaemorrhagic fluid in peritoneal cavity, congested liver.	Died spontaneously.
3	2	♂	550	Dental disease, anorexia, cachexia.	Gross kidney lesions (see case 1).	CT data available.
4	2	♂	1020	Dental disease, anorexia, cachexia.	Gross kidney lesions.	CT data available.
5	5.5	♂	800	Intermittent lameness (score 1), dental disease, anorexia and cachexia.	Cystic kidneys (7.3), end-stage dental disease (Fig. 7.4).	CT data available.
6	2	♀	1140	Intermittent lameness (score 1), anorexia, sudden collapse.	Hydrothorax, hydroperitoneum. Multifocal well-demarcated whitish lesions in the liver.	Died spontaneously. Case 6 was a heterozygote (Sasa).
7	6	♀	900	Profuse diarrhoea followed by shock.	Distended caecum, cystic kidneys.	Died spontaneously.
8	8	♂	1100	Weight loss, polydipsia/polyuria, and intermittent lameness. Collapse and death.	Cystic kidneys.	Non-satina animal. Natural death at old age.

Table 7.1: An overview of clinical and post-mortem findings in studied cases.

### 7.3.2. Blood and urine parameters

The results of routine blood tests are summarized in Table 7.2. Serum biochemistry revealed



Fig. 7.3: A cortical cyst in case 5.



Fig. 7.4: Advanced dental disease in case 5. Exposed ventral aspect of the mandibular bone, showing a large lesion caused by overgrown molar apices (arrow).

most abnormalities. In satin guinea pigs serum calcium and calcium to phosphate ratio were significantly lower and alkaline phosphatase significantly higher than in the controls. In several subjects, calcium phosphorus products were higher than  $100 \text{ mg}^2\text{dl}^{-2}$ , but this was observed in both satin and non-satin groups. Average blood urea nitrogen, alanine aminotransferase and glucose were moderately elevated, but large variations were present within both (satin and non-satin) groups. In all animals, amylase was higher than indicated by the reference range (Suckow et al., 2012).

Haematological profiles were largely within the norm. Sporadically, some values fell beyond the reference range but no trends could be discovered. Case 3 and 4 displayed mild neutrophilia: 13720 and 15670 cells per microliter (reference range 300-12000). All values characterizing red blood cells were recorded with special attention; this is because renal dysfunction may result in mild anemia (Eschbach, 1989). However, no peculiarities in blood smears and red blood cell features were found. Haematocrit of a few individuals was slightly elevated.

Animal group	Ca (mg/dl)	P (mg/dl)	Ca/P	Ca x P ( $\text{mg}^2\text{dl}^{-2}$ )	ALP (IU/l)	BUN (mg/dl)	Cre (mg/dl)	Amy (IU/l)	Alb (g/dl)
Average satin (N=15)	*8.64 ± 2.52	5.49 ± 2.52	*1.92 ± 1.39	49± 29	*117 ± 69	**41 ± 40	0.89 ± 0.61	**1942 ± 813	2.93 ± 0.62
Average control (N=9)	*12.6 ± 3.40	4.71 ± 1.91	*2.84 ± 0.68	65± 40	*51 ± 18	29 ± 13	1.07 ± 0.41	**1945 ± 470	2.91 ± 0.47
Ref. range <sup>1,2</sup>	5.3-12	3-12	-	-	18-28	9-32	0.6-2.2	995-1239	2.1-3.9

Animal group	ALT (IU/l)	TBil (mg/dl)	Glu (mg/dl)	Na (mEq/l)	K (mEq/l)	HCT (%)	MCV (fl)	MCH (pg)	MCHC (g/dl)
Average satin (N=5)	**67 ± 52	0.36 ± 0.12	**160 ± 37	143 ± 4	4.7 ± 0.9	50.5 ± 12.3	79.1 ± 4.7	24.3 ± 1.5	30.7 ± 1.7
Average control (N=9)	**46 ± 12	0.27± 0.05	**190 ± 41	144 ± 8	4.7 ± 0.5	-	-	-	-
Ref. range <sup>1,2</sup>	10-25	0.3-0.9	60-125	132-156	4.5-8.9	34.9-52.3	70-95	23-27	25-40

Table 7.2: Selected serum biochemical and haematological data in satins and controls. ALP – alkaline phosphatase, BUN – blood urea nitrogen, Cre – creatinine, Amy – amylase, Alb – albumin, ALT – alanine aminotransferase, TBil – total bilirubin, HCT – haematocrit, MCV – mean cell volume, MCH – mean cell haemoglobin, MCHC – mean cell haemoglobin content. Reference ranges 1 – Hrapkiewicz and Medina 2007, 2 – Suckow et al., 2012.\* p<0.05, \*\* values outside the reference range, significance unknown.

Only few complete data sets could be obtained from urine tests. The average urine specific density of satin guinea pigs was 1.025± 0.015 g/ml (reference range 1.005-1.030 g/ml); some animals produced concentrated urine (>1.04 g/ml). pH was variable (6.5-8.5), dependent on the condition of the animal. Severely debilitated satin animals had low urine pH values. The average creatinine concentration was found to be 21± 9 mg/dl in satins and 33± 21 mg/dl in controls. Significant proteinuria was detected in the satin group. In cases 1, 3 and 4 the urinary protein concentrations were 1.17, 0.80 and 0.84 g/dl. Combining these data and the corresponding urine and serum creatinine levels allowed estimating the sieving coefficient, defined as the fraction of serum albumin that is filtered by the glomerulus:

$$\text{sieving coefficient} = \frac{[\text{Alb}]_{\text{urine}} [\text{Cre}]_{\text{blood}}}{[\text{Cre}]_{\text{urine}} [\text{Alb}]_{\text{blood}}} \times 100\%$$

It was assumed that the urinary protein was albumin from blood serum and that no post-glomerular protein secretion took place. Sieving coefficients were found to be 3.5, 1.9 and 1.8%, respectively. This is significantly higher than expected for a healthy kidney (Tojo and Kinugasa, 2012). Note that an adult guinea pig has an average urinary output of 90-100 ml per 24 h. Thus, animals with urinary protein concentrations of 0.8-1 g/dl, excreted 0.7 to 1 g of protein daily.

### 7.3.3. Histopathology

#### 7.3.3.1. Integument.

Stained (H&E) specimens of skin of satin and control guinea pigs are shown in Fig. 7.5. No

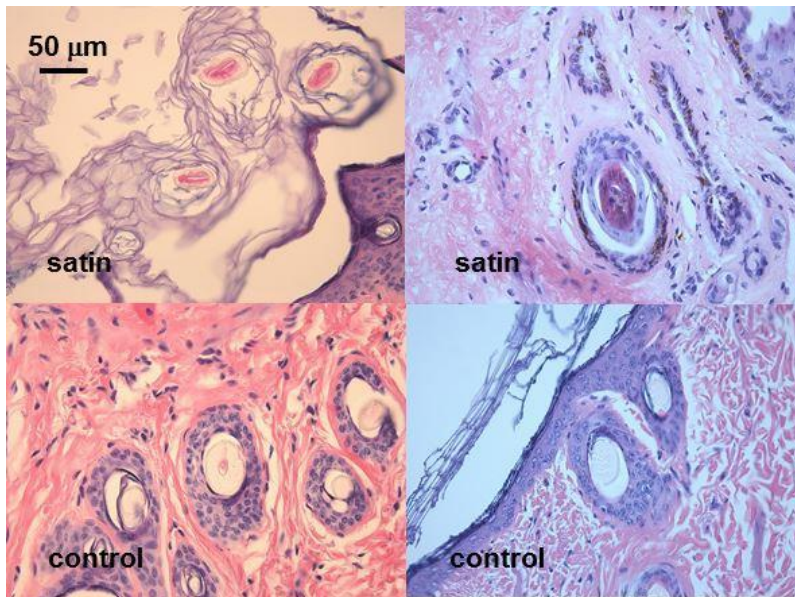


Fig. 7.5: Skin of satin and non-satin guinea pigs. H&E stain.



Fig. 7.6: Hair shafts of satin and control animals. Oil immersion was applied to reduce light scattering by the surface (cuticle) and to display the internal structure.

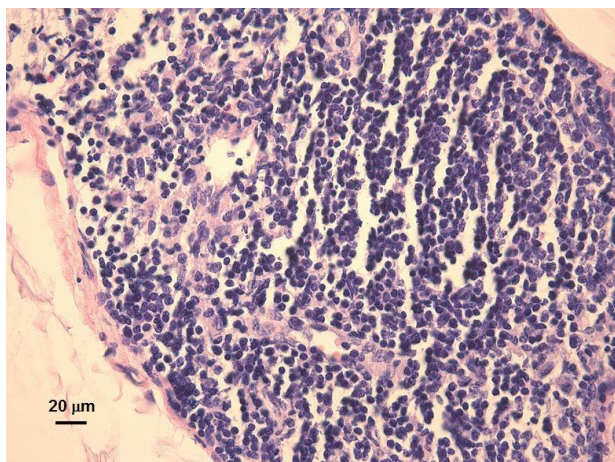


Fig. 7.7: A parathyroid gland of a control (1) guinea pig, showing typical cell strings. H&E stain.

remarkable morphological differences were observed between the groups. There were large variations in the thickness of epidermis, both in satin and control animals. Epidermis of satin guinea pigs was on average thicker ( $26.3 \pm 18.2 \mu\text{m}$ ) than this of controls ( $19.5 \pm 7.0 \mu\text{m}$ ), but the difference was not significant. Hair of satin guinea pigs could be clearly distinguished by its expanded intensely eosinophilic medulla (Fig. 7.5). Unstained oil-immersed pictures of the hair shaft (Fig. 7.6) displayed a strongly reduced network of cortical keratin fibers in satins as compared with controls.

#### 7.3.3.2. Parathyroid

A normal, well demarcated nodular part (*pars compacta*) of the parathyroid gland in a control

animal is shown in Fig. 7.7. Although there were substantial variations within each group, parathyroid glands in satin guinea pigs were found to be much larger than in controls: the average cross-sectional areas were  $4.4 \pm 4.0 \text{ mm}^2$  and  $0.35 \pm 0.3 \text{ mm}^2$  respectively ( $p < 0.05$ ). Abnormal glands (cases 3 and 5) are displayed in Fig. 7.8. A drastically enlarged *pars compacta* was firmly attached to the thyroid. The diffuse part, consisting of chief cells infiltrating the thyroid interfollicular space appeared to be hyperplastic, too. Microscopically, glands of

satin animals contained mainly chief cells with large nuclei and multiple distinct nucleoli, relatively few

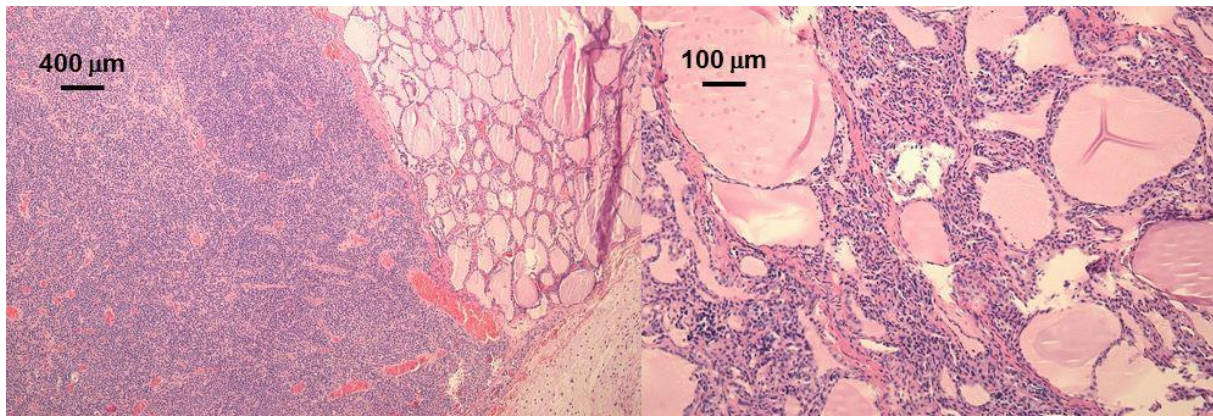


Fig. 7.8: Parathyroid glands of satin guinea pigs. Left (case 3) – pars compacta and pars diffusa within thyroid, right (case 5) – pars diffusa. H&E stain.

oxyphil cells and no fat cells (Fig. 7.9). Large amounts of eosinophilic material were deposited within the parenchyma. The parathyroid gland of a non-satin guinea pig with CKD (case 8) had a similar morphology to the glands of satins.

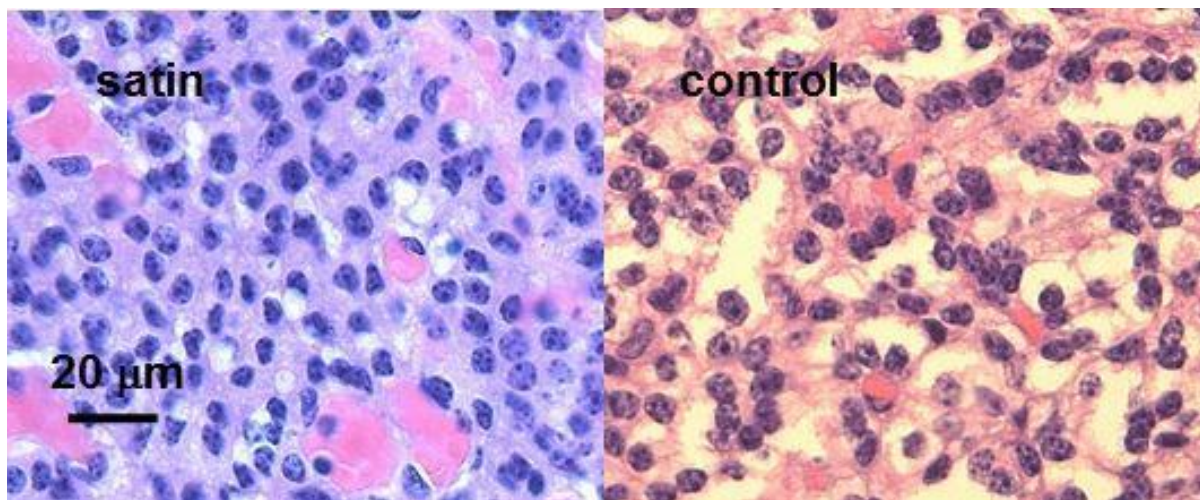


Fig. 7.9: Parathyroid glands of satin (case 5) and control (1) guinea pigs.

#### 7.3.3.3. Bone

Sections of femur diaphysis and distal metaphysis are shown in Fig. 7.10. Diaphyseal bone (cortical or compact bone) of control guinea pigs had in most cases a normal architecture of lamellar bone, with peripheral circumferential and endosteal lamellae enclosing well-delineated, regularly shaped osteons (Haversian systems) in the central cortex region. Metaphyseal sections contained trabecular (cancellous) bone and a growth plate. In small animals such as rats, mice and guinea pigs the growth plate is retained throughout the lifetime (Roach et al., 2003). Trabecular bone of epiphysis had a lamellar structure and the intertrabecular space was filled with red marrow. A close-up of a cortical section is given in Fig. 7.11a. Osteons had a normal structure with their central Haversian canal, surrounded by nearly concentric, smooth lamellae. Thin cement lines (basophilic remnants of past remodeling activities) demarcated the individual lamellae. Lacunae with osteocytes were distributed regularly between the lamellae. However, certain regions of diaphysis had an altered appearance (Fig. 7.11b), characterized by a loss of smooth lamellar structure, presence of broadened, fringed or scalloped cement lines (reversal lines) and chaotic distribution of osteocytes. These features

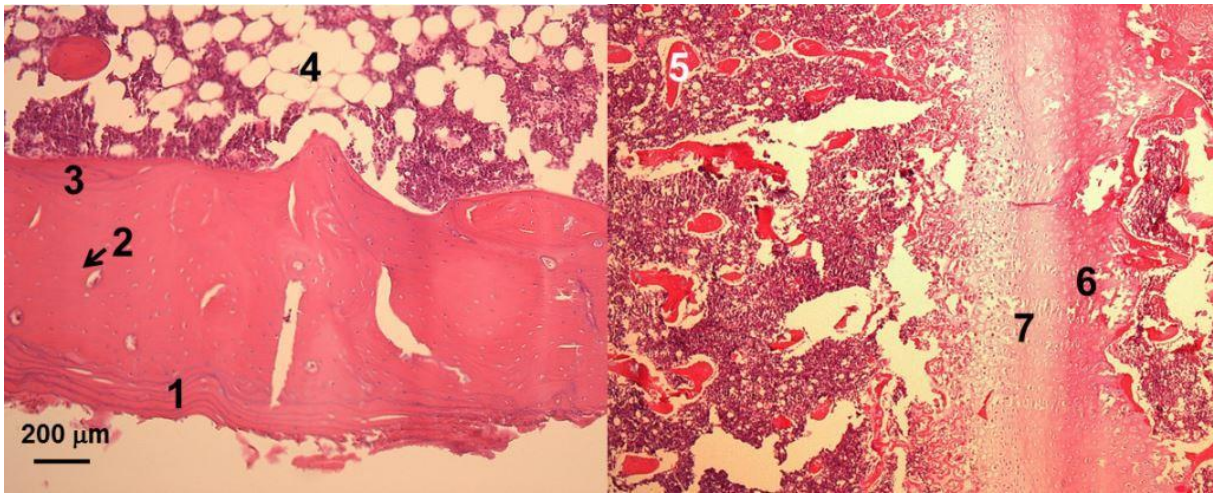


Fig. 7.10: Cortical (left) and trabecular (right) parts of the femoral bone of a control guinea pig (control 1). 1- circumferential lamellae, 2 – Haversian canal, 3 – endosteal lamellae, 4 – bone marrow, 5 – trabeculae, 6 – calcified cartilage, 7 – hypertrophic chondrocytes. H&E stain.

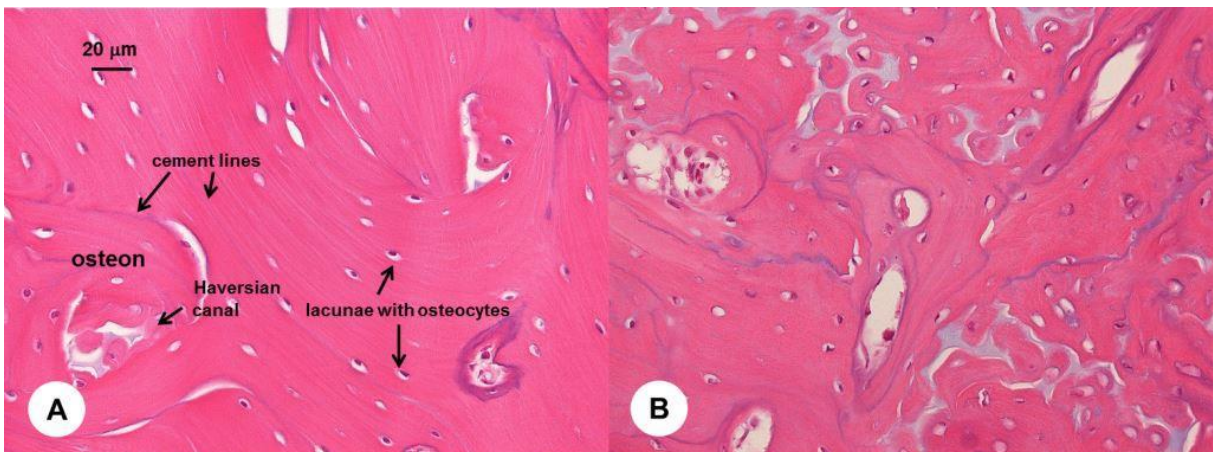


Fig. 7.11: A – femur, cortical bone (control 1). B – femur, cortical bone (control 4). H&E stain.

are typical for woven bone (McGavin and Zachary, 2007). Fig. 7.12 contains an overview of pathological lesions in the femoral diaphysis of a satin guinea pig (case 3). The cortex was remarkably broadened and intact lamellar bone could be only found in the outer (periosteal) region. The normal compact bone structure of diaphysis was largely replaced by a network of pseudo-trabeculae consisting of mixed lamellar and woven bone with thick and irregular cement (reversal) lines. Distinct cement lines demarcated the surface of these structures. The intertrabecular space was remarkably cell-rich (mainly fibroblasts, occasionally macrophages) and filled with vascularized fibrous tissue. Numerous osteoclasts in their Howship's lacunae lined the osteoid surface. The osteoblast population was increased, too. Periosteum was irregular and showed cystic lesions (Fig. 7.13). Bone marrow was suppressed. Similar features were found in all examined satin guinea pigs. Most prominent lesions were present in cases 1, 3, 4 and 5. Femur and tibia of case 2 also contained woven bone, reversal lines and numerous osteoclasts in diaphyseal region, but the normal (cortical) bone structure was better preserved (Fig. 7.14a). Broadened Haversian canals were observed in case 2. Interestingly, case 6 (heterozygote Sasa) had similar lesions to homozygote satin animals (Fig. 7.14b).

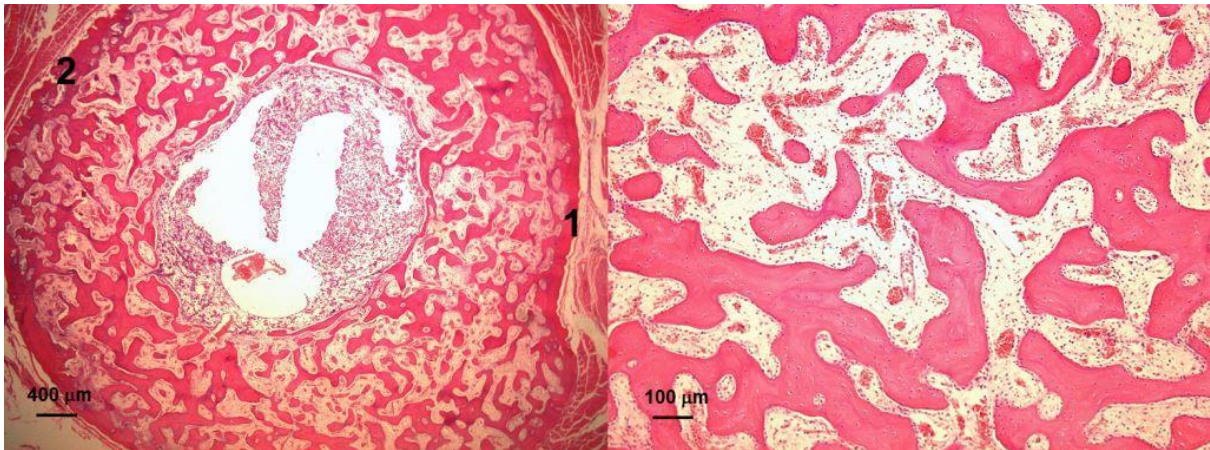


Fig. 7.12: Cortical bone (mid-diaphyseal section of a femur) in a satin guinea pig (case 3). The cortex is drastically expanded; only the periosteal region contains the original lamellar bone (1). Periosteum is poorly delineated and contains cystic lesions (2). Right image: vascularized fibrous tissue is filling spaces between the osteoid islands. H&E stain.

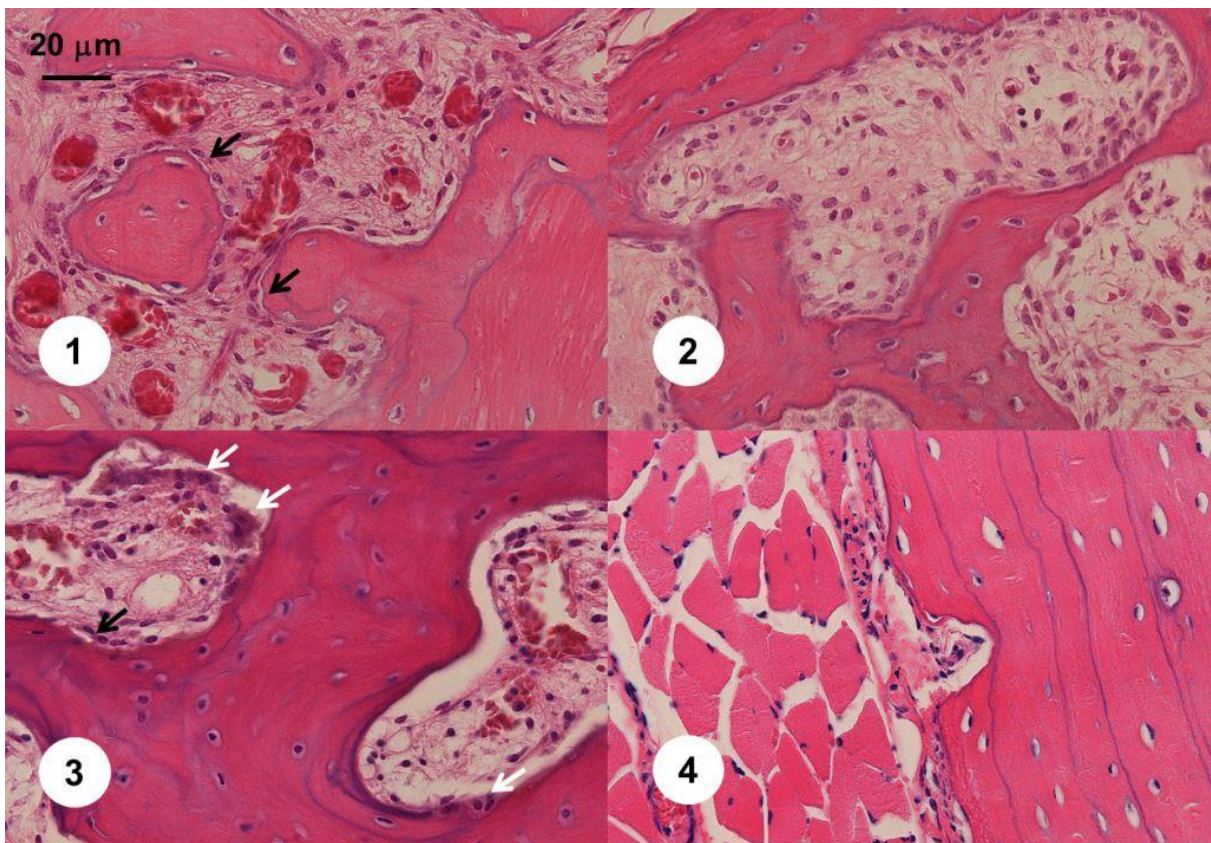


Fig. 7.13: Sections of diaphyseal bone in cases 1-4. 1 – femur of case 1, strongly vascularized connective tissue fills gaps between trabeculae. 2 – femur of case 2, thin trabeculae with irregular and broadened cement lines (reversal lines). 3 – femur of case 3, osteoclasts (white arrows) in their Howship's lacunae line the surface of osteoid. 4 – tibia of case 4, intact circumferential lamellae and periosteum with cavities. There is also increased osteoblastic activity (black arrows). H&E stain.

#### 7.3.3.4. Kidneys

Macroscopic kidney lesions were found in all examined satin guinea pigs and in none of the Dunkin-Hartley controls. Microscopically, abnormalities were observed both in controls and in satin animals, but the satin group was more severely affected.

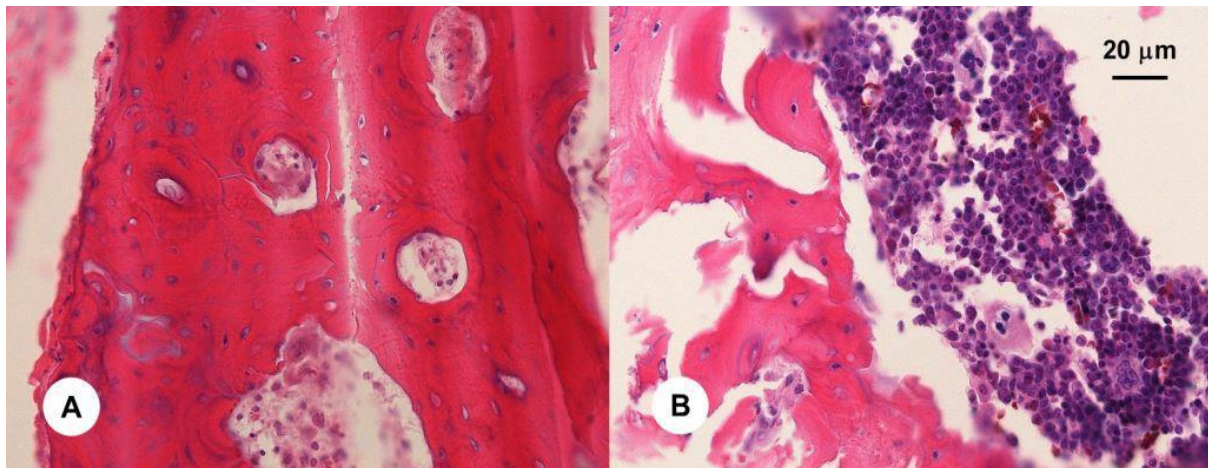


Fig. 7.14: Diaphyseal sections of the femur. A – case 2, reversal lines and osteoclasts in broadened Haversian canals, B – case 6 (heterozygote *Sasa*).

Guinea pig renal cortex with its normal architecture can be seen in Fig. 7.15. In non-satin cavies large regional variations were present within the same kidney. Most of the parenchyma had a normal appearance; focal lesions could be found. Fig. 7.16 compiles the most notable observations in the control group. In control 1, irregular glomeruli with endocapillary proliferation were found in certain regions; capillaries contained numerous PAS-positive Foa-Kurloff cells. These features were also

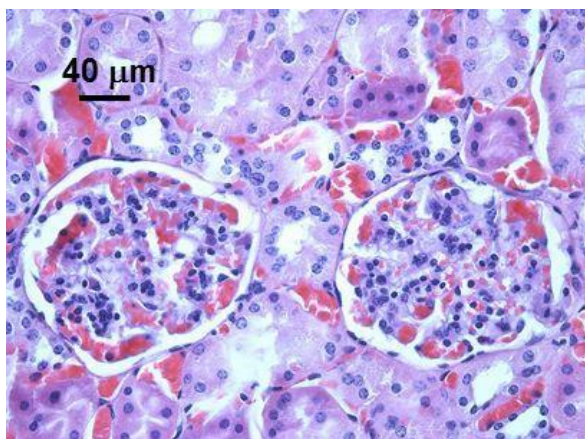


Fig. 7.15: Cortex and normal glomeruli (control 2). H&E stain.

present in control 2, but to a lesser extent. In 1, 3 and 4, kidneys contained zones with focal segmental to generalized glomerulosclerosis, accompanied by marked dilation of the Bowman space. The latter was in some cases filled with eosinophilic substance. Glomerular basal membranes (BM) were moderately thickened. Samples were negative for amyloid and collagen.

Kidney lesions in satin guinea pigs were diffuse; very few unaffected glomeruli could be found. A gallery of typical histological findings is presented in Figs 7.17-20. Most pronounced changes were found in case 5. Severely affected cortex displayed cystic degeneration (Fig. 7.17). Strongly dilated Bowman capsules contained remnants of sclerotic glomeruli. A close-up image is shown in Fig. 7.18, revealing end-stage glomeruli with deformed capsules and drastically thickened BM. There was moderate fibrosis of the capsule and interstitium. Large deposits of PAS-positive material were present in interstitium. Distal tubules and collecting ducts were dilated. Proximal tubular cells appeared larger than in the control group. Similar lesions were found in all other satin guinea pigs (Figs 7.19-20). In case 1 and 2 marked expansion (Fig. 7.19a) and nodular sclerosis (Fig. 7.19b) of mesangium were observed; such changes are often referred to as lobular simplification (Maryniak et al., 1985). In case 7, sclerotic glomeruli as well as interstitium were infiltrated by Foa-Kurloff cells. Interestingly, both the heterozygote *Sasa* (case 6) and the non-satin animal with CKD (case 8)

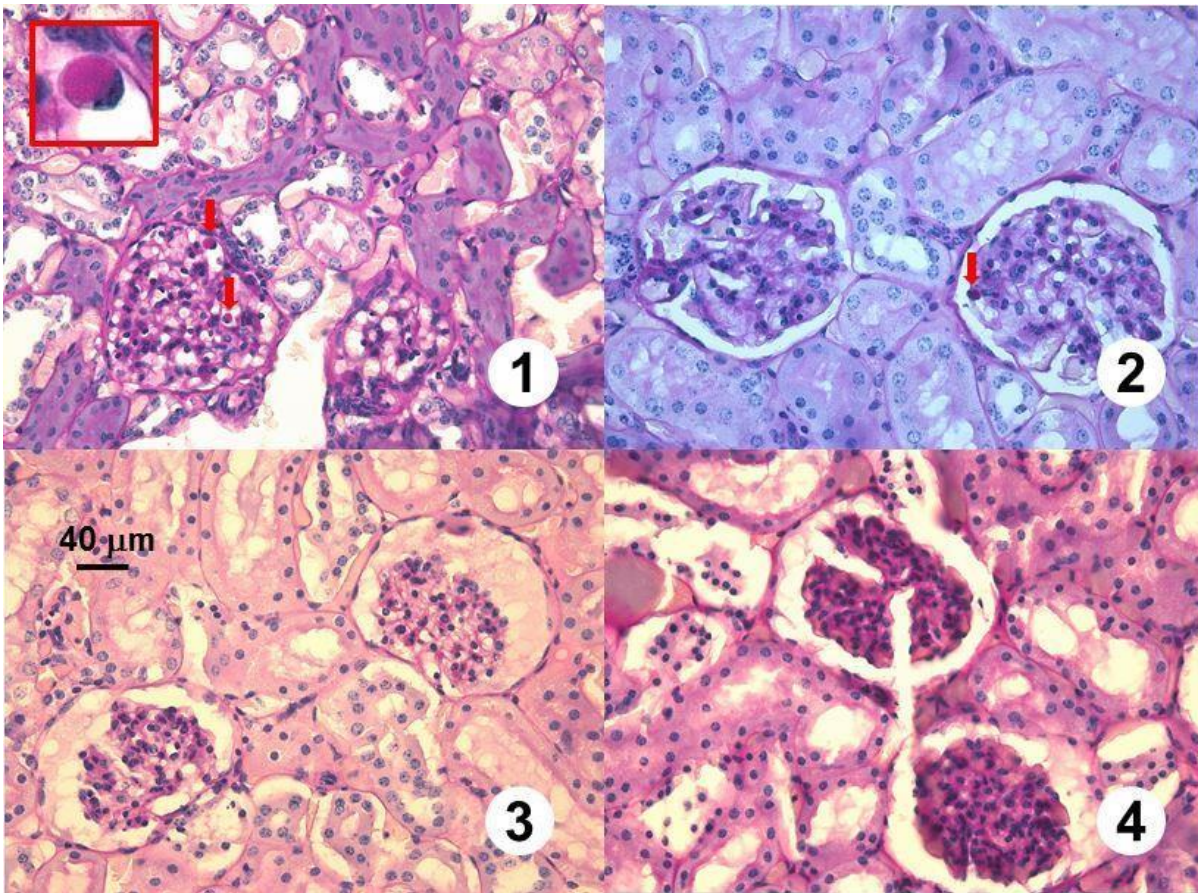


Fig. 7.16: Cortex specimens of controls (1-4). Control 2 displays a normal histological architecture. Hypercellularity, segmental sclerosis and thickened glomerular basal membranes are seen in 1 and 4. In 3 and 4 the dilated Bowman space is filled with eosinophilic exudate. Foa-Kurloff cells are present 1 and 2 (arrows). Insert: a single Foa-Kurloff cell with its PAS positive intracytoplasmic inclusion. PAS stain.

displayed similar patterns of renal disease as the homozygote satin group (Fig. 7.21). Samples were negative for amyloid.

Precipitation of calcium salts in distal tubules and collecting ducts was observed in nearly all examined animals. Renal calcinosis was quantified by analyzing Von Kossa stained sections of medulla and renal pelvis (Fig. 7.22). Calcinosis score (CS) was defined as the percentage of the total cross-sectional kidney area occupied by calcium deposits.

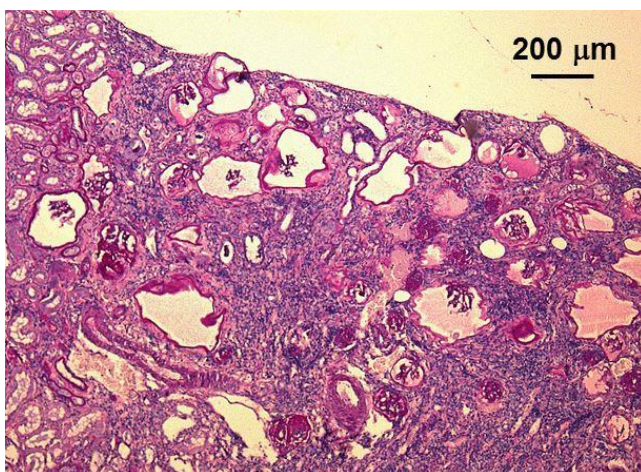


Fig. 7.17: An overview of a severely disordered kidney in a satin guinea pig (case 5). PAS stain.

Kidneys of both satin and non-satin guinea pigs displayed some degree of abnormality; however, this degree appeared higher in the satin group. The most prominent qualitative findings in the kidneys of satin guinea pigs in comparison with the control group were: expanded mesangium or glomerular sclerosis, thickened parietal and visceral Bowman capsule (basal membrane), expanded glomeruli, dilated Bowman spaces and enlarged (hypertrophic) proximal tubular

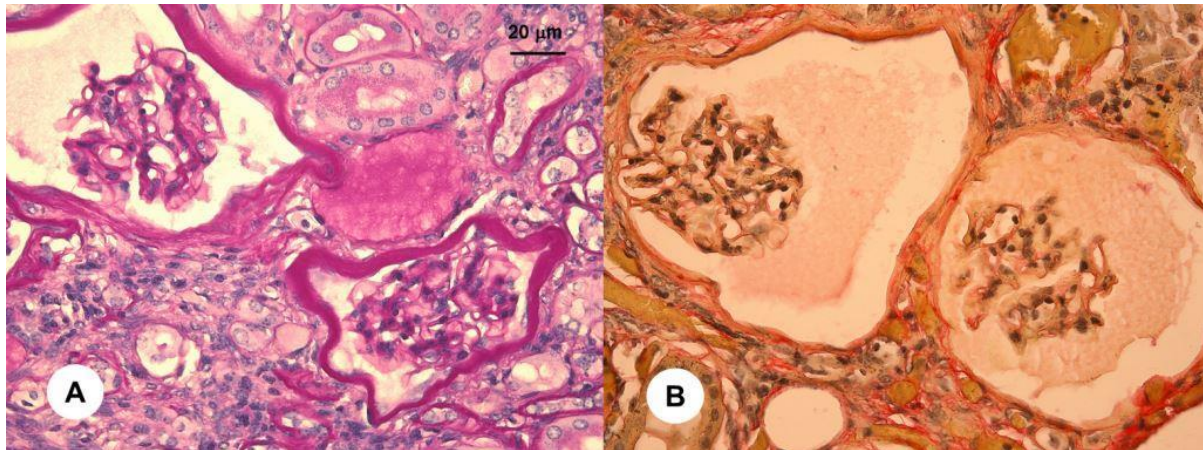


Fig. 7.18: Glomeruli of a satin guinea pig (case 5). A – PAS, B – Van Gieson.

cells. To assess the significance of observed differences, numerical values of the basal membrane (BM) thickness, the Bowman space thickness, cross-sectional areas of the glomerulus (G) and proximal tubular cells (CA), and calcinosis scores (CS) were analyzed statistically. The results are summarized in Table 7.3. The following parameters were significantly different: the thickness of the glomerular basal membrane was higher in the satin group, case 5 had dilated Bowman space and case 7 had enlarged proximal tubular cells. Calcinosis scores were higher in cases 5 and 6, and in control 3. A histogram displaying BM thickness is given in Fig. 7.23.

Animal ID	BM ( $\mu\text{m}$ )	BS ( $\mu\text{m}$ )	G ( $\mu\text{m}^2$ ) $\cdot 10^{-4}$	CA ( $\mu\text{m}^2$ )	CS (%)
Case 1	7.9 $\pm$ 4.7	15.7 $\pm$ 6.3	1.26 $\pm$ 0.98	140 $\pm$ 35	0.085
Case 2	6.5 $\pm$ 4.5	12.0 $\pm$ 6.4	1.31 $\pm$ 0.34	178 $\pm$ 47	0.052
Case 3	3.4 $\pm$ 1.0	6.0 $\pm$ 2.1	0.86 $\pm$ 0.20	136 $\pm$ 26	0.006
Case 4	4.6 $\pm$ 2.1	16.8 $\pm$ 10.2	0.87 $\pm$ 0.25	103 $\pm$ 39	0.023
Case 5	10.9 $\pm$ 5.5	56.1 $\pm$ 41.5*	1.85 $\pm$ 1.11	148 $\pm$ 55	0.166
Case 6	5.3 $\pm$ 2.7	12.7 $\pm$ 9.2	0.89 $\pm$ 0.27	125 $\pm$ 54	0.242
Case 7	6.1 $\pm$ 2.8	18.6 $\pm$ 13.6	1.61 $\pm$ 0.57	282 $\pm$ 55*	0.000
Case 8	8.8 $\pm$ 6.4	22.1 $\pm$ 17.9	1.62 $\pm$ 0.53	211 $\pm$ 40	ND

Control 1	4.4± 1.8	8.8± 2.8	0.74± 0.17	118± 40	0.054
Control 2	3.1± 1.3	9.8± 1.8	1.25± 0.29	186± 48	0.137
Control 3	1.6± 1.0	16.3± 5.5	0.81± 0.13	131± 38	0.269
Control 4	2.3± 1.1	17.8± 5.0	1.07± 0.15	121± 23	0.009
<b>Total score satins</b>	<b>6.4± 4.2***</b>	<b>18.6± 20.4</b>	<b>1.21± 1.01</b>	<b>165± 69</b>	<b>0.09± 0.08</b>
<b>Total score controls</b>	<b>2.8± 1.7</b>	<b>13.2± 5.6</b>	<b>0.71± 0.30</b>	<b>145± 50</b>	<b>0.11± 0.11</b>

Table 7.3: Numerical values of: glomerular basal membrane thickness (BM), Bowman space thickness (BS), glomerular area (G, in tens of thousands of micrometers), proximal tubular cell area (CA), calcinosis score (CS). \* significantly different outcome of pairwise t-tests.\*\*\* significant cell means difference (p<0.001).

#### 7.4. DISCUSSION

The presented findings are suggestive of hyperparathyroidism, abnormally increased bone turnover and extensive renal damage in satin cavies. Scrutinous analysis of blood and urine parameters and microscopic lesions in affected organs may provide hints with regard to the nature of these deviations.

##### 7.4.1. Blood and urine parameters

Blood serum profiles featured low serum calcium, low calcium to phosphate ratio and elevated alkaline phosphatase (ALP). However, one cannot yet speak of hypocalcaemia, because calcium levels were still within the (nominal) normal range. These findings are highly indicative of a disturbed calcium metabolism, but such deviation is not necessarily caused by renal dysfunction. As discussed in Chapter 4, Sections 4.3.1 and 4.4.3, serum calcium and phosphate are poor predictors of renal disease. Interestingly, the calcium phosphorus product was in a range in which the risk of tissue calcification becomes substantial (Block et al., 2004). Although metastatic calcification was not specifically investigated in this study, it might contribute to morbidity and mortality in satin syndrome and in other metabolic disorders in guinea pigs. This issue deserves further investigation.

Alkaline phosphatase is a non-specific marker of intestinal, hepatic or biliary pathology, cancer, bone disease and many others (Rosalki and Foo, 1984). Isolation of tissue-specific isoforms provides a more reliable diagnostic method (Rosalki and Foo, 1984), but is not routinely performed in animals. In practical situations, elevated ALP in conjunction with normal liver-related parameters (ALT, bilirubin) and abnormal calcium levels is strongly suggestive of bone disease. Furthermore, BUN was slightly higher in the satin group; however, there was no simultaneous rise in creatinine. One cannot conclude on the relevance of elevated BUN, because the examined animals were in a terminal stage and pre-renal factors (dehydration) might have contributed to the increase in blood urea. High haematocrit

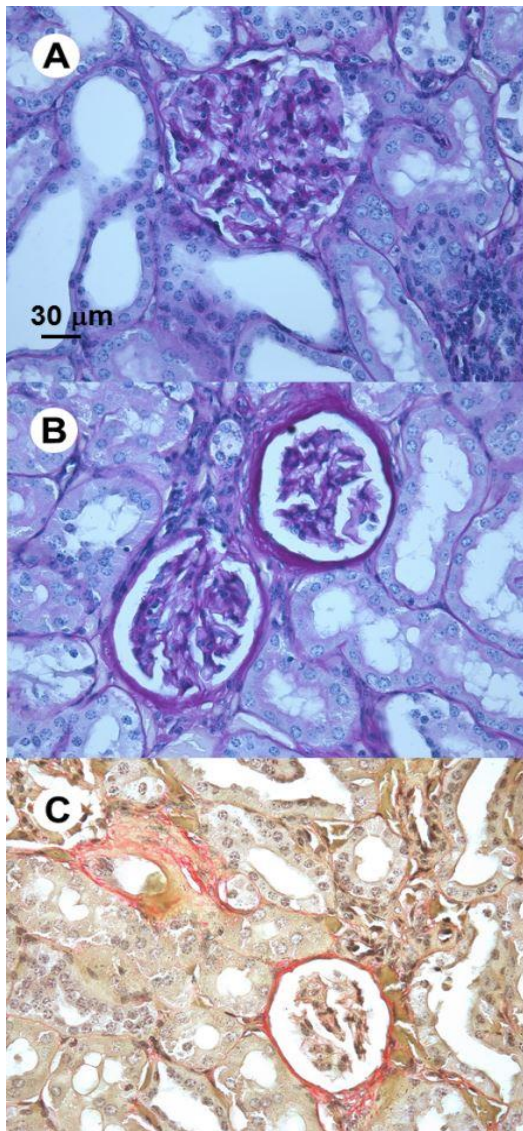


Fig. 7.19: Cortical lesions in case 1. A – tubular dilatation and thickened visceral BM (PAS), B – thickened BM and expanded Bowman space (PAS), C – moderate capsular and interstitial fibrosis (Van Gieson).

weight of the animals. Interestingly, there was no severe hypoalbuminaemia and no edemas. This suggests that compensatory mechanisms in guinea pigs may be more efficient than in humans.

#### 7.4.2. Parathyroid glands

Hyperparathyroidism may be difficult to diagnose in practice (Cope et al., 1957). As discussed in Chapter 4, Section 4.3.1, serum PTH levels are difficult to measure and not always informative in renal failure. A preliminary indication of hyperparathyroidism might be deduced from routine blood tests. Since hyperparathyroidism often induces acute pancreatitis (Lenz et al., 2010), elevated serum amylase has been proposed as an indirect marker for an increased parathyroid activity (Cope et al., 1957; Jacob et al., 2006). Amylase in satin guinea pigs was higher than the reference range, but the significance of this finding could not be verified. Serum amylase tests are easy to carry out; however,

values would rather support the pre-renal origin of uraemia. Serum amylase was somewhat elevated, which could be compatible with low-grade pancreatitis. Alternatively, amylase has been implicated to be a marker of renal insufficiency in rabbits (Harcourt-Brown, 2002). In any case, careful interpretation is necessary, because there was practically no difference between satin and control groups. In routine urine tests, high urinary protein concentration was the only remarkable outcome. Although only few data points for satin guinea pigs could be obtained, one can state that these animals suffered from severe proteinuria. In humans, urinary protein loss of 3.5 g or more per 24 h is considered severe. Proteinuria is part of the so-called nephrotic syndrome or protein-losing nephropathy (Orth and Ritz, 1998), further featuring hypoproteinaemia, edema and hyperlipidaemia. The latter is due to a compensatory mechanism in the liver, which upregulates protein and lipoprotein production in response to renal protein wasting. Nephrotic syndrome is always attributed to glomerular nephropathy; however, there is no *a priori* relation between the severity of proteinuria and the degree of glomerular damage. As a matter of fact, the overwhelming majority of human nephrotic syndrome cases are due to minimal change glomerulopathy in which glomeruli appear normal in light microscopy (Jennette and Spargo, 1999).

In satin guinea pigs, estimated daily protein losses were about 1 g, which is extremely high considering the

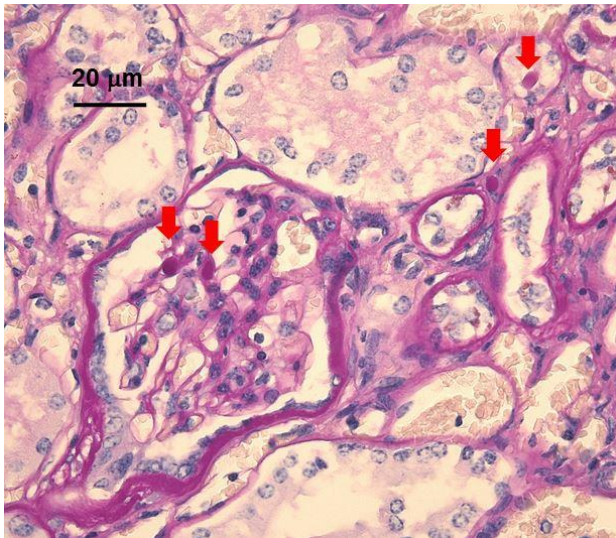


Fig. 7.20: Glomeruli of case 7. Arrows: Foa-Kurloff cells. PAS stain.

reliability of amylase as a marker for parathyroid function is subject to discussion (Jacob et al., 2006). Therefore, histopathological findings are expected to deliver more trustworthy evidence.

The parathyroid glands of satin animals were hyperplastic and displayed characteristic changes: proliferation of endocrine (chief) cells, repression of oxyphil and fat cells, and deposition of eosinophilic material in parenchyma. In contrast to the control group, no lobuli, cell strings or acini could be distinguished. Thus, hyperplasia was of the diffuse type. This is in contrast to the nodular type, where cells arranged in large clusters are

delimited by bands of connective tissue (Tominaga et al., 1996). In humans, both nodular and diffuse hyperplasia may occur in primary as well as secondary (e.g. renal) hyperparathyroidism (Tominaga et al., 1996). On the other hand, in humans oxyphil cells are numerous in renal hyperparathyroidism (Fukuda et al., 1993), while proliferation of chief cells is more typical for primary hyperparathyroidism (Gogusev et al., 1997). The nature of eosinophilic casts in the glands of satin guinea pigs has not yet been clarified; however, similar features may be present in human hyperparathyroidism (Leedham and Pollock, 1970). Extrapolation of the human data requires a certain degree of prudence, because microscopic manifestation of different types of hyperparathyroidism in guinea pigs may be different from the one in humans. One can conclude that the macro- and microscopic features of parathyroid glands in satin guinea pigs are strongly indicative of hyperparathyroidism. However, unambiguous identification of the type of hyperparathyroidism (primary versus secondary) solely on the base of histological findings is not achievable at this stage. Keeping in mind that primary hyperparathyroidism is extremely rare in domestic animals (McGavin and Zachary, 2007), and that kidney and parathyroid gland abnormalities were coincident in all satin guinea pigs, the observed features are tentatively

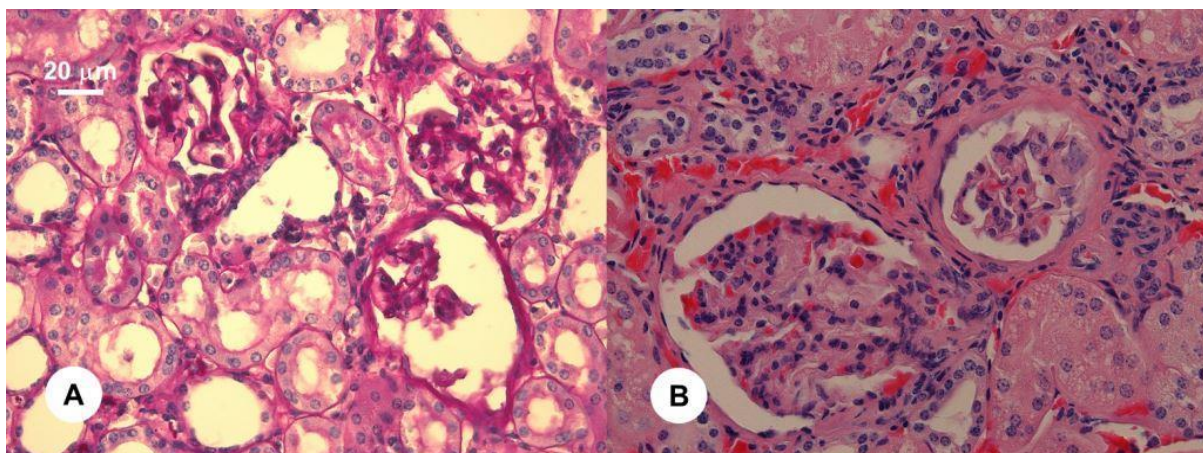


Fig. 7.21: Glomeruli of: A - the heterozygote satin (case 6) and B - non-satin CKD animal (case 8). PAS and H&E.

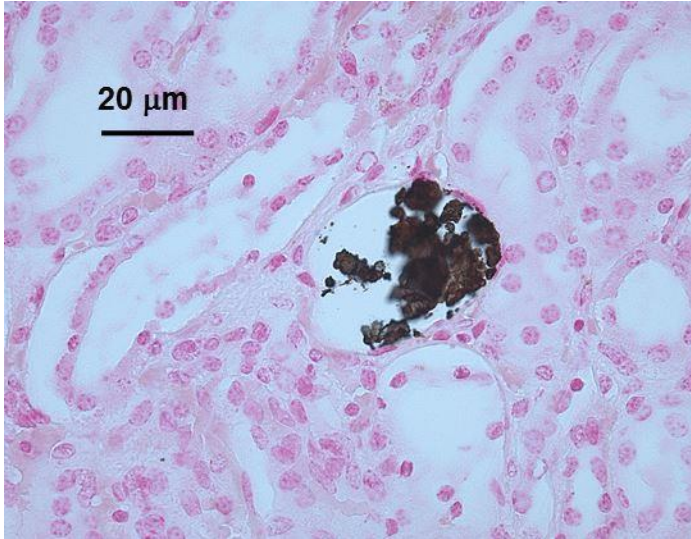


Fig. 7.22: Calcium salt precipitation in renal medulla (case 1). Von Kossa stain.

attributed to secondary hyperparathyroidism.

### 7.4.3. Bones

Bones of satin animals showed macroscopic as well as microscopic abnormalities. Microscopic features such as expansion of the cortex, suppression of the medullary cavity, loss of the osteon structure and the replacement of lamellar cortical bone by woven “trabecular” bone are explicit signs of a pathological process. Enlarged Haversian canals, broadened and irregular cement lines,

osteocytes scattered chaotically through the bone matrix and cystic subperiosteal lesions result from an abnormally increased bone remodeling activity (Jaffe and Bodansky, 1930; McGavin and Zachary, 2007). This is consistent with the presence of large numbers of osteoclasts and osteoblasts, and elevated serum alkaline phosphatase. In fact, the spaces between the pseudo-trabeculae are large resorption lacunae created by osteoclasts in compact bone (Schiller and Teitelbaum, 1999). To gain insight in bone resorption and new bone formation processes, one ought to selectively visualize the calcification front (osteoid seam, see Chapter 5). Osteoid seam consists of unmineralized osteoid which is deposited by osteoblasts at the surface of trabeculae. Within the current staining protocol, selective staining of osteoid seam could not be accomplished. However, in many specimens cement lines delineated the surface of pseudo-trabeculae (Fig. 7.22), which indicates that at these locations

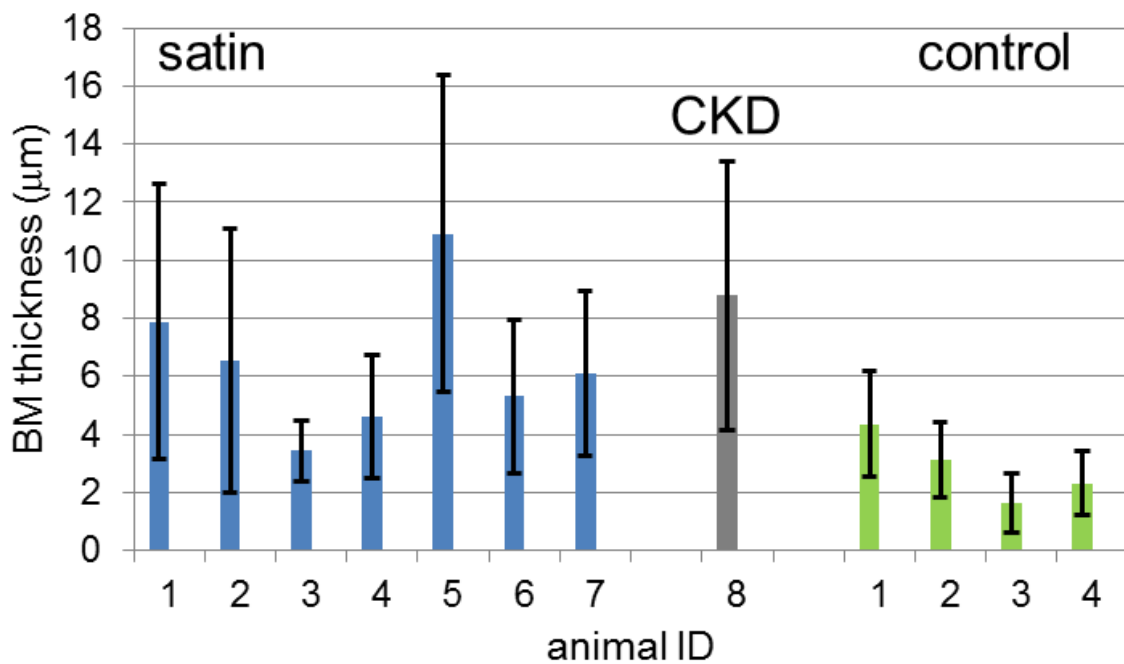


Fig. 7.23: Basal glomerular membrane thicknesses in the studied cases.

osteoid seam was reduced. This may have various reasons. For example, new bone formation may be not able to keep up with osteolytic processes. Alternatively, the global remodeling activity may be arrested because of exhaustion of the parathyroid response (Gogusev et al., 1997; Slatopolsky et al., 1999). In either case, the above features demonstrate that pathologically enhanced bone resorption has taken place. Additional clues, such as hypercellularity, fibrosis and strong vascularization of the intertrabecular space point in the direction of a metabolic bone disease, and more specifically, hyperparathyroidism (Schiller and Teitelbaum, 1999). There are three manifestations of hyperparathyroidism: fibrous osteodystrophy where bone turnover and cellular activity are abnormally high, and the two low-turnover forms – osteomalacia and adynamic bone disease (see also Chapters 2 and 5). Fibrous osteodystrophy is the most common spontaneous presentation of hyperparathyroidism. Osteomalacia in renal disease is specific to humans and associated with aluminum toxicity and/or phosphate depletion due to treatment with phosphate binders (Malluche, 2002). Adynamic bone disease may be induced by excessive supplementation with vitamin D (Toussaint et al., 2006), or may occur spontaneously in diabetes mellitus (Krakauer et al., 1995); the exact mechanisms are not yet fully resolved. Fibrous osteodystrophy can be easily differentiated from other presentations of metabolic bone disease, and also from other conditions that affect bone turnover, such as osteoporosis and Paget disease of bone. In osteomalacia, adynamic bone disease and osteoporosis the bone remains quiescent. The overall cell activity is low which is reflected by hypocellularity of the bone, attenuated trabeculae and unapparent cement lines (Aswar et al., 2012). In osteomalacia, osteoid seam is thicker than normal while in osteoporosis and adynamic bone disease it is strongly reduced (Woods et al., 1968; Hruska and Teitelbaum, 1995). Paget disease (*osteitis deformans*) can in certain cases mimic severe fibrous osteodystrophy, particularly with regard to hypercellularity and osteoclastic activity. Typical for Paget disease are large osteoclasts containing hundreds of nuclei. However, unlike in fibrous osteodystrophy, there is no net bone resorption in Paget disease. Contrariwise, the resulting bone appears sclerotic and microscopically is composed of dense osteoid arranged in mosaic-like fibers (Schiller and Teitelbaum, 1999). Such features were not observed in satin guinea pigs.

Microscopically, fibrous osteodystrophy is characterized by so-called tunneling resorption (Schiller and Teitelbaum, 1999): osteoclasts invade the cortex via periosteum and Haversian canals and bore channels that are further caverned out resulting in an open pseudo-trabecular structure. This is termed *osteitis dissecans*. Furthermore, fibrous tissue fills up peritrabecular spaces and replaces bone marrow (*osteitis fibrosa*). As the disease progresses, large cavities (*osteitis cystica fibrosa*) and eventually brown tumors are formed. These structures contain fibrous tissue, hemosiderin-laden macrophages and giant cells (osteoclasts). Epiphyseal (trabecular) bone is the primary target for resorption, because it normally undergoes most intensive remodeling. In advanced disease, diaphyseal (compact) bone is also affected. Radiographic studies reveal mineral loss in diaphyseal cortex, which is also confirmed by the current study (Chapter 6). Osteocytes have been implicated to play a role in cortical bone resorption (Hruska and Teitelbaum, 1995). However, this condition is infrequent in humans, presumably due to early intervention that prevents such devastating damage

Pathophysiological changes to bones in renal osteodystrophy are in a very good agreement with the observations in both homozygotic and heterozygotic satin guinea pigs. Histological bone lesions correspond to the first stage of fibrous osteodystrophy – *osteitis dissecans*. Additionally, in cases 3, 4 and 5, computed tomography imaging (Chapter 6) revealed severe degrees of bone deformation in the jaws, accompanied by significantly reduced bone density in the skull and extremities. In case 3 and 4, suppression of bone marrow was a prominent radiographic finding. This is compatible with the second stage of renal bone disease, *osteitis fibrosa*. No brown tumors were found in histology specimens. However, numerous cystic lesions were diagnosed by computed tomography in another group of satin animals (Chapter 6). Such features are compatible with the end-stage renal osteodystrophy – *osteitis cystica fibrosa* (Schiller and Teitelbaum, 1999).

Affected bones become extremely soft and easy to deform by applying gentle pressure. In human and animal species, jaws are the predilection site of bone lesions in hyperparathyroidic osteodystrophy (Lautenbach et al., 1968; Cooper, 1989). In the mandibula, advanced fibrous osteodystrophy manifests as “rubber jaws” (Hogg, 1947). A human analogue is *leontiasis ossea* (Lee et al., 1996).

It is remarkable that the severity of bone lesions at histopathology was not necessarily in proportion to the severity of clinical symptoms (lameness) and radiographic signs (Chapter 6). In the studied group, large diversity in clinical presentation was observed. Advanced bone lesions were present in nearly all satin animals, while lameness score 4 (see scoring system in Chapter 3, Section 3.2.2) could be assigned to only one animal (case 1). In cases 3-5, there was statistically significant reduction of bone mineral density, but lameness was not apparent. Note that a typical time scale of bone remodeling is several months (Kearns and Kallmes 2008). Vast lesions such as observed in satin guinea pigs must result from a long period of abnormal bone remodeling.

Finally, the control group consisting of aged animals (about 4 years) also displayed microscopic bone abnormalities, be it lower grade than in satins. This suggests that bone defects are common in guinea pigs and may be associated with old age.

#### **7.4.4. Kidneys**

Histopathological data on kidneys reveal several peculiarities. Firstly, calcium crystals were found in medullae of nearly all animals. Thus, renal calcinosis is certainly not specific to satin guinea pigs. Apparently there is no correlation between the number of calcium crystals precipitated in distal tubules and collecting ducts and renal calcium wasting. Non-satin guinea pigs often displayed higher grades of calcinosis than satins, without obvious signs of hyperparathyroidism and bone resorption. Possibly, other factors are of more importance for developing renal calcinosis, such as the age of the animal, dietary calcium intake and local urine chemistry (e.g. the concentration of urinary calcification inhibitors, Schlieper et al., 2007). These factors could not be uniformized in the current study.

Interestingly, numerous Foa-Kurloff cells were found in three of the examined animals (two Dunkin-Hartley controls and case 7). Foa-Kurloff cells are unique to guinea pigs and capybaras. These mononuclear leukocytes contain a characteristic large inclusion body, composed of glycosylated proteins (PAS-positive). Although the exact function of Foa-Kurloff cells has not been resolved, it is generally accepted that they are an important part of the innate immune system. Foa-Kurloff cells are poor phagocytes, but they have a pronounced NK activity (Revell, 1977). Many factors stimulate

expression of these cells: sex hormone level changes, viraemia or neoplasia (Revell, 1974; Debout et al., 1995). In the current context, the presence of Foa-Kurloff cells may be regarded as accidental finding with no relation to renal pathology. However, it remains an abnormal feature. One has to keep in mind that many unidentified disorders may be present in laboratory and domestic animals. Their impact on experimental results is unknown.

The most striking abnormalities were mesangial expansion, focal segmental to generalized glomerulosclerosis and lobular simplification followed by thickening of the basal membrane. These features were significantly more pronounced in the satin group. The microarchitecture of tubules, interstitium, collecting ducts and renal pelvis did not indicate generalized damage such as infarcts, inflammation or fibrosis. There were also no apparent signs of tubular pathology. Occasionally, some abnormalities were observed in distal portions of the nephron, but these could be explained by primary glomerular nephropathy, proteinuria and/or calcium wasting. For example, tubular dilation (Fig. 7.19) may be due to calcinosis and obstructions in the distal region. Hypertrophy of proximal tubular cells is often seen as a compensatory change in massive proteinuria, where tubular cells increase their phagocytic activity to remove proteins from the filtrate (Amsellem et al., 2010). One can thus conclude that the pattern of renal disease was glomerular rather than tubulo-interstitial. Naturally, certain tubular defects cannot be fully excluded at this stage, because the applied histological procedures were not suitable for demonstrating molecular changes (e.g. altered expression of a receptor or a channel, or presence of immune complexes).

The observed glomerulopathy displays a characteristic pattern – mesangial proliferation followed by focal segmental sclerosis with markedly thickened glomerular basal membranes. The first two features are compatible with a chronic progressive disease and represent a common and aspecific response to glomerular injury. Activation and proliferation of mesangial cells are antecedents of sclerosis (Klahr et al., 1988). Mesangial cells can be activated by deposited immunoglobulines in mesangioproliferative or membranoproliferative glomerulonephritis, such as in IgA nephropathy or lupus (D'Amico 1987; Jennette and Spargo 1999), or by hypertensive damage to the capillary endothelium (Diamond and Karnovsky, 1988). Similar changes to glomeruli were described in 5/6 nephrectomized rats, where hypertension in the local renal circulation plays an important role (Floege et al., 1992). However, the combination of mesangium expansion or sclerosis with thickened basal membranes can be considered unique. In fact, it has an analogue in human pathology: diabetic glomerulosclerosis. Despite extensive research efforts, there are still many unresolved issues in the pathogenesis of diabetic glomerulosclerosis. The primary cause is thought to be diabetes-induced vascular sclerosis with increased synthesis of basal membranes by microvasculature (Jennette and Spargo, 1999). Hypertension in the renal circulation, which is a common sequel to vascular and metabolic changes in diabetes, has been also implicated to contribute (Diamond and Karnovsky, 1988; Sowers et al., 2001). A different mechanism, based on altered biochemical properties of the basal membrane has been investigated by several authors (Kefalides 1974, Parthasarathy and Spiro 1982). More specifically, altered glycosylation of BM proteins has been shown to increase adhesion of albumin, fibrinogen and immune complexes. This causes trapping of these molecules in the subendothelial space. Such a mechanism is essentially different from the more common membranous

glomerulopathy, which is caused by antibody binding to antigens that are present in, or deposited on the BM. Microscopical lesions in diabetic glomerulopathy can be easily recognized. In early stages, thickening of glomerular basal membranes is accompanied by moderate increase of mesangial cellularity. These lesions have been reproduced in diabetic eNOS knock-out mice (Nakagawa et al., 2007). Protein deposits may be found adjacent to the parietal Bowman capsule (“capsular drops”) or in the subendothelial space (“fibrin drops”). This condition progresses to focal segmental sclerosis, lobular simplification and nodular lesions termed Kimmelstiel-Wilson nodules (Sandison et al., 1992). Diabetic glomerulosclerosis is one of the important causes of proteinuria, and the leading cause of renal failure in diabetic patients (Jennette and Spargo, 1999). Lesions reminiscent of diabetic nephropathy were found in kidneys of satin guinea pigs, particularly in case 1, 2, 6 and 7 (Figs 7.19, 7.20 and 7.21). In other cases (Fig. 7.18) no characteristic features could be distinguished due to advanced degeneration (end-stage glomeruli). Comparative histological presentation of human diabetic glomerulosclerosis and satin guinea pig lesions is shown in Fig. 7.24.

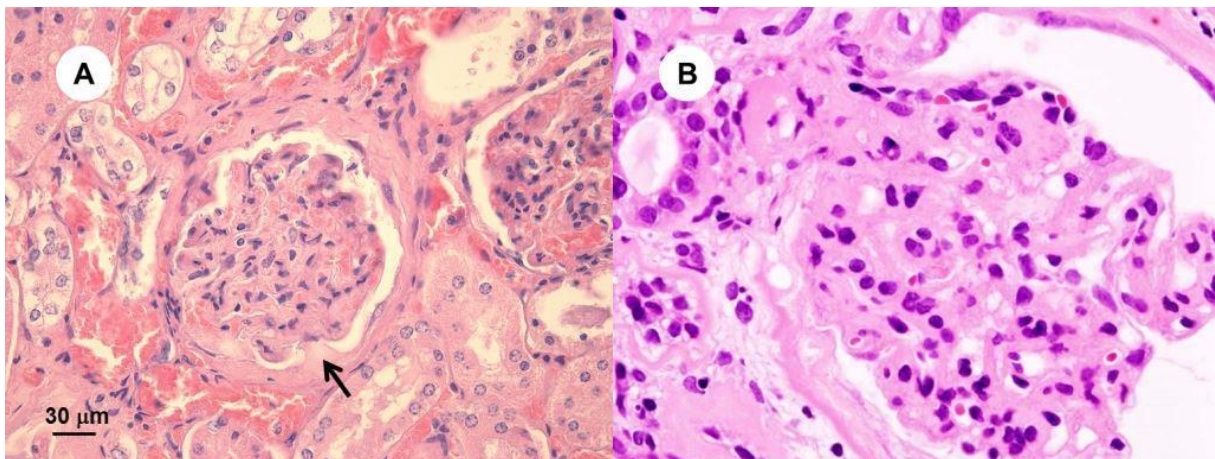


Fig. 7.24: Glomerular sclerosis and thickening of BM in A – satin guinea pig (case 2) and B – human diabetic nephropathy (source: Wikipedia Commons). Note a protein droplet close to the parietal BM in A (arrow).

It has to be noted that the parallel between human diabetic nephropathy and the kidney disease of satins has been drawn purely on the base of the microscopic appearance of glomerular lesions. Further investigations are necessary to verify whether other analogies are present. Diabetes is believed to be common in guinea pigs (Vannevel, 1999; Richardson, 2000) but in many cases it is difficult to diagnose. Moderate elevation of serum glucose, such as in the animals involved in the current study (Table 7.2) does not provide sufficient evidence. At this stage it can be only stated that glomerulopathy is the dominant kidney lesion found in homozygotic and heterozygotic satin cavies, and that it also occurs in non-satins, but it is premature to judge on its mechanism.

Note that despite advanced glomerular degeneration most of the animals were not uraemic and had normal serum creatinine levels. Uraemia and raised serum creatinine are diagnosed only when glomerular filtration rate is reduced to 25-30% of its normal value (Guyton and Hall, 2000). In veterinary practice it is often difficult to differentiate between pre-renal (hypovolaemia, e.g. in dehydration), renal and post-renal (obstruction) factors that influence GFR. Thus, elevated urea and creatinine are not diagnostic for a kidney disorder. A renal cause of uraemia would be a reduction of

the number of functional (permeable) nephrons (Guyton and Hall, 2000), but this was clearly not the case here. Large amounts of protein-rich filtrate were found in dilated Bowman spaces. Glomeruli, although damaged, were still permeable.

A glomerular rather than tubulo-interstitial pattern of renal disease is not an entirely unexpected finding. As discussed in Chapter 4, urine concentration, pH and mineral handling relies mainly on the tubular function. Most of the nutrient wasting syndromes can be explained by defects in reabsorption or acid-base regulation (e.g. tubular necrosis, Fanconi syndrome, RTA). However, neither blood nor urine tests support this diagnosis. The kidneys could acidify and concentrate the urine. There was no wasting of sodium, potassium, phosphate or glucose, because their serum concentrations were not below the normal limits. There were also no abnormalities in the haematology profiles. Mild to moderate anemia would be expected in tubulo-interstitial nephropathy, where interstitial fibroblasts fail to produce erythropoietin (EPO) (Eschbach, 1989).

In the current context, it is not plausible that the observed abnormalities in calcium metabolism are due to impaired tubular calcium handling. The remaining question is: can glomerular nephropathy explain renal calcium wasting, activation of the renal-bone axis and bone destruction to such a degree that the skeleton becomes a loose network of fine bony threads? The solution to this problem has been sought after in Chapter 4 by analyzing codependences of calcium and protein excretion. Glomerular damage results in proteinuria (Jennette and Spargo, 1999). Satin guinea pigs display severe proteinuria with glomerular sieving coefficients as high as 3.5%. In Chapter 4, Section 4.5.3 it has been shown that moderate to severe proteinuria with sieving coefficients of the order of a few percent can increase calcium losses by 10-30%, which is beyond the compensation capacity of the kidney. This leads inevitably to activation of the renal-bone axis and to massive bone loss. The time needed to form large bone lesions, such as observed in the current study, is estimated to be of the order of several months (Kearns and Kallmes, 2008). This is in agreement with typical time scales for progression of the lameness in satins (Chapter 3).

## 7.5. CONCLUSION

The current study clearly demonstrates high degrees of glomerular nephropathy and proteinuria in satin guinea pigs. This can account for calcium wasting and attendant secondary renal hyperparathyroidism. The kidney disorder is of a chronic progressive type, which provides sufficient time to affect the bones to the observed extent. Glomerular nephropathy can induce the bone disease observed in the satin syndrome.

## **8. GENERAL REMARKS AND CONCLUSIONS**

### **8.1. WHAT HAVE WE LEARNED FROM GUINEA PIGS?**

#### **8.1.1. Lesions in satins and satin carriers**

This study has demonstrated that satin guinea pigs have a lower vitality (“fitness”) as compared with their non-satin peers. This is expressed by their significantly lower adult weight and a reduced life expectancy (Chapter 3). Based on histopathology and medical imaging findings, it is beyond any doubt that hyperparathyroidism and attendant bone disease are an essential part of the satin syndrome. It is also shown that, to a high degree of probability, a slowly progressive degenerative kidney disease is the underlying cause of this disorder. Modeling results (Chapter 4) support the observed phenomena. Unexpectedly, lesions in kidneys and bones typical to homozygotic (*sasa*) animals were also found in a heterozygote (*Sasa*). This fact may shed new light on the inheritance pattern of the satin factor. At present, the satin mutation (*sa*) that accounts for the phenotypic features of the coat is commonly acknowledged to be autosomal recessive (Robinson and Seaborne 1988). On the other hand, there are large phenotypic variations in the coat appearance (Chapter I), while no quantitative genomic techniques have been applied to establish the genetic background of satin animals. Consequently, the phenotype-genotype association is often vague. Besides, the linkage of genes coding for the hair properties and the disease remains unclear to date. The fact that the satin heterozygote was affected to an extent comparable to homozygotes suggests at least codominance of the disease-related genes. This issue requires further investigation and collection of statistical evidence.

#### **8.1.2. Is the satin syndrome an “exotic” disorder?**

This issue has not been addressed in previous studies. However, for a veterinary practitioner that observes many guinea pig patients it may be a naturally rising question. It is not clear whether the satin syndrome is unique to satin cavies. First of all, establishing a sound diagnosis of the satin syndrome in living animals poses a genuine challenge. The major complication is the lack of specificity of disease symptoms in satin guinea pigs, and the ubiquity of “satin-like” symptoms (lameness, dental problems) in the whole population of guinea pigs.

Diagnosis of chronic kidney disease (CKD) is not evident because kidney disorders produce vague symptoms and have no fully reliable markers. Uraemia and elevated serum creatinine may be observed only when the glomerular filtration rate is drastically reduced (Guyton and Hall, 2000). Other “evident” signs of a kidney disorder such as polydipsia and polyuria manifest when no adequate urine concentration can be accomplished, e.g. in certain tubulo-intestinal patterns of nephropathy (Hildebrandt et al., 1992). This is not always the case, as has been demonstrated in the current study. Despite extensive kidney damage in the examined animals, none of the blood tests indicated uraemia of renal origin, and only one animal displayed polydipsia and polyuria. To the author’s knowledge, serum kidney parameters and water intake are poor predictors of CKD in guinea pigs.

Diagnosis of hyperparathyroidism and osteodystrophy is at least equally challenging. Radiographic signs are seen in advanced bone pathology (Jordan, 2008) but may be easily missed in

mildly affected animals (Chapter 6). Quantitative techniques such as CT bone densitometry may be helpful in establishing a reliable diagnosis, but are not easy to apply in veterinary practice. In the light of the current results, diagnosis based on serum biochemistry may be state of the art. Satin guinea pigs have significantly altered serum biochemical profiles, particularly with regard to alkaline phosphatase, calcium and calcium to phosphate ratio, and often the calcium phosphorus product. Although none of these parameters can be regarded as a specific marker for metabolic bone disease, their conjunction provides a fairly reliable indication. Naturally, prudence and critical analysis of other blood parameters are recommended.

Interpretation of the causal relationships between nephropathy and bone disease on one hand, and reduced life expectancy, poor physical condition and discomfort on the other hand is possibly the most difficult task. Especially attributing clinical relevance to the observed macroscopic and microscopic lesions requires utmost caution. Because of diversity of renal diseases and presence of numerous disease-modulating factors, kidney lesions and symptoms of kidney disease are not related by any one-to-one function. The same is valid for the lesions and symptoms of bone disease. Thus, not all affected animals develop pronounced clinical symptoms and conversely, severe symptoms do not always result from dramatic pathological changes. This has been confirmed by the present study.

From the results presented in Chapter 7 it follows that kidney and bone lesions are ubiquitous in guinea pigs. There are no lesions that are specific to satin guinea pigs; instead, various degrees of damage are present in virtually all breeds and varieties. All observed changes are indicative of a chronic degenerative disease. In this sense, bone and kidney lesions match each other. Renal failure must be of a slowly progressive type in order to provide enough time for the bone lesions to form (Kearns and Kallmes, 2008).

Apparently, only the combination of two criteria – a sufficiently high degree of kidney damage and a sufficiently long duration of this pathological condition – is the true determinant of the clinical manifestation of the satin disease. Obviously, a large fraction of satin guinea pigs meets these criteria. However, there are no scientific grounds to deny the existence of similar disorders in guinea pigs of other breeds. To the author's knowledge, macroscopic kidney lesions are very common post-mortal findings, especially in aged animals. Progressive weight loss and motoric disorders at old age are not infrequent, too. Possibly, the satin or "satin-like" syndrome can be understood in a broader sense as secondary renal hyperparathyroidism with fibrous osteodystrophy.

The author's experience with diseases and symptoms in geriatric guinea pigs allows a tentative conclusion that the satin syndrome in a broader sense is not specific to satin guinea pigs. This issue should be elaborated in the future research.

## 8.2. WHAT CAN WE LEARN FROM GUINEA PIGS?

Patterns of bone alterations in satin guinea pigs can be fully explained in terms of pathophysiological responses to hyperparathyroidism. In contrast, the observed kidney abnormalities appear to be fairly unique and therefore more intriguing. There is striking morphological resemblance of satin kidney lesions to glomerulopathy concomitant to diabetes in humans and mice (Jennette and Spargo, 1999; Nakagawa et al., 2007). Future research may reveal more parallels. Many related

issues, such as soft tissue calcification, hypertension and the circulatory disease should be addressed as well.

Although the study of the satin syndrome seems to be purely curiosity-driven, some practical implications may arise. Research on kidney diseases in guinea pigs is still in its infancy. There are only few reports of spontaneous kidney failure in guinea pigs (Richardson, 2000; Holowaychuk, 2006); most of the cases were described in terms of acute renal failure due to intoxication. Richardson argued that chronic renal failure may be the underlying cause of weight loss, polydipsia, polyuria and early death, but considered this condition to be relatively rare. Expanding the database on kidney diseases in pet guinea pigs may prove valuable to veterinary practitioners specialized in exotic companion animals.

The role of a satin guinea pig in biomedical research is less evident. Unlike rats and mice, guinea pigs are no popular models for chronic renal failure. CKD in a guinea pig induced by 5/6 nephrectomy has been occasionally used in biomedical research (Ohashi et al., 1999); however, there are not so many advanced CKD models in guinea pigs as there are in rats (Moe et al., 2009). It is difficult to evaluate the potential of a satin guinea pig as a CKD model. There are not many models that can compete with transgenic animal technologies. On the other hand, satin guinea pigs feature spontaneous non-uraemic CKD with characteristic patterns for which specific applications may be identified. As explained in Chapter 5, spontaneous models may provide a closer approximation of the human pathology. Moreover, there is much interest in the common genetic background of human and animal CKD. Analysis of quantitative trait loci in rats and mice demonstrated much conformity (Korstanje and DiPetrillo, 2004). Exploration of the genetic basis of spontaneous guinea pig nephropathy may provide additional insights.

The challenging complexity and possible applications of the satin syndrome merit further research effort.

## 9. REFERENCES

- Alberts B, Bray D, Lewis J, Raff M, Roberts K, Watson JD. (1994) *Molecular Biology of the Cell*. Garland Publishing.
- Amsellem S, Gburek J, Hamard G, Nielsen R, Willnow TE, Devuyst O, Nexo E, Verroust PJ, Christensen EI, Kozyraki R. (2010) Cubilin Is Essential for Albumin Reabsorption in the Renal Proximal Tubule. *J. Am. Soc. Nephrol.* 21:1859–1867.
- Aronson PS, Nee J, Suhm MA. (1982) Modifier role of internal  $H^+$  in activating  $Na^+H^+$  exchanger in renal microvillus membrane vesicles. *Nature* 299:161-163.
- Aswar UM, V Mohan V, Bodhankar SL. (2012) Antiosteoporotic activity of phytoestrogen-rich fraction separated from ethanol extract of aerial parts of *Cissus quadrangularis* in ovariectomized rats. *Indian Journal of Pharmacology* 44:345-350.
- Ba J, Brown D, Friedman PA. (2003). Calcium-sensing receptor regulation of PTH-inhibitable proximal tubule phosphate transport. *American Journal of Physiology-Renal Physiology* 285(6):F1233-F1243.
- Bandarra PM, Pavarini SP, Santos AS, Antoniassi NAB, Cruz CEF, David Driemeier D. (2011) Nutritional fibrous osteodystrophy in goats. *Pesq. Vet. Bras.* 31(10):875-878.
- Barrett KE, Barman SM, Boitano S, Brooks H. (2010) *Ganong's Review of Medical Physiology*. McGraw and Hill.
- Barth H, Aktories K, Popoff MR, Stiles BG. (2004) Binary bacterial toxins: biochemistry, biology, and applications of common *Clostridium* and *Bacillus* proteins. *Microbiol Mol Biol Rev.* 68(3):373-402.
- Berner W, Kinne R, Murer H. (1976) Phosphate transport into brush-border membrane vesicles isolated from rat small intestine. *Biochem. Journal* 160:467-474.
- Berry JL, Davies M, Mee AP. (2002) Vitamin D metabolism, rickets and osteomalacia. *Semin. Musculoskelet. Radiol.* 6(3):173-182.
- Besarab A, Caro JF. (1981) Increased absolute calcium binding to albumin in hypoalbuminaemia. *J. Clin. Pathol.* 34:1368-1374.
- Block GA, Klassen PS, Lazarus JM, Ofsthun N, Lowrie EG, Chertow GM. (2004). Mineral metabolism, mortality, and morbidity in maintenance hemodialysis. *Journal of the American Society of Nephrology* 15(8):2208-2218.
- Bodansky A, Blair JE, Jaffe HL. (1930) Experimental hyperparathyroidism in guinea pigs leading to osteitis fibrosa. *J. Biol. Chem.* 88:629-647.
- Boehmer E, Crossley D. (2009) Objective interpretation of dental disease in rabbits, guinea pigs and chinchillas. *Tierärztliche Praxis Kleintiere* 37 (K):250-260.
- Bonucci E. (1970) Fine structure of epiphyseal cartilage in experimental scurvy. *J. Pathol.* 102(4):219-27.
- Bonucci, E. (1978) Matrix vesicle formation in cartilage of scorbutic guinea pigs electron microscope study of serial sections. *Metabolic Bone Disease and Related Research* 1.3: 205-212.
- Bosshardt DD, Schroeder HE. (1996) Cementogenesis reviewed: a comparison between human premolars and rodent molars. *The Anatomical Record* 245(2):267-292.
- Boutroy S, Bouxsein ML, Munoz F, Delmas PD. (2005) In vivo assessment of trabecular bone microarchitecture by high-resolution peripheral quantitative computed tomography. *Journal of Clinical Endocrinology & Metabolism* 90(12):6508-6515.

- Bovee KC, Joyce T, Reynolds R, Segal S. (1978) The Fanconi syndrome in Basenji dogs: a new model for renal transport defects. *Science* 201(4361):1129-1131.
- Brandão J, Vergneau-Grosset C, Mayer J. (2013) Hyperthyroidism and hyperparathyroidism in guinea pigs (*Cavia porcellus*). *The Veterinary Clinics of North America. Exotic Animal Practice* 16(2):407-420.
- Bronner F. (1987) Intestinal calcium absorption: mechanisms and applications. *The Journal of Nutrition* 117(8):1347-52.
- Brouwers JEM, Lambers FM, Gasser JA, Van Rietbergen B, Huiskes R. (2008) Bone degeneration and recovery after early and late bisphosphonate treatment of ovariectomized Wistar rats assessed by in vivo micro-computed tomography. *Calcified Tissue International* 82(3):202-211.
- Brouwers JEM, Van Rietbergen B, Huiskes R, Ito K. (2009) Effects of PTH treatment on tibial bone of ovariectomized rats assessed by in vivo micro-CT. *Osteoporosis International* 20(11):1823-1835.
- Brown AJ, Ritter CS, Finch JL, Slatopolsky EA. (1999) Decreased calcium-sensing receptor expression in hyperplastic parathyroid glands of uremic rats: role of dietary phosphate. *Kidney Int.* 55:1284-1292.
- Bucay N, Sarosi I, Dunstan CR, Morony S, Tarpley J, Capparelli C, Simonet WS. (1998) Osteoprotegerin-deficient mice develop early onset osteoporosis and arterial calcification. *Genes & Development* 12(9):1260-1268.
- Bugg NC, Jones JA. (1998) Hypophosphataemia. Pathophysiology, effects and management on the intensive care unit. *Anaesthesia* 53(9):895-902.
- Burns JJ. (1957) Missing Step in Man, Monkey and Guinea Pig required for the Biosynthesis of L-Ascorbic Acid. *Nature* 180:553.
- Canaan-Kuhl S, Venkatraman ES, Ernst SI, Olshen RA, Myers BD. (1993). Relationships among protein and albumin concentrations and oncotic pressure in nephrotic plasma. *American Journal of Physiology-Renal Physiology* 264(6):F1052-F1059.
- Canning BJ, Chou Y. (2008) Using guinea pigs in studies relevant to asthma and COPD. *Pulm. Pharmacol. Ther.* 21(5):702-20.
- Capello V, Cauduro A. (2008) Clinical technique: application of computed tomography for diagnosis of dental disease in the rabbit, guinea pig, and chinchilla. *Journal of Exotic Pet Medicine* 17(2):93-101.
- Capello V, Lennox AM. (2008) *Clinical Radiology of Exotic Companion Animals*. Wiley-Blackwell.
- Cappuccio FP, Kalaitzidis R, Duneclift S, Eastwood JB. (2000). Unravelling the links between calcium excretion, salt intake, hypertension, kidney stones and bone metabolism. *Journal of Nephrology* 13(3): 169-177.
- Carter AM. (2007) Animal models of human placentation--a review. *Placenta* 28A:S41-7.
- Chang JI, Som PM, Lawson W. (2007) Unique imaging findings in the facial bones of renal osteodystrophy. *Am. J. Neuroradiol.* 28(4):608-9.
- Chanutin A, Ferris EB. (1932) Experimental renal insufficiency produced by partial nephrectomy: I. Control diet. *Archives of Internal Medicine* 49(5):767.
- Chevalier RL. (1982) Glomerular Number and Perfusion during Normal and Compensatory Renal Growth in the Guinea Pig. *Pediatr. Res* 16: 436-440.
- Chen NX, Moe SM. (2004) Vascular calcification in chronic kidney disease. In: *Seminars in Nephrology* 24(1): 61-88. WB Saunders.

- Chen G, Deng C, Li YP. (2012) TGF- $\beta$  and BMP Signaling in Osteoblast Differentiation and Bone Formation. *Int. J. Biol. Sci.* 8(2):272-288.
- Chew FS, Huang-Hellinger F. (1993) Brown tumor. *American Journal of Roentgenology* 160(4): 752-752.
- Chojkier M, Houglum K, Solis-Herruzo J, Brenner, DA. (1989) Stimulation of collagen gene expression by ascorbic acid in cultured human fibroblasts. A role for lipid peroxidation? *Journal of Biological Chemistry* 264(28), 16957-16962.
- Chow KM, Liu ZC, Chang TMS. (2003) Animal Remnant Kidney Model of Chronic Renal Failure Revisited. *Hong Kong Journal of Nephrology* 5(2):57-64.
- Christiansen P. (2001) The skeleton in primary hyperparathyroidism: a review focusing on bone remodeling, structure, mass, and fracture. *APMIS Suppl.* 102:1-52.
- Clarke GL, Allen AM, J. D. Small JD, Lock A. (1980) Subclinical scurvy in the guinea pig. *Vet Pathol* 17:40-44.
- Cochran M, Wilkinson R. (1975) Effect of correction of metabolic acidosis on bone mineralisation rates in patients with renal osteomalacia. *Nephron* 15(2):98-110.
- Cogan MG. (1990) Angiotensin II: a powerful controller of sodium transport in the early proximal tubule. *Hypertension* 15:451-458.
- Cooke RE, Kleeman CR. (1950) Distal tubular dysfunction with renal calcification. *The Yale Journal of Biology and Medicine* 23(3):199.
- Cooper KL. (1989) Radiology of metabolic bone disease. *Endocrinology Metabolism Clinics of North America* 18(4): 955-76.
- Cope O, Culver PJ, Mixter CG, Nardi GL. (1957). Pancreatitis, a diagnostic clue to hyperparathyroidism. *Annals of Surgery* 145(6):857.
- Cowley BD, Gudapaty S, Kraybill AL, Barash BD, Harding MA, Calvet JP, Gattone VH. (1993) Autosomal-dominant polycystic kidney disease in the rat. *Kidney International* 43(3):522.
- Cozzolino M, Dusso AS, Slatopolsky E. (2001) Role of Calcium-Phosphate Product and Bone-Associated Proteins on Vascular Calcification in Renal Failure. *J. Am. Soc. Nephrol.* 12:2511–2516.
- Crosby AH, Edwards SJ, Murray JC, Dixon MJ. (1995). Genomic organization of the human osteopontin gene: exclusion of the locus from a causative role in the pathogenesis of dentinogenesis imperfecta type II. *Genomics* 27 (1):155–160.
- Cross HS, Debiec H, Peterlik M. (1990) Mechanism and regulation of intestinal phosphate absorption. *Mineral and Electrolyte Metabolism* 16(2-3):115.
- D'Amico G (1987) The commonest glomerulonephritis in the world: IgA nephropathy. *Q. J. Med.* 64 (245):709–727.
- Dawson RMC, Elliott DC, Elliott WH, Jones KM. (1987) *Data for Biochemical Research*, 3rd Ed., Oxford Press.

- Debiec H, Lorenc R. (1988) Influence of lactose on phosphate metabolism in rats. *Br. J. Nutr.* 59:87-92.
- Debout C, Taouji S, Izard J. (1995) Increase of a guinea pig natural killer cell (Kurloff cell) during leukemogenesis. *Cancer letters* 97(1):117-122.
- De Bruin C, Meij BP, Kooistra HS, Hanson JM, Lamberts SWJ, Hofland LJ. (2009) Cushing's disease in dogs and humans. *Hormone Research in Paediatrics* 71:140-143.
- De Schutter T. (2012) The calcification paradox. PhD Thesis, University of Antwerp.
- Dhingra R, Sullivan LM, Fox CS, Wang TJ, D'Agostino RB, Gaziano JM, Vasani RS. (2007) Relations of Serum Phosphorus and Calcium Levels to the Incidence of Cardiovascular Disease in the Community. *Arch. Intern. Med.* 167:879-885.
- Diamond JR, Karnovsky MJ. (1988) Focal and segmental glomerulosclerosis: analogies to atherosclerosis. *Kidney International* 33(5):917-924.
- Ding M, Danielsen CC, Hvid I. (2006) Age-Related Three-Dimensional Microarchitectural Adaptations of Subchondral Bone Tissues in Guinea Pig Primary Osteoarthritis. *Calcif. Tissue Int.* 78:113-122
- Duarte CG, Watson JF. (1967) Calcium reabsorption in proximal tubule of the dog nephron. *American Journal of Physiology* 212(6):1355-1360.
- Eschbach JW. (1989) The anemia of chronic renal failure: pathophysiology and the effects of recombinant erythropoietin. *Journal of Perinatal Medicine* 35(1):134-148.
- Evangelista C, Rizzo M, Capasso G. (2004) New concepts of tubular calcium transport in the kidney: clinical implications. *G. Ital. Nefrol.* 21(1):5-15.
- Fain O. (2005) Musculoskeletal manifestations of scurvy. *Joint Bone Spine* 72(2):124-128.
- Floege J, Burns MW, Alpers CE, Yoshimura A, Pritzl P, Gordon K, Johnson RJ. (1992) Glomerular cell proliferation and PDGF expression precede glomerulosclerosis in the remnant kidney model. *Kidney International* 41(2):297-309.
- Foley RN, Parfrey PS, Sarnak MJ. (1998) Epidemiology of cardiovascular disease in chronic renal disease. *J. Am. Soc. Nephrol.* 9(120):S16-23.
- Franceschi RT, Iyer BS, Cui Y. (1994) Effects of Ascorbic Acid on Collagen Matrix Formation and Osteoblast Differentiation in Murine MC3T3-E 1 Cells. *J. Bone Miner. Res.* 9:843-854
- Friedman PA. (1998) Codependence of renal calcium and sodium transport. *Ann. Rev. Physiol.* 60:179-197.
- Friedman PA. (2000) Mechanisms of renal calcium transport. *Experimental Nephrology* 8(6):343-350.
- Friedman PA, Gesek FA. (1993) Vitamin D3 accelerates PTH-dependent calcium transport in distal convoluted tubule cells. *Am. J. Phys. Renal Phys.* 265(2):F300-F308.
- Friedman PA, Gesek FA. (1995) Cellular Calcium Transport in Renal Epithelia: Measurement, Mechanisms, and Regulation. *Physiological Reviews* 75(3):429-471.
- Friedman PA, Figueiredo JF, Maack T, Windhager EE. (1981) Sodium-calcium interactions in the renal proximal convoluted tubule of the rabbit. *American Journal of Physiology-Renal Physiology* 240(6):F558-F568.
- Fukuda N, Tanaka H, Tominaga Y, Fukagawa M, Kurokawa K, Seino Y. (1993) Decreased 1, 25-dihydroxyvitamin D3 receptor density is associated with a more severe form of parathyroid hyperplasia in chronic uremic patients. *Journal of Clinical Investigation* 92(3): 1436.

- Fukagawa M, Kazama JJ, Kurokawa K. (2002) Renal osteodystrophy and secondary hyperparathyroidism. *Nephrology Dialysis Transplantation* 17: 2-5.
- Gagnon RF, Duguid WP. (1983) A reproducible model for chronic renal failure in the mouse. *Urol. Res.* 11: 11-14.
- Geibel J, Giebisch G, Boron WF. (1990) Angiotensin II stimulates both Na-H exchange and Na<sup>+</sup>/HCO<sup>-</sup> cotransport in the rabbit proximal tubule. *Proc. Natl. Acad. Sci. USA* 87:7917-7920,
- Genant HK, Block JE, Steiger P, Glueer CC, Smith R. (1987) Quantitative computed tomography in assessment of osteoporosis. *Seminars in Nuclear Medicine* 17(4): 316-333.
- Gennari L, Merlotti D, De Paola V, Calabro A, Becherini L, Martini G, Nuti R. (2005). Estrogen receptor gene polymorphisms and the genetics of osteoporosis: a HuGE review. *American Journal of Epidemiology*, 161(4):307-320.
- Gilbert L, He X, Farmer P, Boden S, Kozlowski M, Rubin J, Nanes MS. (2000) Inhibition of osteoblast differentiation by tumor necrosis factor-alpha. *Endocrinology* 141(11):3956-64.
- Gilka F, Sugden EA. (1984) Ectopic mineralization and nutritional hyperparathyroidism in boars. *Canadian Journal of Comparative Medicine* 48(1):102.
- Gogusev J, Duchambon P, Hory B, Giovannini M, Goureau Y, Sarfati E, Drüeke TB. (1997) Depressed expression of calcium receptor in parathyroid gland tissue of patients with hyperparathyroidism. *Kidney International* 51(1):328-336.
- Gordon MT, Anderson DC, Sharpe PT. (1991) Canine distemper virus localised in bone cells of patients with Paget's disease. *Bone* 12(3):195-201.
- Gould CF, Ly JQ, Lattin GE, Beall DP, Sutcliffe JB. (2007) Bone tumor mimics: avoiding misdiagnosis. *Current Problems in Diagnostic Radiology* 36(3):124-141.
- Greenspan EM. (1949) Hyperchloremic acidosis and nephrocalcinosis: the syndrome of pure "lower nephron" insufficiency. *Archives of Internal Medicine* 83(3):271.
- Gutierrez O, Isakova T, Rhee E, Shah A, Holmes J, Collerone G, Jüppner H, Wolf M. (2005) Fibroblast Growth Factor-23 Mitigates Hyperphosphatemia but Accentuates Calcitriol Deficiency in Chronic Kidney Disease. *Journal of the American Society of Nephrology* 16(7):2205-2215.
- Guyton AC, Hall JE. (2000) *Textbook of medical physiology*. 10th edition, Saunders Publ.
- Han S, Li T, Ellis E, Strom S, Chiang JY. (2010) A novel bile acid-activated vitamin D receptor signaling in human hepatocytes. *Mol. Endocrinol.* 24(6):1151-64.
- Hawkins MG. Secondary nutritional hyperparathyroidism with fibrous osteodystrophy in three guinea pigs. (2010) Association of Exotic Mammal Veterinarians Scientific Program, San Diego, 121.
- Hawkins MG, Bishop CR. (2012) Disease Problems of Guinea Pigs. In: Quesenberry KE, Carpenter JW (eds). *Ferrets, Rodents and Rabbits*, Elsevier.
- Harcourt-Brown F. (2002) Clinical Pathology. In: *Textbook of Rabbit Medicine*, Butterworth-Heinemann, London, p. 140-164.
- Harcourt-Brown FM. (2007) The progressive syndrome of acquired dental disease in rabbits. *Journal of Exotic Pet Medicine* 16(3):146-157.
- Harmey D, Hessle L, Narisawa S, Johnson KA, Terkeltaub R, Millán JL. (2004) Concerted Regulation of Inorganic Pyrophosphate and Osteopontin by Akp2, Enpp, and Ank: An Integrated Model of the Pathogenesis of Mineralization Disorders. *The American Journal of Pathology* 164(4):1199-1209.

- Hessle L, Johnson KA, Anderson HC, Narisawa S, Sali A, Goding JW, Terkeltaub R, Luis Millan JL, (2002) Tissue-nonspecific alkaline phosphatase and plasma cell membrane glycoprotein-1 are central antagonistic regulators of bone mineralization. *Proceedings of the National Academy of Sciences* 99(14):9445-9449.
- Hildebrandt F, Waldherr R, Kutt R, Brandis M. (1992). The nephronophthisis complex: clinical and genetic aspects. *The Clinical Investigator* 70(9):802-808.
- Ho LT, Sprague SM. (2002) Renal osteodystrophy in chronic renal failure. *Semin Nephrol.* 22(6):488-93.
- Hoenderop JGJ, Mueller D, Van der Kemp AWCM, Hartog A, Suzuki M, Ishibashi K, Imai M, Sweep F, Willems PHGM, Van Os CH, Bindels RJM. (2001) Calcitriol controls the epithelial calcium channel in kidney. *Journal of the American Society of Nephrology* 12(7):1342-1349.
- Hoenderop JGJ, Nilius B, Bindels RJM. (2002) Molecular mechanism of active Ca<sup>2+</sup> reabsorption in the distal nephron. *Annu. Rev. Physiol.* 64:529-49.
- Hogg AH. (1947) Osteodystrophic disease in the dog, with special reference to rubber jaw (renal osteodystrophy) and its comparison with renal rickets in the human. *Veterinaria* 11(11):117.
- Holowaychuk MK. (2006). Renal failure in a guinea pig (*Cavia porcellus*) following ingestion of oxalate containing plants. *The Canadian Veterinary Journal* 47(8):787.
- Hrapkiewicz K, Medina LV. (2007) *Clinical Laboratory Animal Medicine*. Blackwell Publishing.
- Hruska KA, Teitelbaum ST. (1995) Renal osteodystrophy. *New England Journal of Medicine* 333:166-174.
- Hruska KA, Mathew S, Lund R, Qiu P, Pratt R. (2008) Hyperphosphatemia of chronic kidney disease. *Kidney International* 74(2):148-157.
- Ito S, Arima S, Ren YL, Juncos LA, Carretero OA. (1993) Endothelium-derived relaxing factor/nitric oxide modulates angiotensin II action in the isolated microperfused rabbit afferent but not efferent arteriole. *Journal of Clinical Investigation* 91(5):2012.
- Jacob JJ, John M, Thomas N, Chacko A, Cherian R, Selvan B, Seshadri MS. (2006) Does hyperparathyroidism cause pancreatitis? A South Indian experience and a review of published work. *ANZ Journal of Surgery* 76(8):740-744.
- Jaffe HL, Bodansky A. (1930) Experimental fibrous osteodystrophy (*ostitis fibrosa*) in hyperparathyroid dogs. *The Journal of Experimental Medicine* 52(5):669-694.
- Jayawardena CK, Takahashi N, Watanabe E, Takano Y. (2002) On the origin of intrinsic matrix of acellular extrinsic fiber cementum: Studies on growing cementum pearls of normal and bisphosphonate-affected guinea pig molars. *European Journal of Oral Sciences* 110(3):261-269.
- Jennette JC, Sparg BH. (1999) The kidney. In: Rubin E, Farber EL (eds). *Pathology*. Lippincott-Raven.
- Jevtic V. (2003) Imaging of renal osteodystrophy. *European Journal of Radiology* 46(2):85-95.
- Jimenez PA, Glasson SS, Trubetskoy OV, Haimes HB. (1997) Spontaneous osteoarthritis in Dunkin-Hartley guinea pigs: histologic, radiologic and biochemical changes. *Lab. Anmi. Sci.* 47:598-601.
- Jordan J. (2008) Investigation of fibrous osteodystrophy in guinea pigs (*Cavia aparea f. porcellus*) of the satin phenotype. Development of radiographic scoring technique validating the presumptive diagnosis. *Dr. Vet. Med. hesis. Freie Universitat Berlin*.

- Jordan J, Brunnberg L, Ewringmann A, et al., (2009) Clinical, radiological and laboratory investigation of fibrous osteodystrophy in guinea pigs (*Cavia porcellus*) of the satin breed. *Kleintierpraxis* 54:5-13.
- Karsenty G, Lacour B, Ulmann A, Piérandréi E, Drüeke T. (1985) Phosphate fluxes in isolated enterocytes from vitamin D replete and vitamin D deficient rats—early effects of calcitriol. *Pflügers Archiv.* 403(2):151-155.
- Kawata T, Nagano N, Obi M, Miyata S, Koyama C, Kobayashi N, Wakita S, Wada M. (2008) Cinacalcet suppresses calcification of the aorta and heart in uremic rats. *Kidney Int.* 74:1270-1277.
- Kearns AE, Kallmes DF. (2008) Osteoporosis Primer for the Vertebroplasty Practitioner: Expanding the Focus Beyond Needles and Cement. *Am. J. Neuroradiol.* 29:1816-1822.
- Kefalides NA. (1974) Biochemical properties of human glomerular basement membrane in normal and diabetic kidneys. *Journal of Clinical Investigation* 53(2):403.
- Kerjaschki D. (2001) Caught flat-footed: podocyte damage and the molecular bases of focal glomerulosclerosis. *Journal of Clinical Investigation* 108(11):1583-1587.
- Kerstetter JE, O'Brien KO, Insogna KL. (2003) Dietary protein, calcium metabolism, and skeletal homeostasis revisited. *Am. J. Clin. Nutr.* 78:584S-592S
- Kinne R, Schwartz IL. (1978) Isolated membrane vesicles in the evaluation of the nature, localization, and regulation of renal transport processes. *Kidney International* 14:547—556.
- Kinsella JL, Aronson PS. (1980) Properties of the Na<sup>+</sup>-H<sup>+</sup> exchanger in renal microvillus membrane vesicles. *American Journal of Physiology - Renal Physiology* 238:F461-F469
- Kipp DE, McElvain M, Kimmel DB, Akhter MP, Robinson RG, Lukert BP. (1996) Scurvy results in decreased collagen synthesis and bone density in the guinea pig animal model. *Bone* 18:281-288.
- Klahr S, Schreiner G, Ichikawa I. (1988) The progression of renal disease. *The New England Journal of Medicine* 318(25):1657-1666.
- Kolek OI, Hines ER, Jones MD, LeSueur LK, Lipko MA, Kiela PR, Ghishan FK. (2005) 1 $\alpha$ , 25-Dihydroxyvitamin D<sub>3</sub> upregulates FGF23 gene expression in bone: the final link in a renal-gastrointestinal-skeletal axis that controls phosphate transport. *American Journal of Physiology-Gastrointestinal and Liver Physiology* 289(6):G1036-G1042.
- Kopp JB, Smith MW, Nelson GW, Johnson RC, Freedman BI, Bowden DW, Winkler CA. (2008) MYH9 is a major-effect risk gene for focal segmental glomerulosclerosis. *Nature Genetics* 40(10):1175-1184.
- Korstanje R, DiPetrillo K. (2004) Unraveling the genetics of chronic kidney disease using animal models. *American Journal of Physiology-Renal Physiology* 287(3):F347-F352.
- Krakauer IC, McKenna MJ, Buderer NF, Rao DS, Whitehouse FW, Parfitt AM. (1995) Bone loss and bone turnover in diabetes. *Diabetes* 44:775-782.
- Kraus VB, Hoebner JL, Stabler T, Flahiff CM, Setton LA, Fink Ch, Vilim V, Clark AG. (2004) Ascorbic acid increases the severity of spontaneous knee osteoarthritis in a guinea pig model. *Arthritis and Rheumatism* 50:1822-1831.
- Kumar S, Singh R, Vasudeva N, Sharma S. (2012), Acute and chronic animal models for the evaluation of anti-diabetic agents. *Cardiovascular Diabetology* 11:9.
- Kurosu H, Ogawa Y, Miyoshi M, Yamamoto M, Nandi A, Rosenblatt KP, Kurou M. (2006) Regulation of fibroblast growth factor-23 signaling by *klotho*. *Journal of Biological Chemistry* 281(10): 6120-6123.
- Lack EA, Farber EL, Rubin E. (1999) The Endocrine System. In: Rubin E, Farber EL (eds). *Pathology*. Lippincott-Raven.

- Lafont AG, Wang YF, Chen GD, Liao BK, Tseng YC, Huang CJ, Hwang PP. (2011) Involvement of calcitonin and its receptor in the control of calcium-regulating genes and calcium homeostasis in zebrafish (*Danio rerio*). *Journal of Bone and Mineral Research* 26(5):1072-1083.
- Laing CM, Tøye AM, Capasso G, Unwin RJ. (2005) Renal tubular acidosis: developments in our understanding of the molecular basis. *Int. J. Biochem. Cell Biol.* 37 (6):1151–61.
- Laradi A, Sakhrani LM, Massry SG. (1986) Effect of dopamine on sodium uptake by renal proximal tubule cells of rabbit. *Miner. Electrolyte Metab.* 12:303-307.
- Lautenbach E, Dockhorn R. (1968) Osteodystrophia fibrosa generalisata (Recklinghausen's disease; hyperparathyroidism) and its effects on the jaws. *Oral Surg. Oral Med. Oral Pathol.* 25(3):479-484.
- Lee VS, Webb MS, Martinez S, McKay CP, Leight GS. (1996) Uremic leontiasis ossea: "bighead" disease in humans? Radiologic, clinical, and pathologic features. *Radiology* 199(1):233-240.
- Leedham PW, Pollock DJ. (1970) Intrafollicular amyloid in primary hyperparathyroidism. *J. Clin. Pathol.* 23:811-817.
- Legendre, L. F. (2002). Malocclusions in guinea pigs, chinchillas and rabbits. *The Canadian Veterinary Journal* 43(5):385-390.
- Lenz JI, Jacobs JM, De Beeck BO, Huyghe IA, Pelckmans PA, Moreels TG. (2010) Acute necrotizing pancreatitis as first manifestation of primary hyperparathyroidism. *World Journal of Gastroenterology* 16(23):2959-2962.
- Leon NP, Teklegiorgis S, Perez CC. (2008) The bony manifestation of Rickets. A case report. *J. Eritr. Med. Assoc.* 3(1): 49-51.
- Lepage R, Roy L, Brossard JH, Rousseau L, Dorais C, Lazure C, D'Amour P. (1998) A non-(1– 84) circulating parathyroid hormone (PTH) fragment interferes significantly with intact PTH commercial assay measurements in uremic samples. *Clinical Chemistry* 44:805–809.
- Lerner UH. (2006) Deletions of genes encoding calcitonin/alpha-CGRP, amylin and calcitonin receptor have given new unexpected insights into the function of calcitonin receptors and calcitonin receptor-like receptors in bone. *J. Musculoskelet. Neuronal Interact.* 6:87-95.
- Li YC, Amling M, Pirro AE, Priemel M, Meuse J, Baron R, Demay MB. (1998) Normalization of mineral ion homeostasis by dietary means prevents hyperparathyroidism, rickets, and osteomalacia, but not alopecia in vitamin D receptor-ablated mice. *Endocrinology* 139(10):4391-4396.
- Liu FY, Cogan MG. (1988) Angiotensin II Stimulation of Hydrogen Ion Secretion in the Rat Early Proximal Tubule. *J. Clin. Invest.* 82: 601-607.
- Liu SK, Dorfman HD, Hurvitz AI, Patnaik AK. (1977) Primary and secondary bone tumours in the dog. *Journal of Small Animal Practice* 18(5):313-326.
- Lopez I, Aguilera-Tejero E, Felsenfeld AJ, Estepa JC, Rodriguez M. (2002) Direct effect of acute metabolic and respiratory acidosis on parathyroid hormone secretion in the dog. *Journal of Bone and Mineral Research* 17(9):1691-1700.
- Lucke VM. (1968) Renal disease in the domestic cat. *The Journal of Pathology and Bacteriology* 95(1):67-91.
- Lund RJ, Davies MR, Brown AJ, Hruska KA. (2004) Successful treatment of an adynamic bone disorder with bone morphogenetic protein-7 in a renal ablation model. *Journal of the American Society of Nephrology* 15(2):359-369.

- Luo G, Ducey P, McKee MD, Pinero GJ, Loyer E, Behringer RR, Karsenty G. (1997) Spontaneous calcification of arteries and cartilage in mice lacking matrix GLA protein. *Nature* 386:78–81.
- Makishima M, Lu TT, Xie W, Whitfield GK, Domoto H, Evans RM, Mangelsdorf DJ. (2002). Vitamin D receptor as an intestinal bile acid sensor. *Science* 296(5571):1313-1316.
- Malluche HH. (2002) Aluminum and bone disease in chronic renal failure. *Nephrology Dialysis Transplantation* 17:21-24.
- Maryniak RK, First MR, Weiss MA. (1985) Transplant glomerulopathy: evolution of morphologically distinct changes. *Kidney Int.* 27(5):799-806.
- Massop H. (2009) Botaantasting bij de satijncavia. MSc Thesis, Ghent University (in Dutch).
- Maynard LA, Boggs D, Fisk G, Seguin D. (1958) Dietary mineral interrelations as a cause of soft tissue calcification in guinea pigs. *J. Nutr.* 64:85-97.
- McAlindon TE, Jacques P, Zhang Y, Hannan MT, Aliabadi P, Weis P. (1996) Do antioxidant micronutrients protect against the development and progression of knee osteoarthritis? *Arthritis Rheum.* 39:648–56.
- McCarron DA, Pingree PA, Rubin RJ, Gaucher SM, Molitch M, Krutzik S. (1980) Enhanced parathyroid function in essential hypertension: a homeostatic response to a urinary calcium leak. *Hypertension* 2: 162-8.
- McDowell H, Gregory TM, Brown WE. (1977) Solubility of  $\text{Ca}_5(\text{PO}_4)_3\text{OH}$  in the System  $\text{Ca}(\text{OH})_2\text{-H}_3\text{PO}_4\text{-H}_2\text{O}$  at 5, 15, 25, and 37 C. *J. Res. Nat. Bur. Stand. A* 81: 273-281.
- McGavin MD, Zachary JF. (2007) *Pathologic Basis of Veterinary Medicine*. 4<sup>th</sup> edition, Elsevier.
- McMahon C, Will A, Hu P, Shah GN, Sly WS, Smith OP. (2001) Bone marrow transplantation corrects osteopetrosis in the carbonic anhydrase II deficiency syndrome. *Blood* 97: 1947-1950.
- Meister A. (1994) Glutathione-ascorbic acid antioxidant system in animals. *J. Biol. Chem.* 269: 9397-400.
- Meyer JL. (1984) Can biological calcification occur in the presence of pyrophosphate? *Arch. Biochem. Biophys.* 231:1–8.
- Meyer TW, Hostetter TH. (2007) Uraemia. *The New England Journal of Medicine* 357:1316-1325.
- Mirra JM, Brien EW, Tehranzadeh J. (1995) Paget's disease of bone: review with emphasis on radiologic features, part I. *Skeletal Radiology* 24(3):163-171.
- Mocetti P, Ballanti P, Zalzal S, Silvestrini G, Bonucci E, Nanci A. (2000) A histomorphometric, structural, and immunocytochemical study of the effects of diet-induced hypocalcemia on bone in growing rats. *Journal of Histochemistry & Cytochemistry* 48(8):1059-1077.
- Moe SM, Reslerova M, Ketteler M, O'Neill K, Duan D, Koczman J, Westenfeld R, Jahnen-Dechent W, Chen NX. (2005) Role of calcification inhibitors in the pathogenesis of vascular calcification in chronic kidney disease (CKD). *Kidney International* 67:2295-2304.
- Moe S, Drüeke T, Cunningham J, Goodman W, Martin K, Olgaard K, Eknoyan G. (2006) Definition, evaluation, and classification of renal osteodystrophy: a position statement from Kidney Disease: Improving Global Outcomes (KDIGO). *Kidney International* 69(11):1945-1953.
- Moe SM, Chen NX, Seifert MF, Sinderson RM, Duan D, Chen X, Liang Y, Radcliff JS, White KE, Gattone VH. (2009) A rat model of chronic kidney-mineral bone disease. *Kidney International* 75:176-184.

- Morales E. (1995). *The Guinea Pig: Healing, Food, and Ritual in the Andes*. University of Arizona Press.
- Myers JL, Arocho J, Bernreuter W, Dunham W, Mazur MT. (1991) Leiomyosarcoma of bone. A clinicopathologic, immunohistochemical, and ultrastructural study of five cases. *Cancer* 67(4):1051-1056.
- Nagpal S, Na S, Rathnachalam R. (2005) Noncalcemic actions of vitamin D receptor ligands. *Endocrine Reviews* 26 (5):662-87.
- Nakagawa T, Segal M, Croker B, Johnson RJ. (2007) A breakthrough in diabetic nephropathy: the role of endothelial dysfunction. *Nephrology Dialysis Transplantation* 22(10): 2775-2777.
- Neven E, D'Haese PC. (2011) Vascular Calcification in Chronic Renal Failure What Have We Learned From Animal Studies?. *Circulation research* 108(2):249-264.
- O'Dell BL, Morris ER, Pickett EE, Hogan AG. (1957) Diet Composition and Mineral Balance in Guinea Pigs. *J. Nutrition* 63:65-77.
- Ohashi T, Kenmochi M, Kinoshita H, Ochi K, Kikuchi H. (1999) Cochlear function of guinea pigs with experimental chronic renal failure. *Ann Otol. Rhinol. Laryngol.* 108(10):955-62.
- Okada H, Kaneko Y, Yawata T, Uyama H, Ozono S, Motomiya Y, Hirao Y. (1999) Reversibility of adenine-induced renal failure in rats. *Clinical and Experimental Nephrology* 3(2): 82-88.
- Oken DE, Thomas SR, & Mikulecky DC. (1981) A network thermodynamic model of glomerular dynamics: application in the rat. *Kidney Int.* 19(2):359-373.
- O'Neill WC, Sigrist MK, McIntyre CW. (2010) Plasma pyrophosphate and vascular calcification in chronic kidney disease. *Nephrol. Dial. Transplant.* 25:187–191.
- Orth SR, Ritz E. (1998) The nephrotic syndrome. *New England Journal of Medicine* 338(17): 1202-1211.
- Paget J. (1877). On a form of chronic inflammation of bones (osteitis deformans). *Medico-chirurgical Transactions* 60:37.
- Parfitt AM. (2003) Renal bone disease: a new conceptual framework for the interpretation of bone histomorphometry. *Curr. Opin. Nephrol. Hypertens.* 12(4):387-403.
- Parthasarathy N, Spiro RG. (1982) Effect of diabetes on the glycosaminoglycan component of the human glomerular basement membrane. *Diabetes* 31(8):738-741.
- Pei Y, Hercz G, Greenwood CEA, Segre G, Manuel A, Saiphoo C, Fenton S, Sherrard D. (1993) Renal osteodystrophy in diabetic patients. *Kidney International* 44(1):159.
- Peng X, Griffith JW, Lang CM. (1990) Cystitis, urolithiasis and cystic calculi in ageing guineapigs. *Laboratory Animals* 24(2):159-163.
- Pérez AV, Picotto G, Carpentieri AR, Rivoira MA, Peralta López ME, Tolosa de Talamoni NG. (2008) Minireview on Regulation of Intestinal Calcium Absorption. *Digestion* 77:22-34
- Portale AA. (1999) Blood calcium, phosphorus, and magnesium. In Favus MJ (ed): *Primer on the Metabolic Bone Diseases and Disorders of Mineral Metabolism*. Philadelphia, PA, Lippincott, Williams & Wilkins.
- Pratt JH. (1982) Role of angiotensin II in potassium-mediated stimulation of aldosterone secretion in the dog. *Journal of Clinical Investigation* 70(3):667.

- Preedy VR, Watson RR, Sherma Z. (2010) Dietary Components and Immune Function (Nutrition and Health). Totowa, NJ: Humana.
- Prentice A. (2004) Diet, nutrition and the prevention of osteoporosis. *Public Health Nutrition* 7:227-244.
- Preziosi R, Diana A, Florio D, Gustinelli A, Nardini G. (2007) Osteitis deformans (Paget's disease) in a Burmese python (*Python molurus bivittatus*) – a case report. *The Veterinary Journal* 174:669-672.
- Quesenberry KE, Donnelly TM, Mans Ch. (2012) Biology, Husbandry and Clinical Techniques of Guinea Pigs and Chinchillas. In: Quesenberry KE, Carpenter JW (eds). *Ferrets, Rodents and Rabbits, Clinical Medicine and Surgery*, Elsevier.
- Quigley R. (2006) Proximal renal tubular acidosis. *Journal of Nephrology* 19:S41.
- Raggatt LJ, Partridge NC. (2010) Cellular and Molecular Mechanisms of Bone Remodeling. *The Journal of Biological Chemistry* 285:25103-25108.
- Rao DS, Parfitt AM, Villanueva AR, Dorman PJ, Kleerekoper M. (1987) Hypophosphatemic osteomalacia and adult Fanconi syndrome due to light-chain nephropathy: another form of oncogenous osteomalacia. *The American journal of medicine* 82(2):333-338.
- Rapsch-Dahinden Ch, Klawitter A, Sagawe J, Fehr M. (2009) Course of Osteodystrophia fibrosa generalisata in a satin guinea pig. *Schweiz Arch Tierheilkd.* 151(5):233-7.
- Reiter AM. (2008) Pathophysiology of dental disease in the rabbit, guinea pig, and chinchilla. *Journal of Exotic Pet Medicine* 17(2):70-77.
- Remuzzi G, Benigni A, Remuzzi A. (2006) Mechanisms of progression and regression of renal lesions of chronic nephropathies and diabetes. *Journal of Clinical Investigation* 116(2):288-296.
- Revell PA. (1974) Kurloff cell levels in the peripheral blood of normal and oestrogen treated guinea-pigs. *British Journal of Experimental Pathology* 55(6):525.
- Revell PA. (1977) The Kurloff cell. *Int. Rev. Cytol.* 51:275-314.
- Richardson VCG. (2000) *Diseases of Domestic Guinea Pigs*. Blackwell Publishing.
- Riihonen R, Supuran CT, Parkkila S, Pastorekova S, Väänänen HK, Laitala-Leinonen T. (2007) membrane-bound carbonic anhydrases in osteoclasts. *Bone* 40(4):1021-31.
- Ritter CS, Finch JL, Slatopolsky EA, Brown AJ. (2001) Parathyroid hyperplasia in uremic rats precedes down-regulation of the calcium receptor. *Kidney Int.* 60:1737-1744.
- Rix M, Andreassen H, Eskildsen P, Langdahl B, Olgaard K. (1999) Bone mineral density and biochemical markers of bone turnover in patients with predialysis chronic renal failure. *Kidney International* 56(3):1084-1093.
- Roach HI, Mehta G, Oreffo ROC, Clarke NMP, Cooper C. (2003) Temporal Analysis of Rat Growth Plates: Cessation of Growth with Age Despite Presence of a Physis. *J. Histochem. Cytochem.* 51: 373-383.
- Robinson R, Seaborne S. (1988) Satin coat in the guinea pig. *J. Hered.* 79 (3): 214-215.
- Rogers JB, Blumenthal HT. (1960) Studies of Guinea Pig Tumors I. Report of Fourteen Spontaneous Guinea Pig Tumors, with a Review of the Literature. *Cancer Research* 20(2):191-197.
- Rosalki SB, Foo AY. (1984) Two new methods for separating and quantifying bone and liver alkaline phosphatase isoenzymes in plasma. *Clinical Chemistry* 30(7):1182-1186.

- Rosenthal KL. (2006) Calcium metabolism in rabbits: what's new? Proc. North American Veterinary Conference, Orlando, Florida.
- Rosol TJ, Tannehill-Gregg SH, LeRoy BE, Mandl S, Contag CH. (2003) Animal models of bone metastasis. *Cancer* 97(S3):748-757.
- Rowlands IW, Weir BJ. (1974) *The Biology of Hystricomorph Rodents*. Academic Press, 437–446.
- Rubin E, Farber EL. (1999) *Pathology*. Lipincott-Raven.
- Rummens K. (2003) Environmental regulation of fetal mineralization. PhD Thesis. *Acta Biomedica Lovaniensia* 279, Leuven University Press.
- Saddoris KL. (2007) Dietary Factors Affecting Sodium-dependent Phosphate Uptake and Gene Expression of the NaPi-IIb in the Small Intestine of Weanling Pigs. PhD Thesis, Purdue University.
- Sandison A, Newbold KM, Howie AJ. (1992) Evidence for unique distribution of Kimmelstiel-Wilson nodules in glomeruli. *Diabetes* 41(8):952-955.
- Seeman E. (2003). Invited review: pathogenesis of osteoporosis. *Journal of Applied Physiology* 95(5): 2142-2151.
- Sellmeyer DE, Schloetter M, Sebastian A. (2002). Potassium citrate prevents increased urine calcium excretion and bone resorption induced by a high sodium chloride diet. *Journal of Clinical Endocrinology & Metabolism* 87(5):2008-2012.
- Schafer JA, Troutman SL, Andreoli TE. (1974) Volume Reabsorption, Transepithelial Potential Differences, and Ionic Permeability Properties in Mammalian Superficial Proximal Straight Tubules. *The Journal of General Physiology* 64:582-607.
- Schafer C, Heiss A, Schwarz A, Westenfeld R, Ketteler M, Floege J, Muller-Esterl W, Schinke T, Jahnchen-Dechent W. (2003) structural basis of calcification inhibition by alpha 2-Heremans-Schmid glycoprotein/fetuin-A is a systemically acting inhibitor of ectopic calcification. *J. Clin. Invest.* 112(3):357-366.
- Schedl HP, Osbaldiston GW, Mills IH. (1968) Absorption, secretion and precipitation of calcium in the small intestine of the dog. *Am. J. Physiol.* 214: 814–819.
- Schiller AL, Teitelbaum SL. (1999) *Bones and Joints*. In: Rubin E, Farber EL (eds). *Pathology*. Lippincott-Raven.
- Schlieper G, Westenfeld R, Brandenburg V, Ketteler M. (2007) Vascular calcification in patients with kidney disease: inhibitors of calcification in blood and urine. In: *Seminars in Dialysis* vol. 20(2): 113-121). Blackwell Publishing Ltd.
- Schwarz T, Störk CK, Megahy IW, Lawrie AW, Lochmüller EM, Johnston PEJ. (2001) Osteodystrophia fibrosa in two Guinea pigs. *J Am Vet Med Assoc*:219, 63-66.
- Shah S, Hussain T. (2006) Enhanced Angiotensin II-Induced Activation of Na<sup>+</sup>, K<sup>+</sup>-ATPase in the Proximal Tubules of Obese Zucker Rats. *Clin. Experimental Hypertension* 28(1): 29-40.
- Shobeiri N, Adams MA, Holden RM. (2010) Vascular calcification in animal models of CKD: a review. *American Journal of Nephrology* 31(6):471-481.
- Shroff RC, Shah V, Hiorns MP, Schoppet M, Hofbauer LC, Hawa G, Rees L. (2008). The circulating calcification inhibitors, fetuin-A and osteoprotegerin, but not matrix Gla protein, are associated with vascular stiffness and calcification in children on dialysis. *Nephrology Dialysis Transplantation* 23(10): 3263-3271.

Sigrist MK, Taal MW, Bungay P, McIntyre CW. (2007) Progressive vascular calcification over 2 years is associated with arterial stiffening and increased mortality in CKD 4 and 5 patients. *Clin. J. Am. Soc. Nephrol.* 2:1241-1248.

Simpson DP. (1983) Citrate excretion: a window on renal metabolism. *Am. J. Physiol.* 244: F223-234.

Slatopolsky E, Finch J, Denda M, Ritter C, Zhong M, Dusso A, Brown AJ. (1996). Phosphorus restriction prevents parathyroid gland growth. High phosphorus directly stimulates PTH secretion in vitro. *Journal of Clinical Investigation* 97(11):2534.

Soriano JR. (2002) Renal tubular acidosis: the clinical entity. *Journal of the American Society of Nephrology* 13(8): 2160-2170.

Sowers JR, Epstein M, Frohlich ED. (2001) Diabetes, hypertension, and cardiovascular disease an update. *Hypertension* 37(4):1053-1059.

Spitzer A, Brandis M. (1974) Functional and Morphologic Maturation of the Superficial Nephrons: relationship to total kidney function. *The Journal of Clinical Investigation* 53:279-287.

Spring KR, Giebisch, G. (1977) Kinetics of Na (+) transport in necturus proximal tubule. *The Journal of General Physiology* 70(3):307-328.

Steeve KT, Marc P, Sandrine T, Dominique H, Yannick F. (2004) IL-6, RANKL, TNF-alpha/IL-1: interrelations in bone resorption pathophysiology. *Cytokine & Growth Factor Reviews* 15(1): 49-60.

Stoffels E, Stoffels WW. (1994) Electrons, ions and dust in a radio-frequency discharge. PhD Thesis, Eindhoven University of Technology.

Stover EH, Borthwick KJ, Bavalia C, Eady N, Fritz DM, Rungroj N, Karet FE. (2002) Novel ATP6V1B1 and ATP6V0A4 mutations in autosomal recessive distal renal tubular acidosis with new evidence for hearing loss. *Journal of Medical Genetics* 39(11):796-803.

Suckow MA, Stevens KA, Wilson RP. (2012) *The Laboratory Rabbit, Guinea Pig, Hamster and Other Rodents.* Academic Press.

Suda T, Takahashi N, Udagawa N, Jimi E, Gillespie MT, Martin TJ. (1999) Modulation of osteoclast differentiation and function by the new members of the tumor necrosis factor receptor and ligand families. *Endocrine Reviews* 20(3):345-357.

Suki WS, Rouse D, Ng RCK, Kokko J. Calcium Transport in the Thick Ascending Limb of Henle. Heterogeneity of function in the medullary and cortical segments. *Journal of Clinical Investigation* 66:1004.

Sutton RA, Wong NL, Dirks JH. (1979) Effects of metabolic acidosis and alkalosis on sodium and calcium transport in the dog kidney. *Kidney international* 15(5): 520.

Tencer J, Frick IM, Oquist BW, Alm P, Rippe B. (1998) Sizeselectivity of the glomerular barrier to high molecular weight proteins: upper size limitations of shunt pathways. *Kidney International* 53:709–715.

Theoleyre S, Wittrant Y, Tat SK, Fortun Y, Redini F, Heymann D. (2004) The molecular triad OPG/RANK/RANKL: involvement in the orchestration of pathophysiological bone remodeling. *Cytokine & Growth Factor Reviews* 15(6):457-475.

Thomas SR Dagher G. (1994) A kinetic model of rat proximal tubule transport—load-dependent bicarbonate reabsorption along the tubule. *Bulletin of Mathematical Biology* 56(3):431-458.

Thomas SR, Layton AT, Layton HE, Moore LC. (2006) Kidney modelling: status and perspectives. *Proc. IEEE* 94(4):740-752.

- Thomas SR, Mikulecky DC. (1978) A network thermodynamic model of salt and water flow across the kidney proximal tubule. *American Journal of Physiology-Renal Physiology* 235(6):F638-F648.
- Tigges S, Nance EP, Carpenter WA, Erb R. (1995) Renal osteodystrophy: imaging findings that mimic those of other diseases. *American Journal of Roentgenology* 165:143-148.
- Tojo A, Kinugasa S. (2012) Mechanisms of Glomerular Albumin Filtration and Tubular Reabsorption. *International Journal of Nephrology* 2012: Article ID 481520.
- Tominaga Y, Kohara S, Namii Y, Nagasaka T, Haba T, Uchida K, Takagi H. (1996). Clonal analysis of nodular parathyroid hyperplasia in renal hyperparathyroidism. *World Journal of Surgery* 20(7):744-752.
- Toussaint N, Cooney P, Kerr PG. (2006) Review of dialysate calcium concentration in hemodialysis. *Hemodial. Int.* 10:326-337.
- Triantafillidou K, Zouloumis L, Karakinaris G, Kalimeras E, Iordanidis F. (2006) Brown tumors of the jaws associated with primary or secondary hyperparathyroidism. A clinical study and review of the literature. *Am J Otolaryngol.* 27(4):281-6.
- Vanbrugghe B, Blond L, Carioto L, Carmel EN, Nadeau ME. (2011) Clinical and computed tomography features of secondary renal hyperparathyroidism. *Can. Vet. J.* 52(2):177-180.
- Vannevel J. (1999) Diabetes in the guinea pig--not uncommon. *Can. Vet. J.* 40(9): 613.
- Veighey K, Cunningham J. (2011) Renal bone disease. *Medicine* 39(7): 417-420.
- Verdenius HHW, Alma L. (1958) A quantitative study of decalcification methods in histology. *J. Clin. Pathol.* 11(3): 229-236.
- Verstuyf A, Carmeliet G, Bouillon R, Mathieu C. (2010) Vitamin D: a pleiotropic hormone. *Kidney International* 78(2):140-145.
- Wada M, Ishii H, Furuya Y, Fox J, Nemeth EF, Nagano N. (1998) NPS R-568 halts or reverses osteitis fibrosa in uremic rats. *Kidney International* 53(2):448-453.
- Walter WG, Baldwin DE. (1963) Observations on the parathyroid glands of guinea pigs affected with metastatic calcification. *Can. J. Comp. Med. Vet. Sci.* 27(6): 140-141, 142-146.
- Watson ML, Rao JK, Gilkeson GS, Ruiz P, Eicher EM, Pisetsky DS, Seldin MF. (1992) Genetic analysis of MRL-lpr mice: relationship of the Fas apoptosis gene to disease manifestations and renal disease-modifying loci. *The Journal of Experimental Medicine* 176(6):1645-1656.
- Witteman JC, Kok FJ, Van Saase JL, Valkenburg HA. (1986) Aortic calcification as a predictor of cardiovascular mortality. *Lancet* 2(8516):1120-1122.
- Woods CG, Morgan DB, Paterson CR, Gossmann HH. (1968) Measurement of osteoid in bone biopsy. *J. Pathol.* 95: 441-447.
- Wronski TJ, Dann LM, Scott KS, Cintron M. (1989) Long-term effects of ovariectomy and aging on the rat skeleton. *Calcif. Tissue Int.* 45:360-366.
- Wyngaarden JB, & Dunn JT. (1957). 8-Hydroxyadenine as the intermediate in the oxidation of adenine to 2, 8-dihydroxyadenine by xanthine oxidase. *Archives of Biochemistry and Biophysics* 70(1):150-156.
- Yokozawa T, Oura H, Okada T. (1982) Metabolic effects of dietary purine in rats. *J. Nutr. Sci. Vitaminol.* 28: 519-526.

